Title

Rutting of Caltrans Asphalt Concrete and Asphalt-Rubber Hot MixUnder Different Wheels, Tires and Temperatures — AcceleratedPavement Testing Evaluation

Authors

Harvey, John
Popescu, Lorina

Publication Date

2000

UCPRC-RR-2000-01

Rutting of Caltrans Asphalt Concrete and Asphalt-Rubber Hot Mix Under Different Wheels, Tires and Temperatures – Accelerated Pavement Testing Evaluation

Research Report Prepared for

CALIFORNIA DEPARTMENT OF TRANSPORTATION

by

John Harvey and Lorina Popescu

January 2000
Pavement Research Center
Institute of Transportation Studies
University of California, Berkeley

TABLE OF CONTENTS

List of Tables vii

List of Figures ix

1.0 Background and Scope 1

1.1 Background – Caltrans Flexible Overlay Strategies 1

1.2 Scope of this Report 5

2.0 Laboratory and HVS Experiment Designs 7

2.1 HVS Test Experiment Design 8

2.1.1 Layout of Test Sections 9

2.1.2 Pavement Structures 10

2.1.3 Materials 21

2.2 HVS Test Conditions, Instrumentation and Data Collection 31

2.2.1 Trafficking 31

2.2.2 Tires and Wheels 31

2.2.3 Wheel Speed and Direction 34

2.2.4 Instrumentation and Data Collection 36

2.2.5 Heating and Temperature Control 38

3.0 Heavy Vehicle Simulator Test Results 41

3.1 Pavement Temperatures 41

3.2 Rutting Results 45

3.2.1 Comparison of Tire/Wheel Types 54

3.2.2 Comparison of Overlay Types 56

3.2.3 Comparison of Pavement Temperature 59

3.3 Contribution to Rutting of Shear and Densification of Different Layers 61

3.3.1 Profile changes 61

3.3.2 Air-void content changes 62

3.3.3 Thickness Changes 66

3.3.4 Identification of Shear and Densification 71

3.4 Rutting in the Underlying Layers 78

3.5 Late Bonding of Layers 80

4.0 Conclusions and Recommendations 83

4.1 Conclusions 83

4.2 Recommendations 85

5.0 References 87

Appendix A: Caltrans ARHM-GG/DGAC Thickness Equivalencies 89

Appendix B: Thickness Data from Cores and Trench Slabs 91

Appendix C: Air-Void Content Data 101

Appendix D: Deflections and Back-Calculated Moduli 111

Appendix E: Temperature Data..... 113

Appendix F: Average Transverse Surface Profiles versus Load Repetitions 115

Appendix G Transverse Profiles from AC Slabs from Trenches..... 125

Appendix H Development of Rut and Hump Volume Under Trafficking from Transverse Surface Profiles 137

Appendix I Transverse Aggregate Base Surface Profiles at Termination of Trafficking..... 147

LIST OF TABLES

Table 1 Matrix of HVS test experiment variables and test numbers..... 9

Table 2 Asphalt concrete layer thicknesses (mm) adjacent to rutting test sections measured from cores and slabs..... 13

Table 3 Summary of thicknesses (mm) by layer and overlay type. 14

Table 4 Approximate thicknesses of underlying layers. 14

Table 5 Air-void contents prior to HVS trafficking, from cores..... 16

Table 6 Summary of average air-void contents prior to trafficking (percent) by layer and overlay type. 16

Table 7 Summary data of measured deflections (microns) and back-calculated moduli (MPa) before overlay construction, 1 March, 1997 19

Table 8 Summary data of measured deflections (microns) and back-calculated moduli (MPa)after overlay construction, 1 April, 1997 19

Table 9 Summary of extracted gradation and binder content for DGAC overlay mix. 24

Table 10 Summary of extracted gradation, binder content and rubber content for ARHM-GG mix. 25

Table 11. Summary of extracted gradation and binder content for Goal 1 asphalt concrete mix..... 29

Table 12 Calculated surface contact durations for tire/wheel types included in study, assuming average unidirectional wheel speed. (18)..... 35

Table 13. Comparison of single variables from HVS test section results..... 41

Table 14 Summary of pavement temperatures and thermocouple depths during HVS trafficking. 42

Table 15 Temperature gradients in asphalt bound layers, assuming linear gradient between top and bottom thermocouples. 45

Table 16 Average maximum rut depth and load repetitions at completion of HVS trafficking. 51

Table 17 Load repetitions to 6.25 mm and 12.5 mm average maximum rut depth. 53

Table 18 Air-void contents before and after HVS trafficking, from cores. 63

Table 19 Final wheelpath air-void contents by tire/wheel type and layer type..... 65

Table 20 Final hump air-void contents by tire/wheel type and layer type. 66

Table 21. Thicknesses before and after HVS trafficking, from slabs. 67

Table 22 Thicknesses before and after HVS trafficking, from cores. 68

Table 23 Thickness of ATPB before and after HVS trafficking, from cores. 68

Table 24 Summary averages for percent change in thickness of asphalt concrete layers under HVS trafficking. 70

Table 25 Percent change of layer thickness from slabs and cores, and change of air-void content from cores at end of HVS trafficking. 72

Table 26 Volume of wheelpaths and humps, percent of rut volume attributed to shear (ratio of hump to wheelpath volume) and densification (1-shear), average across all data acquisitions during HVS trafficking. 76

Table 27 Volume of wheelpaths and humps, percent of rut volume attributed to shear (ratio of hump to wheelpath volume) and densification (1-shear), at 13 mm rut depth. 76

Table 28 Summary averages of percent of rut volume attributed to shear and densification. 77

Table A-1 California Structural Equivalencies. 89

Table A-2 California Reflective Crack Retardation Equivalencies 89

Table B-1 Thickness Data from Before Trafficking. 92

Table B-2 Thickness in the Wheelpaths after Trafficking. 95

Table B-3 Thickness of the Humps After Trafficking. 98

Table C-1 Air-Void Contents Before Trafficking. 102

Table C-2 Air-Void Contents in Wheelpaths After Trafficking. 105

Table C-3 Air-Void Contents in Humps after Trafficking. 108

Table D-1 Deflection data on rutting test sections (3/1/1997). 111

Table D-2 Deflection data on rutting test section after construction (4/1/1997). 112

Table E-1 Average Temperature, Sections 510RF and 511RF. 113

Table E-2 Average Temperature, Section 512 RF 113

LIST OF FIGURES

Figure 1. Layout of Goal 3 HVS tests sections. 10

Figure 2. Drained pavement structure. 11

Figure 3. Undrained pavement structure. 11

Figure 4. Locations of deflection measurements and HVS rutting test sections..... 18

Figure 5. Sensor 1 and Sensor 7 deflections along deflection lines, prior to overlay construction. 20

Figure 6. Back-calculated moduli for granular layers and subgrade before overlay. 22

Figure 7. Average back-calculated moduli for granular layers and subgrade before and after overlay construction..... 23

Figure 8. Extracted aggregate gradations for DGAC and ARHM-GG overlay mixes (sieve sizes to 0.45 power), and Superpave maximum density lines. 28

Figures 9a and 9b. Aluminum reflector with resistance-heating element and infrared lamps. 40

Figure 10. Average pavement temperature profiles during HVS trafficking. 44

Figure 11. Average pavement temperature profiles during HVS trafficking for three overlays under dual-radial wheel. 46

Figure 12. Average pavement temperature profiles during HVS trafficking for three overlays under wide-base single wheel. 47

Figure 13. Average pavement temperature profiles during HVS trafficking for four tire types on DGAC overlay. 48

Figure 14. Average pavement temperature profiles during HVS trafficking for two temperatures, wide-base single wheel, DGAC overlay. 49

Figure 15. Plot of average maximum rut depth versus load repetitions for all test sections..... 50

Figure 16. Plot of average maximum rut development versus load repetitions for four tire/wheel types on DGAC overlay..... 55

Figure 17. Plot of average maximum rut development versus load repetitions for DGAC, 38 mm ARHM-GG and 62 mm ARHM-GG overlays under dual/radial tires..... 57

Figure 18. Plot of average maximum rut development versus load repetitions for DGAC, 38 mm ARHM-GG and 62 mm ARHM-GG overlays under wide-base single tire. 58

Figure 19. Plot of average maximum rut development versus load repetitions for DGAC overlay at two different temperatures. 60

Figure 20. Percent change in layer thickness versus air-void content change from HVS trafficking in the wheelpath. 74

Figure 21. Percent change in layer thickness versus air-void content change from HVS trafficking in the wheelpath. 75

Figure F-1. Profilometer data from Section 505RF. 116

Figure F-2. Profilometer data from Section 506RF. 117

Figure F-3. Profilometer data from Section 507RF. 118

Figure F-4. Profilometer data from Section 508RF. 119

Figure F-5. Profilometer data from Section 509RF. 120

Figure F-6. Profilometer data from Section 510RF. 121

Figure F-7. Profilometer data from Section 511RF. 122

Figure F-8. Profilometer data from Section 512RF. 123

Figure F-9. Profilometer data from Section 513RF. 124

Figure G-1. Transverse profile of trenched AC slab from Section 504RF. 126

Figure G-2. Transverse profile of trenched AC slab from Section 505RF. 127

Figure G-3. Transverse profile of trenched AC slab from Section 506RF. 128

Figure G-4. Transverse profile of trenched AC slab from Section 507RF. 129

Figure G-5. Transverse profile of trenched AC slab from Section 508RF. 130

Figure G-6. Transverse profile of trenched AC slab from Section 509RF. 131

Figure G-7. Transverse profile of trenched AC slab from Section 510RF. 132

Figure G-8. Transverse profile of trenched AC slab from Section 511RF. 133

Figure G-9. Transverse profile of trenched AC slab from Section 512RF. 134

Figure G-10. Transverse profile of trenched AC slab from Section 513RF. 135

Figure H-1. Development of Rut and Hump Volume Under Trafficking from Transverse Surface Profiles, Section 505RF. 138

Figure H-2. Development of Rut and Hump Volume Under Trafficking from Transverse Surface Profiles, Section 506RF. 139

Figure H-3. Development of Rut and Hump Volume Under Trafficking from Transverse Surface Profiles, Section 507RF. 140

Figure H-4. Development of Rut and Hump Volume Under Trafficking from Transverse Surface Profiles, Section 508RF. 141

Figure H-5. Development of Rut and Hump Volume Under Trafficking from Transverse Surface Profiles, Section 509RF. 142

Figure H-6. Development of Rut and Hump Volume Under Trafficking from Transverse Surface Profiles, Section 510RF. 143

Figure H-7. Development of Rut and Hump Volume Under Trafficking from Transverse Surface Profiles, Section 511RF. 144

Figure H-8. Development of Rut and Hump Volume Under Trafficking from Transverse Surface Profiles, Section 512RF. 145

Figure H-9. Development of Rut and Hump Volume Under Trafficking from Transverse Surface Profiles, Section 513RF. 146

Figure I-1. Transverse Aggregate Base Surface Profile at Termination of Trafficking, Section 505RF. 148

Figure I-2. Transverse Aggregate Base Surface Profile at Termination of Trafficking, Section 506RF. 149

Figure I-3. Transverse Aggregate Base Surface Profile at Termination of Trafficking, Section 507RF. 150

Figure I-4. Transverse Aggregate Base Surface Profile at Termination of Trafficking, Section 508RF. 151

Figure I-5. Transverse Aggregate Base Surface Profile at Termination of Trafficking, Section 509RF. 152

Figure I-6. Transverse Aggregate Base Surface Profile at Termination of Trafficking, Section 510RF. 153

Figure I-7. Transverse Aggregate Base Surface Profile at Termination of Trafficking, Section 511RF. 154

Figure I-8. Transverse Aggregate Base Surface Profile at Termination of Trafficking, Section 512RF. 155

Figure I-9. Transverse Aggregate Base Surface Profile at Termination of Trafficking, Section 513RF. 156

1.0 BACKGROUND AND SCOPE

1.1 Background – Caltrans Flexible Overlay Strategies

Overlays are the primary rehabilitation strategy for flexible pavements that have cracking or ride quality problems. The traditional material used for overlays of flexible pavements is dense graded asphalt concrete (DGAC). Caltrans has also used asphalt-rubber hot mix gap-graded (ARHM-GG) for overlays for approximately the last 20 years (1).

Although Caltrans has many years of experience with ARHM-GG overlays, the strategy is not used routinely. It has been estimated that ARHM-GG is used on about 5 percent of the lane-km overlaid in the late 1990s (exact figures are not readily available from Caltrans). According to the 1995 Caltrans State of the Pavement Report (2), Caltrans overlaid about 990 lane-kilometers (615 lane-miles) per year between 1990/01 and 1994/95. Using the five percent estimate, only about 50 lane-kilometer (31 lane-miles) were ARHM-GG.

In 1993, the average cost of Type A DGAC was $31.5 per ton for quantities of 5,000 tons or more. In the same year, the average cost per ton of ARHM-GG was $56.5 per ton for quantities of 1,000 to 10,000 tons, and $40.8 for 10,000 or more tons. Thus, the cost per ton of ARHM-GG is between about 30 to 80 percent more than that of DGAC. (3)

The Caltrans design method for DGAC overlay thickness for structural overlays is based on surface deflections and component analysis, and empirical estimates of thickness to retard reflections cracking (California Test Method 356 [4]). The thickness design method for ARHM-GG overlays is based on the DGAC design thickness and other criteria, which are included in a thickness design guide document published by the Caltrans Engineering Service Center (1). The

structural and reflection cracking equivalencies of ARHM-GG compared to DGAC have evolved over the years, primarily based on observations of test section performance. The latest equivalencies are summarized in Appendix A (1).

Following Caltrans guidelines, the maximum ARHM-GG overlay thickness is 60 mm, and the minimum is 30 mm. ARHM-GG to DGAC equivalence ratios range between 1.5 and 2.0 for structural applications where fatigue cracking is the expected distress mode, and 1.5 to 2.33 where reflection cracking is the expected is distress mode. The structural and reflection cracking ratios are larger if a Stress Absorbing Membrane Interlayer (SAMI) is placed between the existing pavement and the ARHM-GG overlay.

Selection of optimum binder content in the mix design for DGAC is performed following California Test Method 367 (4). The criteria for DGAC binder content selection are minimum value for Hveem stabilometer (CTM 366 [4]), four percent air-void content under standard kneading compaction (CTM 304, 308 [4]), and a "flushing" criterion in which the technician determines whether the mix looks over-asphalted. The minimum Hveem stabilometer value for 19-mm maximum aggregate size DGAC Type A is 37.

Mix design for ARHM-GG is performed following guide documents published by the Caltrans Engineering Service Center. The current criteria are a minimum Hveem stabilometer value of 23, a minimum air-void content of four percent under standard kneading compaction, and a minimum 18 percent Voids in the Mineral Aggregate (VMA). The air-void content under laboratory compaction criterion is three percent when less than about 35,000 equivalent single axle loads (ESALs) are expected in the 10-year design life of the overlay, or when the maximum ambient air temperature is not expected to exceed 35°C. The air-void content criterion is five

percent in desert areas where more than about 3,500,000 ESALs are expected in the 10-year design life. (1)

In addition to these requirements, allowable binder contents for ARHM-GG are constrained to be within the range of 7.0 to 9.5 percent (by mass of aggregate). Dense graded asphalt rubber hot mix (ARHM-DG) must be within 6.5 and 8.5 percent (by mass of aggregate). (1)

These mix design requirements are based on experience gained through a trial and error process over the past 20 years. That process has included many successful applications of ARHM-GG overlays, and a few severe rutting failures on ARHM-GG overlay projects in desert areas with heavy traffic which lead to the current version of the mix design requirements. Caltrans has recently been working on performance based specifications for ARHM. In several cases, a performance based mix design procedure developed as part of the Strategic Highway Research Program (SHRP) at the University of California, Berkeley has indicated the need for lower binder contents for ARHM-GG than were recommended using the Caltrans criteria. These cases were primarily in hot desert locations and locations with heavy traffic. The UCB procedure includes the use of the Repeated Simple Shear Test at Constant Height (RSST-CH)

The relatively small proportion of ARHM-GG overlays compared to DGAC overlays is likely due to the following considerations:

- Relative life cycle cost of ARHM-GG versus DGAC, given that the cost per ton in place of ARHM-GG is greater than the cost of DGAC (although the cost data from 1993 indicate that the differential is more than offset by use of reduced thicknesses), and

- Uncertainty about ability of the Caltrans mix design criteria to prevent rutting failures, in part because ARHM-GG does not meet the criteria for Hveem stabilometer values used for DGAC, and despite the performance history which suggests that ARHM-GG typically has adequate rutting performance as used by Caltrans.

It has been suggested that greater use of ARHM-GG as an overlay strategy by Caltrans is warranted provided that the material can be routinely designed and constructed to provide performance that results in a lower life cycle cost than the DGAC overlay strategy. However, if life cycle costs for ARHM-GG are greater than those for DGAC, then the use of ARHM-GG is not warranted. ARHM is assumed to be as recyclable as DGAC.

The objective of CAL/APT Goal 3 is to evaluate the long-term and short-term performance of the two overlay strategies. Long-term performance is defined as failure from fatigue cracking, reflection cracking or rutting of the unbound pavement layers. Short-term performance is defined as failure by rutting of the asphalt bound materials, including the overlay, underlying asphalt concrete or asphalt treated permeable base (ATPB). Life cycle cost is dependent upon both long-term and short-term performance.

Rutting of the asphalt-bound layers, in particular the newly laid overlay, can occur within a few years after rehabilitation. Typically, a rutting failure will occur within five years after construction, before aging of the asphalt and strain-hardening and densification from trafficking significantly increase the resistance of the mix to permanent shear deformation.

1.2 Scope of this Report

This report presents results from accelerated pavement tests using the Caltrans Heavy Vehicle Simulator (HVS) of DGAC and ARHM-GG overlays placed at the University of California, Berkeley Pavement Research Center. The results in this report are from tests conducted at elevated temperatures to evaluate the rutting performance of the two overlay strategies. The tests also investigated the effects of tire type, temperature and thickness of the ARHM-GG overlay.

The overlays were placed on existing flexible pavement structures, sections of which were previously tested as part of CAL/APT Goal 1 (5-9). The mix designs and thickness designs for the overlays and their construction are included in References (10, 11).

2.0 LABORATORY AND HVS EXPERIMENT DESIGNS

The laboratory test and Heavy Vehicle Simulator (HVS) test experiments for this project were designed to meet the following objectives:

1. Validate existing Caltrans mix design methods for DGAC and ARHM-GG with respect to rutting of the mix (stability);
2. Validate mechanistic-empirical procedures for predicting rutting behavior, developed by the University of California, Berkeley as part of the Strategic Highway Research Program;
3. Evaluate the shear frequency sweep (FS-S) and repeated simple shear test at constant height (RSST-CH) tests as simple performance tests for rutting;
4. Evaluate the effects of laboratory specimen compaction methods on RSST-CH test results;
5. Provide input and validation data for mechanistic modeling of rutting in combination with the VRSPTA test results previously produced by CAL/APT (3-D Load Cell) data (12);
6. Compare rutting caused by radial tires on dual wheels, bias-ply tires on dual wheels, wide base single tires (super single), and high-pressure aircraft type tires;
7. Compare the rutting behavior of typical Caltrans DGAC and ARHM-GG overlay materials; and
8. Quantify the effects of construction variation on rutting performance.

Results relating to Objectives 1, 5, 6 and 7 are included in this report. Additional information relating to completion of the remaining objectives will be included in other reports on the Goal 3 rutting experiments.

2.1 HVS Test Experiment Design

The experiment design for the HVS tests on the Goal 3 overlays included the following variables:

- Overlay type: asphalt-rubber hot mix gap-graded (ARHM-GG) and dense graded asphalt concrete (DGAC).
- Overlay thickness: design thicknesses for the ARHM-GG overlays were 38 and 62 mm; design thicknesses for the DGAC overlays were 62 and 75 mm. The DGAC overlay thicknesses were assumed to be equal for the experiment design.
- Tire/wheel type: the four combinations were bias-ply tires on dual wheels, radial tires on dual wheels, a wide base single tire/wheel, and an aircraft tire/wheel.
- Pavement temperature: one test was performed with a target temperature of 40°C at a depth of 50 mm. All other tests were performed with a target temperature of 50°C at a depth of 50 mm.

The matrix of primary experiment variables and associated test numbers, and the additional tests are shown in Table 1.

Table 1 Matrix of HVS test experiment variables and test numbers.

	ARHM-GG Overlay		**DGAC Overlay ****	
	50°C at 50 mm depth		50°C at 50 mm depth	40°C at 50 mm depth
Dual Radial	38 mm* thick	62 mm* thick		
Dual Bias-ply	510RF	509RF	506RF	
Wide-base Single			505RF	
Aircraft	511RF	508RF	507RF	512RF
			513RF	

* design thickness
**design thicknesses of 62 and 75 mm; actual thicknesses varied

One test not shown in Table 1, 504RF, was performed on the surface of the Goal 1 pavement prior to placement of the Goal 3 overlays. Test 504RF was performed using the wide-base single wheel and a target temperature of 45°C at 50 mm depth.

2.1.1 Layout of Test Sections

The Goal 3 Rutting test sections were located on the RFS pavement structures as shown in Figure 1. The overlay sections included in the HVS rutting tests were in locations where the underlying pavement structure from Goal 1 had not been trafficked. The top and bottom lifts of the underlying Goal 1 structure were therefore uncracked. The layout of the rutting test sections was also situated so that it avoided the transition zones between different pavement structures and areas where cores had been taken from the underlying Goal 1 structure. It should be noted that a portion of Section 513RF was placed over an area where some cores had been taken; that portion of the rut test section was affected.

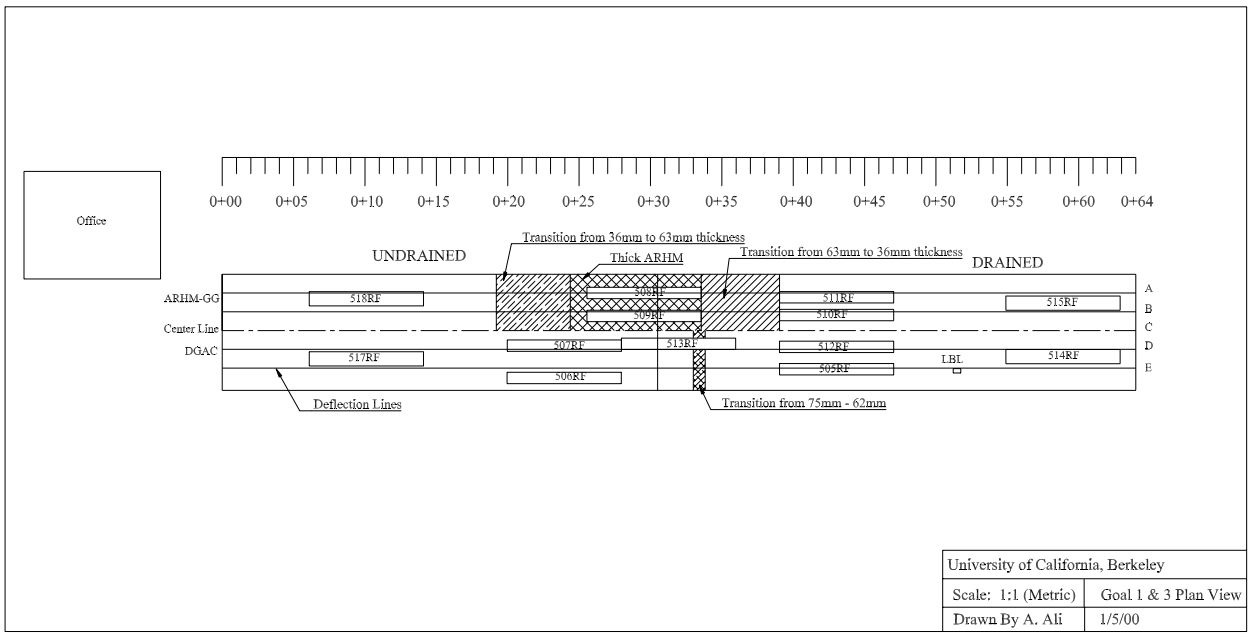

Figure 1. Layout of Goal 3 HVS tests sections.

2.1.2 Pavement Structures

The Goal 3 overlays were constructed upon the Goal 1 pavement structures. The Goal 1 structures included two types: "drained" containing an Asphalt Treated Permeable Base (ATPB) layer, and "undrained" containing no ATPB layer. The underlying Goal 1 structure type was ignored in the selection of the HVS rutting test sections, as can be seen in Figure 1. It was assumed that at the elevated temperatures used for the HVS rutting tests, all of the rutting would occur in the asphalt concrete and none would occur in the underlying layers.

The drained pavement structure is shown in Figure 2, and the undrained structure in Figure 3.

The design of the Goal 1 drained and undrained pavement structures is presented in detail in Reference (5). The design of the Goal 3 ARHM-GG and DGAC overlays are presented in detail in References (10,11).

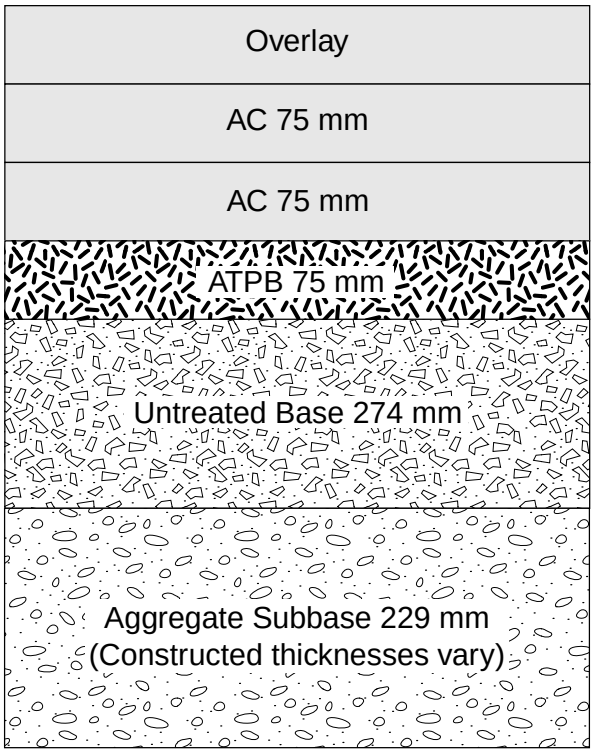

Figure 2. Drained pavement structure.

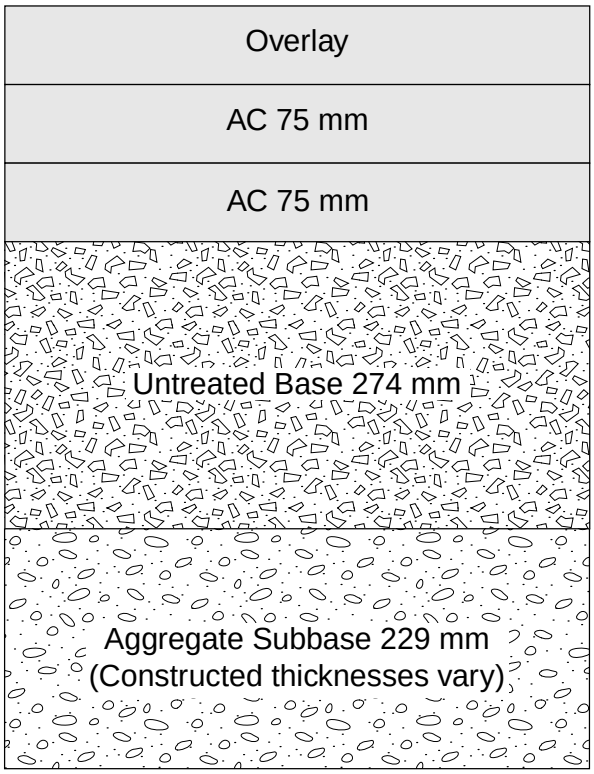

Figure 3. Undrained pavement structure.

2.1.2.1 Thicknesses Prior to HVS Trafficking

Thicknesses of the asphalt concrete layers prior to HVS trafficking were determined from cores outside the trafficked areas and from slabs of untrafficked asphalt concrete removed from trenches. The asphalt concrete layer thicknesses before HVS trafficking were measured on the cores and slab locations adjacent to the test sections, yet outside the rut and upheaval caused by the trafficking. Thickness measurements are summarized in Table 2, and indicate that similar thicknesses were measured using the slabs and cores. The thicknesses of the asphalt concrete layers of Section 504RF are assumed to be similar to those of Section 508RF due to their close longitudinal proximity and same transverse location. Complete data is included in Appendix B.

Thickness measurements are summarized by overlay type in Table 3. In the experiment design, the assumption that the DGAC overlay has essentially same thickness across the five sections with that overlay type is not strictly valid, as the data presented in Table 3 show. The thicknesses of the ARHM-GG overlays are more uniform across the two sections with each design thickness. The thicknesses of the top and bottom lifts of the Goal 1 asphalt concrete are consistent across the test sections.

It can be assumed that the thicknesses of the Goal 1 top and bottom lifts are similar to the average values shown in Table 3. Cores and slabs could not be taken on Section 504RF because of time constraints before the Goal 3 overlays were placed, and the need to reuse that section for a later HVS test.

Thicknesses of the layers beneath the asphalt concrete layers were determined from elevations at the surface of each layer measured during construction of the Goal 1 structures. The thicknesses for each rutting test section were interpolated from the various survey locations.

Table 2 Asphalt concrete layer thicknesses (mm) adjacent to rutting test sections measured from cores and slabs.

Section	Cores		Slabs	
	Average	Standard Deviation	Average	Standard Deviation
504RF – Top Lift	76	1	78	1
Bottom Lift	82	2	81	1
505RF - DGAC Overlay	61	3	54	3
Top Lift	75	0	72	2
Bottom Lift	75	0	77	3
506RF – DGAC Overlay	78	3	78	2
Top Lift	79	3	80	3
Bottom Lift	78	4	81	4
507RF – DGAC Overlay	78	1	76	1
Top Lift	76	2	76	1
Bottom Lift	76	1	74	1
512RF – DGAC Overlay	52	1	49	2
Top Lift	69	3	65	4
Bottom Lift	72	0	77	5
513RF – DGAC Overlay	77	1	80	2
Top Lift	67	3	72	1
Bottom Lift	78	3	78	2
508RF – ARHM 62 mm Overlay	66	2	73	5
Top Lift	75	2	76	1
Bottom Lift	82	5	75	2
509RF – ARHM 62 mm Overlay	70	1	75	0
Top Lift	70	4	74	1
Bottom Lift	70	3	72	1
510RF – ARHM 38 mm Overlay	34	6	35	1
Top Lift	61	3	66	1
Bottom Lift	74	5	77	0
511RF – ARHM 38 mm Overlay	38	2	35	-
Top Lift	69	3	66	-
Bottom Lift	83	3	77	-

Table 3 Summary of thicknesses (mm) by layer and overlay type.

	Cores				Slabs			
	Average	**Std. Dev.**	**Max**	**Min**	**Average**	**Std. Dev.**	**Max**	**Min**
DGAC	72	10	82	51	68	14	81	47
ARHM, 62 mm	67	3	71	64	74	4	78	70
ARHM, 38 mm	36	5	40	26	35	1	36	34
Top Lift	72	6	84	58	73	6	84	61
Bottom Lift	77	5	88	67	78	4	86	71

The estimated thicknesses are shown in Table 4. Thicknesses of the ATPB layer were measured from cores.

Table 4 Approximate thicknesses of underlying layers.

	504RF	505RF	506RF	507RF	512RF	513RF	508RF	509RF	510RF	511RF
ATPB		73			70				75	81
AB	274	183	274	274	183	274	274	274	183	183
ASB	306	185	177	233	230	243	306	289	253	276

Note: ATPB – asphalt treated permeable base, AB – aggregate base, ASB – aggregate subbase.
Note: AB and ATPB thicknesses for sections 508RF, 509RF, and 513RF transition to those of the drained structure over a portion of each test section).

2.1.2.2 Air-Void Contents Prior to Trafficking

Compaction of the Goal 1 asphalt concrete layers and the Goal 3 overlays was performed following the Caltrans method specification. Compaction was performed following the complete method specification for the Goal 1 layers. Very good compaction was achieved in those layers due to the excellent temperature control the contractor was able to exercise. A short haul distance from the plant, the relatively short project length, and the building in which the sections were constructed aided the temperature control.

For the Goal 3 overlays, target air-void contents of 8 to 10 percent for the DGAC and 7 to 11 percent for the ARHM-GG were specified to better replicate typical Caltrans results. Compaction was to be stopped by UCB if air-void contents went below the target range. The DGAC overlay air-void contents went below the target range when the method compaction specification was only partially completed, and compaction was stopped. The method compaction specification was completed on the ARHM-GG overlay. The ARHM-GG mix cooled faster than the DGAC mix, particularly in the areas where the design thickness was 38 mm. Compaction of the overlay mixes was somewhat different between HVS tests sections, as is shown in Table 5.

The average air-void content of 7.2 percent across the DGAC overlays was somewhat below typical air-void contents of about 8 percent achieved on Caltrans QC/QA projects in the field (Table 6). The DGAC overlay average air-void contents ranged between 4.7 percent on Section 506RF and 10.2 percent on Section 512RF. As is discussed in Reference (11), the dense graded overlay material arrived at the site hotter and retained heat longer during compaction than did the gap-graded ARHM material. The thicker ARHM-GG lift at Sections 508RF and 509RF retained heat longer than did the thinner ARHM-GG layer in Sections 510RF and 511RF; the air-void contents of the two overlay thicknesses show that the different cooling rates had a tremendous effect (Table 6). The thick ARHM-GG overlay sections are located between the thin ARHM-GG overlays, and were therefore placed at exactly the same time and subjected to the same roller passes.

Table 5 Air-void contents prior to HVS trafficking, from cores.

Section	Air-Void Content (percent)	
	Average	**Standard Deviation**
504RF – Top Lift	5.2	0.3
Bottom Lift	4.6	1.8
505RF – DGAC Overlay	5.8	0.4
Top Lift	7.3	1.7
Bottom Lift	4.7	1.2
506RF – DGAC Overlay	4.7	0.9
Top Lift	6.4	0.7
Bottom Lift	6.5	0.6
507RF – DGAC Overlay	7.9	0.6
Top Lift	5.9	0.3
Bottom Lift	5.9	1.3
512RF – DGAC Overlay	10.3	2.1
Top Lift	8.5	1.1
Bottom Lift	4.8	0.1
513RF – DGAC Overlay	7.1	1.0
Top Lift	8.0	1.1
Bottom Lift	6.5	0.5
508RF – ARHM 62 mm Overlay	12.5	2.2
Top Lift	6.4	0.7
Bottom Lift	3.5	0.9
509RF – ARHM 62 mm Overlay	10.0	0.7
Top Lift	8.7	2.4
Bottom Lift	4.9	1.7
510RF – ARHM 38 mm Overlay	15.2	3.6
Top Lift	4.7	0.4
Bottom Lift	6.5	1.7
511RF – ARHM 38 mm Overlay	17.9	0.5
Top Lift	6.4	0.8
Bottom Lift	3.3	1.5

Table 6 Summary of average air-void contents prior to trafficking (percent) by layer and overlay type.

Material	Average Air-Void Content
DGAC overlay	7.2
ARHM 62 mm	11.2
ARHM 38 mm	16.6
Top Lift	6.0
Bottom Lift	4.2

The average air-void content for the top and bottom lifts of Goal 1 asphalt concrete were also considerably smaller than those typically obtained on Caltrans projects in the field. The top lift average air-void content ranged between 4.6 percent on Section 507RF and 8.7 percent on Section 509RF. The average air-void content for the bottom lift ranged between 2.9 percent on Section 505RF and 6.5 percent on Section 510RF. The average air-void content of the ATPB measured from cores from Section 510RF was 30.8 percent.

Complete air-void content data from the cores is included in Appendix C.

2.1.2.3 Deflections Prior to Rutting Study

Surface deflection measurements were made with a Dynatest Model 3031 Heavyweight Deflectometer (HWD) immediately before (1 March 1997) and after construction of the overlays (1 April 1997), prior to the beginning of the HVS rutting tests. Layer moduli were back-calculated using ELMOD Version 3.0 and 4.0 (12). Deflection measurement locations are shown relative to the HVS rutting test sections in Figure 4. Deflections and moduli for the HVS rutting test sections, included in Tables 7 and 8, were assumed to be those of the nearest deflection line. Pavement temperatures at the time of both sets of deflection measurements were approximately 20°C.

The Sensor 7 deflection measurements, which are taken farthest from the load, indicate that subgrade conditions in the rutting test sections were fairly uniform before and after overlay construction, as shown in Tables 7 and 8. The Sensor 1 deflections, taken at the load, indicate that the total pavement structures were fairly similar prior to construction, except at one end of

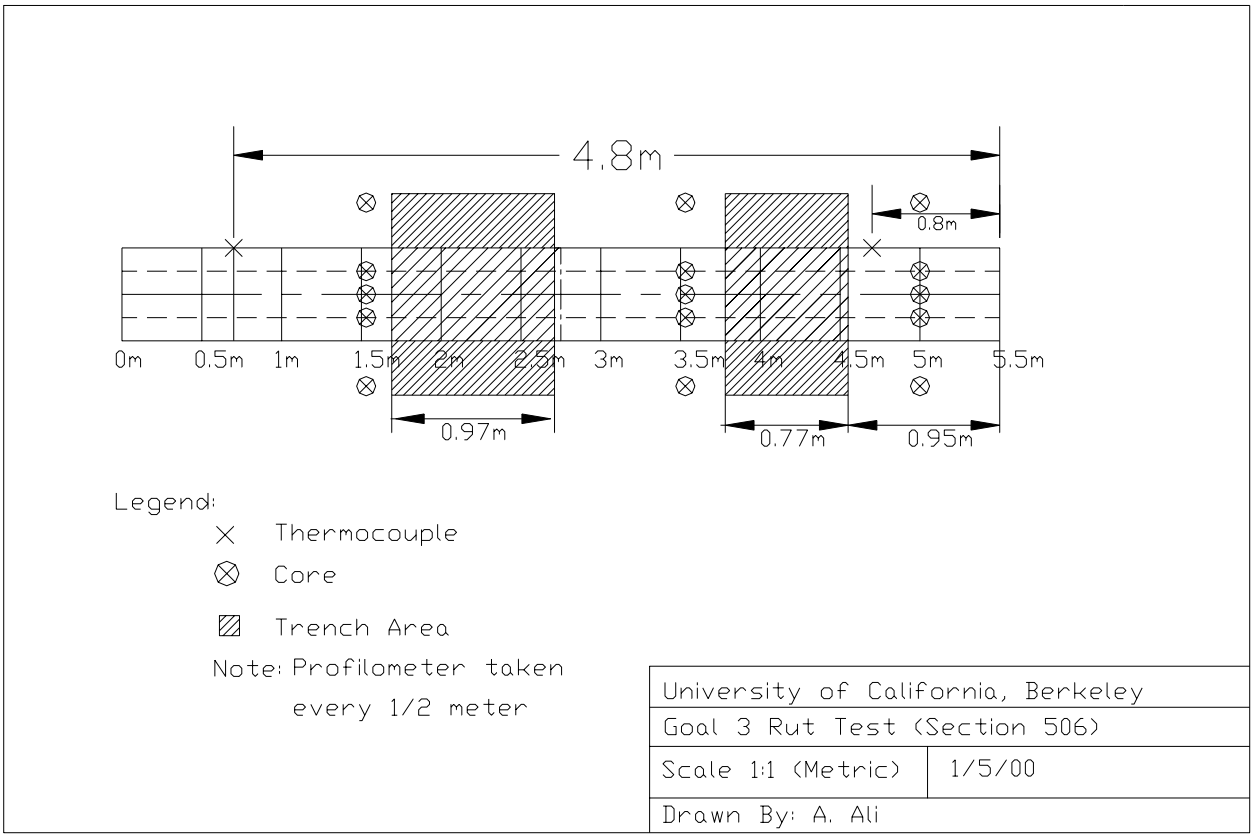

Figure 4. Locations of deflection measurements and HVS rutting test sections.

Section 513, which had been subjected to coring (Table 7, Figure 5). The Sensor 1 deflections after overlay construction were less than those measured before construction, and the Sensor 7 deflections were the same before and after construction, as expected.

All pavement structures were modeled as three layer systems for back-calculation of elastic moduli. All asphalt concrete layers were considered as Layer 1 including the overlay, Goal 1 asphalt concrete, and where applicable, the asphalt treated permeable base. The granular layers, consisting of aggregate base and aggregate subbase were considered as Layer 2, and the Subgrade as Layer 3.

Table 7 Summary data of measured deflections (microns) and back-calculated moduli (MPa) before overlay construction, 1 March, 1997

Section	D1 Avg.	D1 Std. Dev.	D7 Avg.	D7 Std. Dev.	E1 Avg.	E1 Std. Dev.	E2 Avg.	E2 Std. Dev.	E3 Avg.	E3 Std. Dev.
504 RF	82	5.51	21	0.58	5859.5	654.2	587.9	70.7	102.2	6.3
505 RF	82	3.61	18	1.53	3147.6	367.6	501.8	63.4	105.5	13.8
506 RF	91	5.75	23	0.58	3737.2	711.4	529.5	4.9	92.5	17.2
507 RF	91	5.48	20	0.58	4320.5	176.6	450	66.4	116.6	13.6
508 RF	88	4.58	21	0.58	6614.4	189.3	499.6	37.9	79.9	1.2
509 RF	87	5.03	18	1.53	5879.5	296.6	471.1	44.7	139.1	24.6
510 RF	70	5.69	18	1.15	6182.2	618.5	376.3	65.9	88.6	1.3
511 RF	69	4.27	18	0.76	6371.2	379	397	49.4	84.4	49.4
512 RF	76	4.48	18	1.26	4664.9	477.6	439.1	55.5	97	7.5
513 RF	111	22.95	20	0.76	3918.7	477.7	365.8	41.9	100	12.3

Table 8 Summary data of measured deflections (microns) and back-calculated moduli (MPa)after overlay construction, 1 April, 1997

Section	D1 Avg.	D1 Std. Dev.	D7 Avg.	D7 Std. Dev.	E1 Avg.	E1 Std. Dev.	E2 Avg.	E2 Std. Dev.	E3 Avg.	E3 Std. Dev.
504 RF	74.7	2.5	20.3	0.6	7553.9	443.2	677.0	26.5	105.7	4.2
507 RF	77.7	3.8	20.0	0.0	7082.8	701.7	505.2	88.3	208.9	13.4
508 RF	79.3	6.4	20.3	0.6	8776.0	1844.2	538.6	64.9	94.7	17.0
509 RF	78.7	3.1	20.0	0.0	7237.5	485.7	476.5	54.4	208.9	13.3
510 RF	67.0	4.4	18.7	1.2	6337.7	655.9	343.7	66.1	174.9	22.8
511 RF	65.3	3.6	18.3	1.4	6919.9	93.0	381.4	75.2	129.4	15.0
512 RF	67.0	4.4	18.7	1.2	6337.7	655.9	343.7	66.1	174.9	22.8
513 RF	78.3	3.5	19.7	0.6	7334.8	649.9	473.2	51.4	190.8	25.3

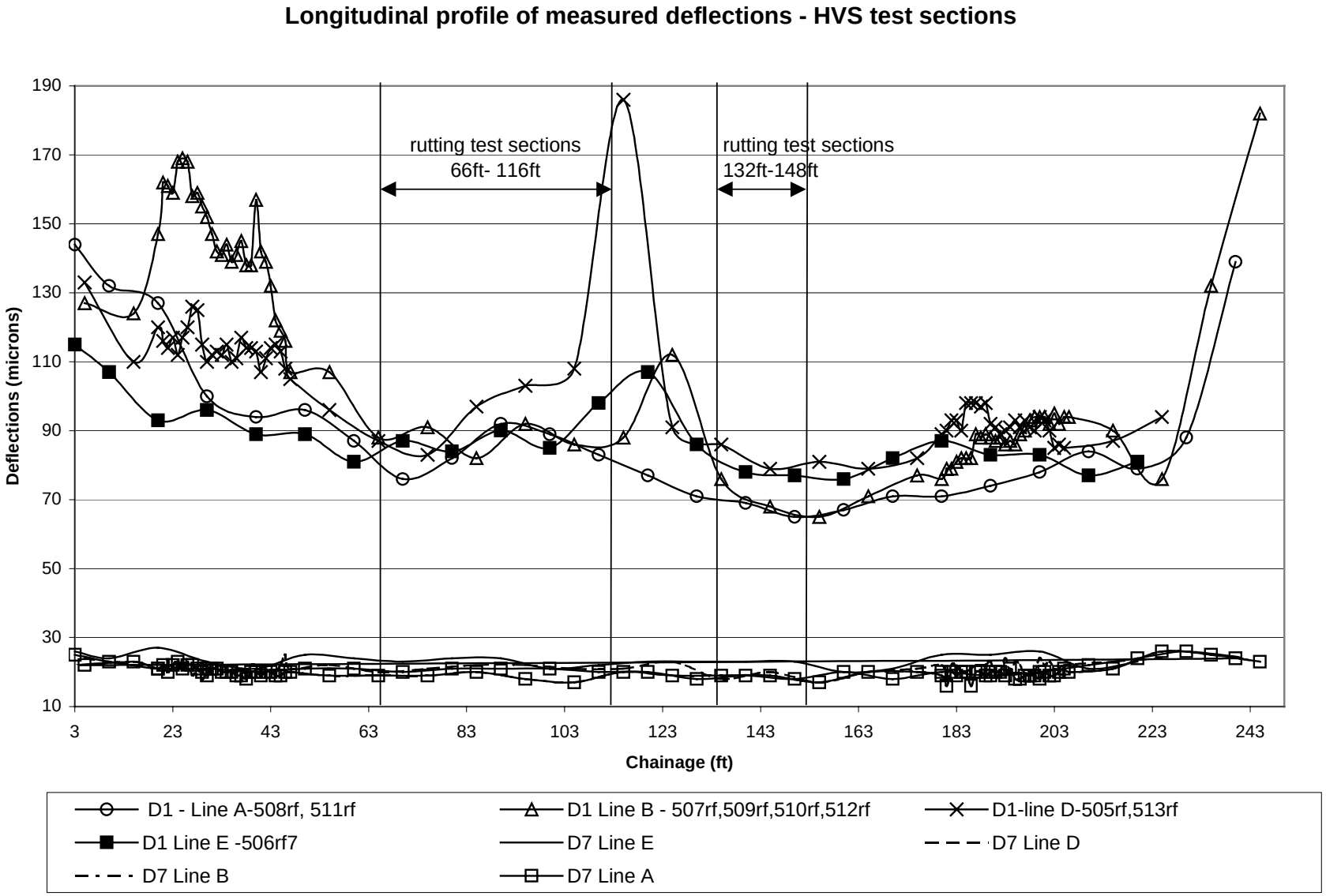

Figure 5. Sensor 1 and Sensor 7 deflections along deflection lines, prior to overlay construction.

The back-calculated subgrade moduli nearest each of the test sections prior to overlay (Figure 6) are fairly consistent across all of the test sections. The granular layers have more variability (Figure 6). This variability is typical of back-calculated moduli from field sites, and includes variability in materials properties, construction quality, and differences between assumed and actual layer thickness, as well as deflection measurement variability.

The back-calculated moduli of the granular layers did not appear to change much before and after construction, and across the test sections averaged between 344 and 677 MPa (Figure 6). The back-calculated moduli of the subgrade were also fairly similar before and after construction of the overlays, and averaged between 80 and 209 MPa.

The back-calculated moduli and deflection data indicate that the structures beneath the asphalt concrete in the HVS test sections can be assumed to be fairly uniform. Details of the deflection data are included in Appendix D.

2.1.3 Materials

The pavement materials in the rutting test sections are described in detail in previous reports. The materials and construction of the pavement structure beneath the overlays is described in Reference (5). The overlay materials and construction are described in Reference (11). The materials properties important to understanding the rutting performance of the rutting test sections are summarized in this report.

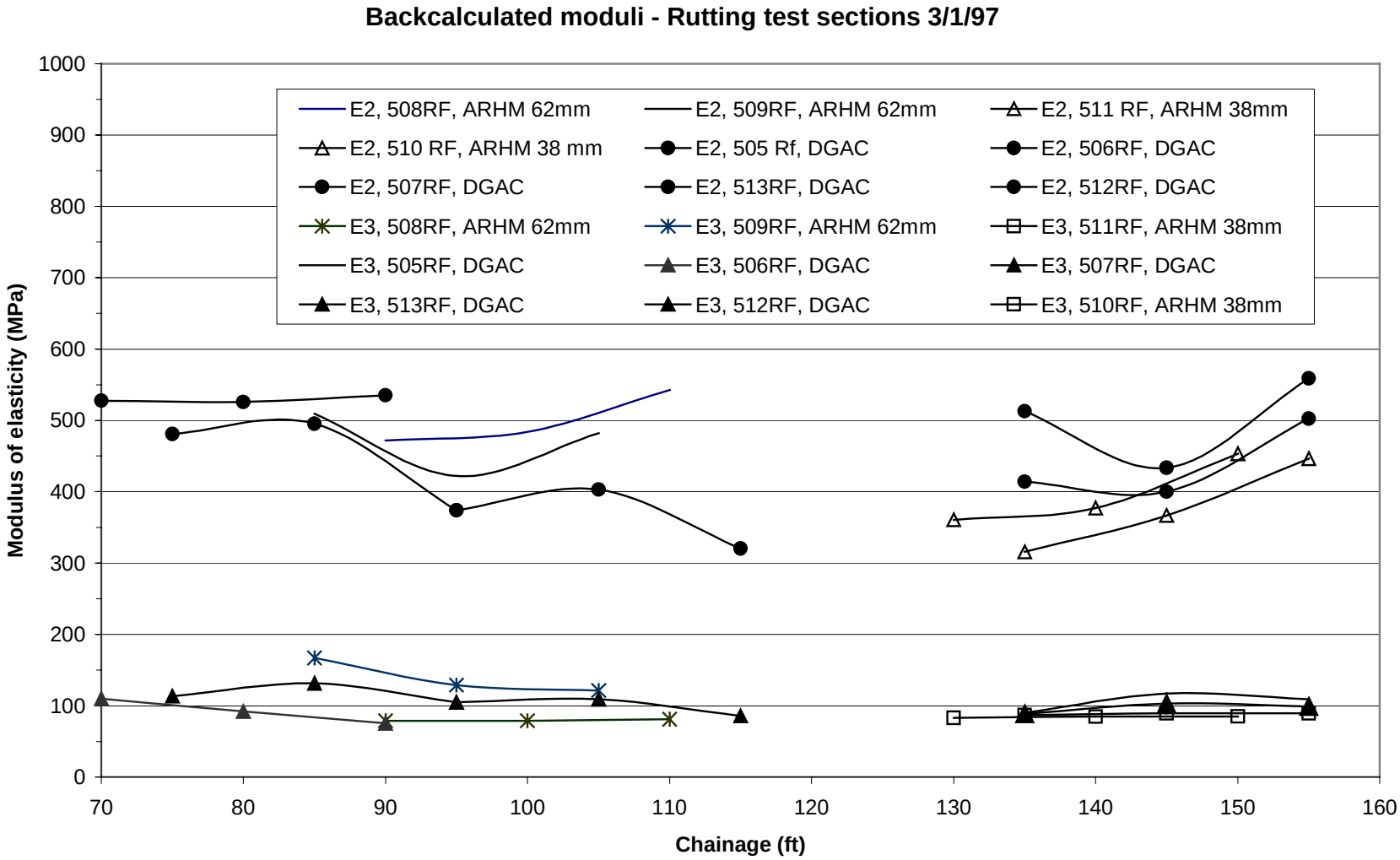

Figure 6. Back-calculated moduli for granular layers and subgrade before overlay.

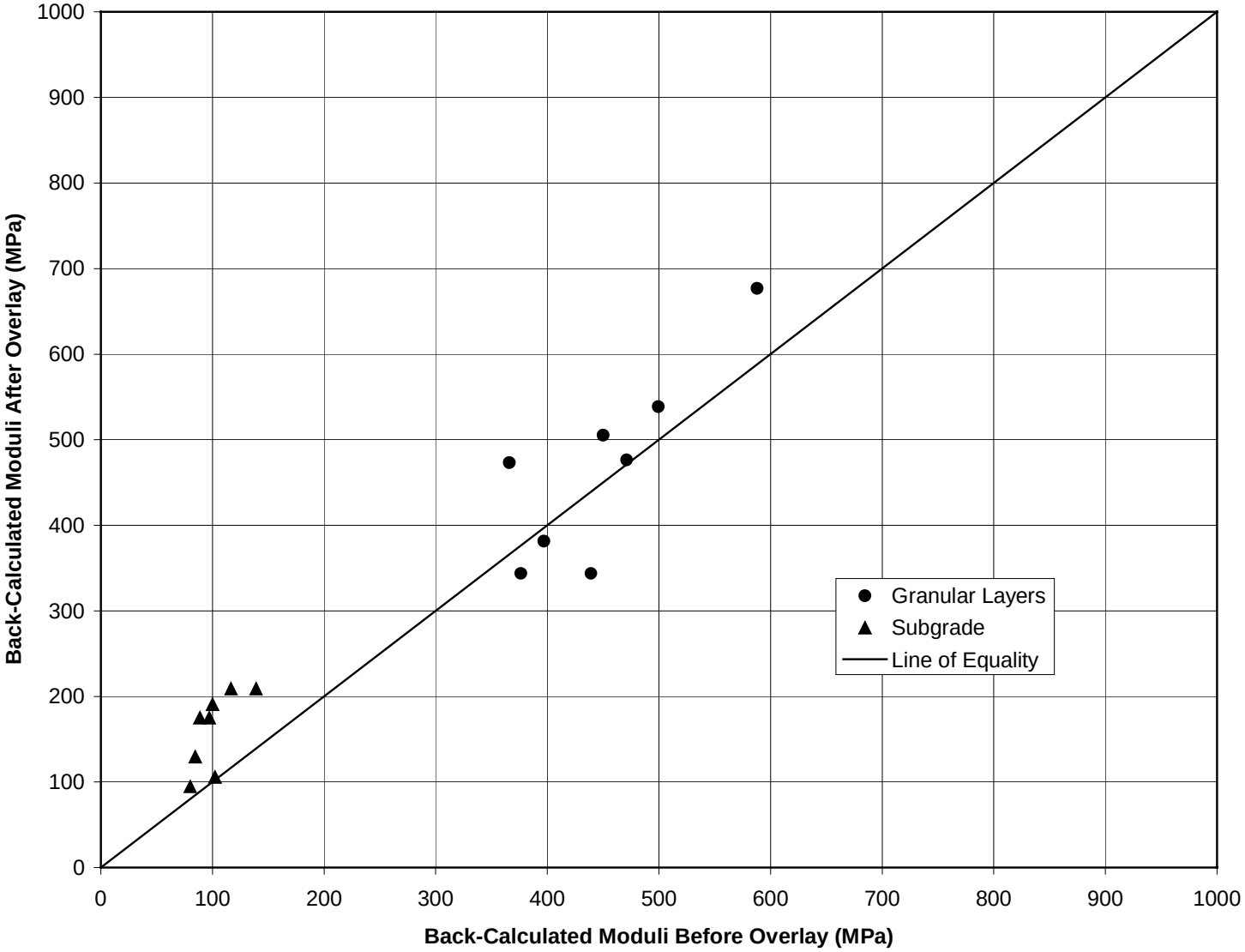

Figure 7. Average back-calculated moduli for granular layers and subgrade before and after overlay construction.

2.1.3.1 Overlay Mixes

The ARHM-GG and DGAC materials were specified as follows in the bid documents for the Goal 3 overlays:

> *DGAC shall meet Caltrans Standard Specifications for 19 mm (3/4 in.) Type A, coarse gradation asphalt concrete.*
>
> *ARHM-GG shall meet Caltrans Standard Special Provisions for 12.5 mm (1/2 in.) Type 2, gap-graded asphalt rubber hot mix. The mix design shall be based on a 4 percent air-void content.*

The mix design aggregate gradations, contract compliance ranges determined following Caltrans standard specifications, and results of extractions from belt samples taken at the plant are shown in Tables 9 and 10. Both mix design gradations were within Caltrans specifications for target limits.

The binder for the DGAC mix was an AR-4000 meeting Caltrans specifications, manufactured by Huntway in Benicia. The PG classification for the DGAC binder is PG 64-16. The binder formulation for the ARHM-GG mix included 76.5 percent (by mass) Shell AR-4000,

Table 9 Summary of extracted gradation and binder content for DGAC overlay mix.

Percent Passing Sieve Size (mm)	Mix Design	Permissible Operating Range **	Extracted (average)	Extracted (Std. Dev.)
19	100	90-100	99.8	0.6
12.5	93		95.2	1.9
9.5	73	60-75	76.4	2.6
4.75	50	45-55	52.3	2.0
2.36	39	34-44	36.6	1.5
1.18	27		27.4	1.1
0.60	18	13-23	22.3	1.0
0.30	11		17.2	0.7
0.15	6		9.3	0.5
0.075	5	3-7	6.8	0.3
Binder Content* (%)	5.0-5.3		5.1	0.1

* Percent by mass of aggregate
** Per Section 39 Caltrans Standard Specifications (5, 13).

Table 10 Summary of extracted gradation, binder content and rubber content for ARHM-GG mix.

Percent Passing Sieve Size (mm)	Mix Design	Permissible Operating Range ***	Extracted (average)	Extracted (Std. Dev.)
19	100	100	100.0	
12.5	98	90-100	97.3	1.2
9.5	85	81-91	84.4	2.6
4.75	33	28-38	34.0	2.5
2.36	21	18-26	22.7	1.8
1.18	15		16.7	1.4
0.60	10	7-15	12.7	1.2
0.30	6		9.2	0.9
0.15	4		6.1	0.8
0.075	3	3-7	4.6	0.6
Binder Content* (%)	7.6-7.9		6.9	0.5
Rubber Content** (%)	21		15.9	3.3

* Percent by mass of aggregate
** Percent by mass of binder
*** Per applicable Caltrans Special Provisions (11)

2.5 percent Witco cutter oil, 15.75 percent 10 mesh crumb rubber, and 5.25 percent high natural rubber. Both of the rubber components were manufactured by BAS. The binder was formulated to meet the appropriate Caltrans special provisions at the time the mix design was performed. The PG classification for the ARHM-GG binder is PG 82-28. (11)

The binder contents were selected following Caltrans standard procedures. The binder content for the DGAC mix was selected based on the Caltrans "flushing" criterion. At the design binder content of 5.3 percent (by mass of aggregate), the Hveem stabilometer value was 42; the air-void content under standard kneading compaction was 5.5 percent. The Caltrans minimum permissible Hveem stabilometer value is 37 for this mix. By Caltrans criteria, the DGAC overlay mix should have a low probability of rutting in the field.

The binder content for the ARHM-GG mix was selected based on the Caltrans criterion for air-void content under standard kneading compaction. At the design binder content of 7.9 percent (by mass of aggregate), the Hveem stabilometer value was 23; the air-void content under standard kneading compaction was 4.0 percent. (11)

The extracted aggregate gradations indicate that the constructed gradations were within nearly all of the Caltrans specification operating ranges (Tables 9 and 10). The DGAC mix was somewhat coarser than the target gradations for the coarse sizes, and finer than the targets for the fine sizes (Table 9). The ARHM-GG gradation nearly matched the target value for all sizes (Table 10).

The extracted binder contents from the DGAC mix were within the mix design range. The extracted binder contents from the ARHM-GG mix had much greater variability, and were below the mix design range. Assuming that there were no difficulties with the extraction process for asphalt-rubber binders, the average binder content was found to be 0.7 to 1.0 percent less than the target range (by mass of aggregate).

It has been found that maximum density for an aggregate gradation can typically be obtained when the gradation follows a line between the maximum aggregate size and the origin on a plot of percent aggregate passing each sieve size by mass, and the sieve sizes raised to the 0.45 power.

Following the definition used by the Superpave specifications (14), the DGAC and ARHM-GG overlay materials have a nominal maximum aggregate size of 19 mm and a maximum aggregate size of 25 mm. When plotted on the 0.45 power curve, the DGAC overlay gradation can be seen to follow the maximum density line except for the 19 mm sieve (Figure 8).

In particular, the DGAC overlay gradation follows the maximum density line between the 4.75 and 0.3 mm sieves and therefore passes through the "restricted zone" of the Superpave specifications.

The gap graded ARHM-GG overlay material passes well above the maximum density line for sieve sizes above 10 mm and below the line for the smaller sieves.

2.1.3.2 Goal 1 Asphalt Concrete Mix

The Goal 1 asphalt concrete mix designs and the results of previous laboratory tests on field cores and laboratory compacted specimens are summarized in Reference (5). The same asphalt concrete mix was used for the top and bottom lifts of the Goal 1 structures. It met all Caltrans standard specifications for Type A, 19-mm maximum size, coarse gradation mix. The aggregate sources and asphalt source were not the same as those used for the DGAC overlay mix, and the two mixes were produced by different plants.

The asphalt binder met Caltrans requirements for AR-4000 and was produced by the Shell refinery at Benicia. The binder content selected following Caltrans test methods was 4.9 percent by mass of aggregate, and the mix design recommended range was 4.6 to 4.9 percent. The binder content was selected based on the Caltrans "flushing" criterion. The Hveem stabilometer value at 4.9 percent asphalt content was 47, and the air-void content under standard kneading compaction was 4.4 percent. Mix design target gradations, the Caltrans operating ranges, and gradation analyses from extraction and plant belt samples are shown in Table 11.

It can be seen that the aggregate gradations obtained from the mix were all within the permissible operating ranges. The asphalt contents found from extractions on the top lift of

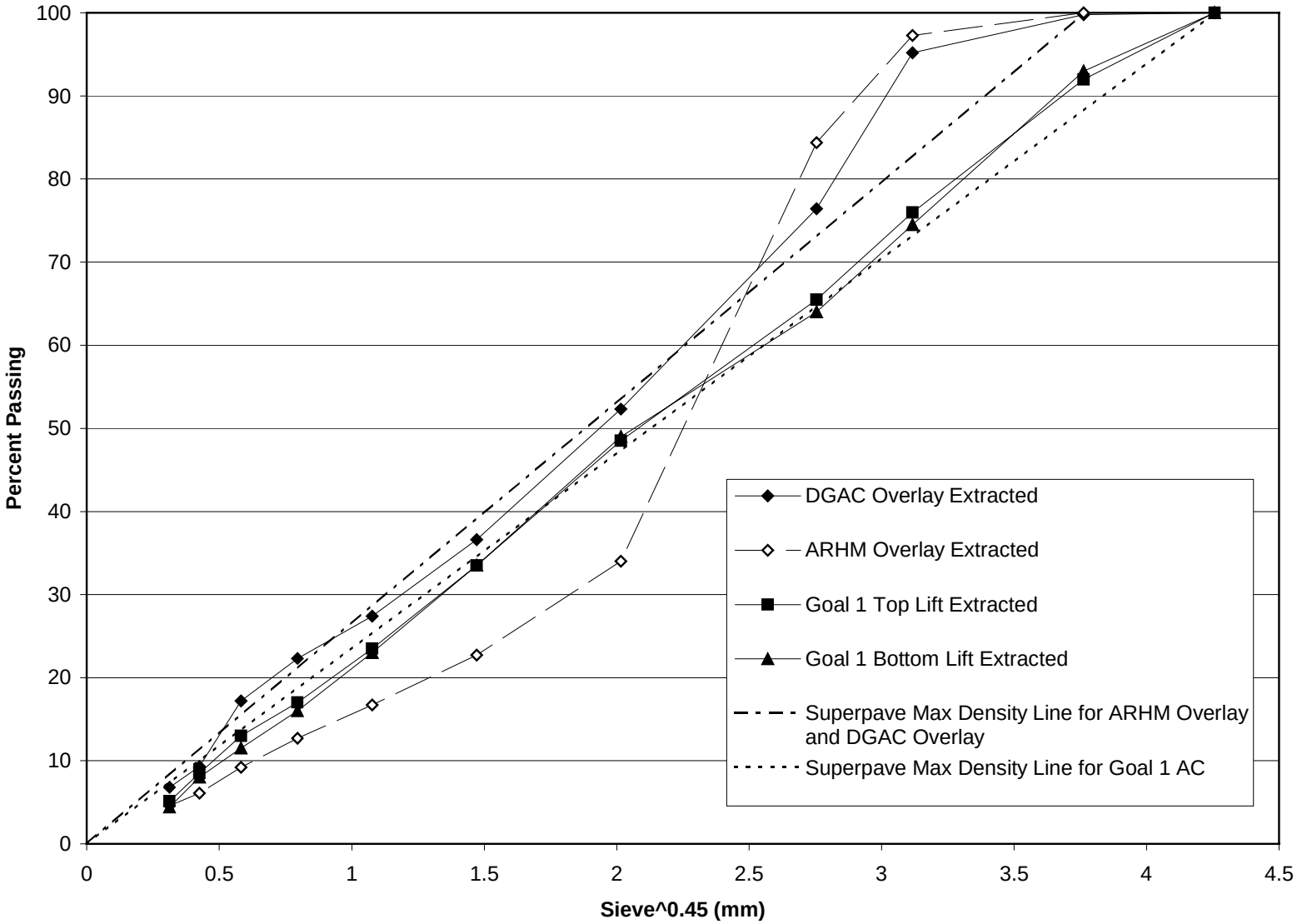

Figure 8. Extracted aggregate gradations for DGAC and ARHM-GG overlay mixes (sieve sizes to 0.45 power), and Superpave maximum density lines.

Table 11. Summary of extracted gradation and binder content for Goal 1 asphalt concrete mix.

Percent Passing Sieve Size (mm)	Mix Design	Permissible Operating Range ***	Top Lift Extracted (average)	Top Lift Extracted (Std. Dev.)	Bottom Lift Extracted* (average)	Top Lift Extracted (Std. Dev.)
25	100	100	100.0	0.0	100.0	0.0
19	99	90-100	92.0	7.1	93.0	1.4
12.5	80		76.0	8.5	74.5	0.7
9.5	67	60-75	65.5	4.9	64.0	2.8
4.75	49	45-55	48.5	4.9	49.0	2.8
2.36	33	29-39	33.5	3.5	33.5	2.1
1.18	22		23.5	2.1	23.0	1.4
0.60	14	10-20	17	1.4	16.0	1.4
0.30	9		13	1.4	11.5	0.7
0.15	6		8.5	0.7	8.0	0.0
0.075	3	3-7	5.1	0.1	4.4	0.6
Binder Content** (%)	4.6-4.9		5.25		4.8	

* Aggregate gradations include plant belt samples and extracted values
** Percent by mass of aggregate
*** Per Section 39 Caltrans Standard Specifications (5, 13)

asphalt concrete are somewhat higher than the recommended range from the mix design. Despite the high asphalt contents, stabilometer tests on material collected from the top lift during construction were found to have typical values between 46 and 48. The asphalt contents from extractions on the bottom lift are within the recommended range. Stabilometer test values on site samples of the bottom lift averaged 46. The minimum Hveem stabilometer value permitted by Caltrans for this mix is 37. These results indicate that by Caltrans criteria the Goal 1 mix should have a low probability of rutting in the field.

Although they meet the same Caltrans specifications, the Goal 1 asphalt concrete and the DGAC overlay material have different nominal maximum aggregate sizes following the Superpave specifications. The Goal 1 asphalt concrete is a 25-mm gradation following Superpave specifications, while the DGAC overlay material is a 19-mm gradation. The Goal 1

asphalt concrete nearly exactly follows the 25-mm maximum density line as defined by Superpave specifications (Figure 8). The Goal 1 gradation passes through the Superpave "restricted zone," as does the DGAC overlay.

2.1.3.3 Underlying Materials

The asphalt treated permeable base (ATPB) material under some of the HVS rutting sections meets Caltrans standard specifications. Cores and slabs taken from the rutting test sections showed no signs of stripping or other damage. The aggregate base (AB) material meets all Caltrans standard specifications for Class 2 Aggregate Base. R-value tests of the AB had values between 78 and 83. The aggregate base relative density at the time of compaction ranged between 99 and 103 percent and the water contents were at or just below the optimum water content. The Caltrans standard specification requires 95 percent relative compaction. (5)

The aggregate subbase (ASB) met all requirements for Caltrans Class 2 Aggregate Subbase. R-value tests of five samples ranged between 55 and 82, averaging 70 with a standard deviation of 10. The relative density of the ASB ranged between 95 and 100 percent. The Caltrans standard specification requires 95 percent relative compaction. The upper two meters of the subgrade soil are a high-plasticity clay, with a USCS classification of CH, and an AASHTO classification of A-7-6. The liquid limit ranges between 39 and 55 and the plasticity index between 27 and 41. R-value tests of the subgrade produced values between 4 and 30. The relative compaction of the subgrade was between 91 and 98 percent, averaging about 95 percent. Caltrans standard specifications require a minimum average relative compaction of 95 percent. The groundwater table is at depths of about 3.5 to 4.8 m below the surface of the subbase. (5, 13)

2.2 HVS Test Conditions, Instrumentation and Data Collection

2.2.1 Trafficking

The HVS test sections were 8 m in length. Pavement performance in the 1.5-m lengths at each end of the trafficked section (the "turnaround zone") were not included in the performance evaluations because the HVS wheel speed varies in these areas. All trafficking was channelized, with no side shift permitted. The decision to channelize the traffic was based on the following observations:

- Once a rut begins to develop, radial tires tend to track in the wheelpath with little or no wander, and so forcing a wander pattern might be farther from actual conditions than channelizing the traffic.
- Better control of high pavement temperatures could be obtained by channelizing the traffic, which permitted the placement of the heaters at the edge of the wheelpath.
- Actual wander patterns once a rut has begun to develop have not been quantified for most tires, and in particular for wide-based singles and dual radials.
- Rutting would develop faster with channelization, and could be compared to a forced wander pattern with results from the Cal/APT Pilot Study in South Africa (15).

2.2.2 Tires and Wheels

Four types of tires and wheels were included in the study, divided between two types of tires on dual wheels, and two types of tires on single wheels. Dual wheels are most commonly used in the United States, accounting for about 97 to 99 percent of all commercial truck wheels,

excluding steering axles. A larger percentage of trucks use wide-base singles in Europe, approaching 30 percent of all truck tires in France, and the majority of truck tires in Britain and Germany. Factors associated with wide-base singles that are pushing their greater use in Western Europe are larger payloads permitted by reduced vehicle weight, lower tire costs, reduced rolling resistance leading to reduced fuel consumption, and high taxes on vehicle weight and fuel. (16)

Prior to the development of modern radial tires in the 1960s, most trucks used bias-ply tires. Currently, it has been estimated that more than 90 percent of dual tires used in the United States are radials, and the remainder are bias-ply tires. A recent study of trucks entering Oregon found that less than one percent of tires on commercial trucks were bias-ply (17).

2.2.2.1 Bias-ply Duals

Goodyear 10.00-20, Load Range G tires on 10-cm wide rims were used for this study. The tire tread consists of six plies of nylon cord with a sidewall of 1 ply nylon cord. The maximum dual load rating is 28.09 kN (6,300 lbs.) at 620 kPa (90 psi) cold inflation pressure. The test load used for this study was 40 kN on the dual, which results in 20 kN (4,500 lbs.) on each tire. The inflation pressure was 620 kPa. This tire/wheel was used on Section 505RF.

2.2.2.2 Radial Duals

Goodyear G159A, 11R22.5, Load Range G tires on 11-cm wide rims were used in this study. The tire tread consists of six plies of steel cord with a sidewall of one ply steel cord. The maximum dual load rating is 25.64 kN (5,750 lbs.) at a cold inflation pressure of 723 kPa (105

psi). The test load used for this study was 40 kN on the dual, or 20 kN on each tire, at the rated inflation pressure. This tire/wheel was used on Sections 506RF, 509RF.

2.2.2.3 Wide-Base Single

The wide-base single used for this study was a Goodyear G286, 425/65R22.5, Load Range J, which was mounted on a 33-cm wide rim. The tire tread consists of five plies of steel cord, with a sidewall of one ply of steel cord. The maximum load rating is 46.82 kN (10,500 lbs.) at a cold inflation pressure of 758 kPa (110 psi). The test load for this study was 40 kN at the rated inflation pressure. The wide-base single was used on Sections 504RF, 507RF, 508RF, 511RF and 512RF.

2.2.2.4 Aircraft Single

An aircraft wheel and tire was included in the study for two reasons:

- To obtain data of use in relating field observations of rutting performance between highway and airfield locations, and
- To provide an upper bound for performance as truck tire/wheel technology continues to move towards greater loads and inflation pressures.

The aircraft tire used in this study was a BF Goodrich TSO C62C, 46 × 16, tubeless, reinforced thread, 0.42 skid. The maximum load rating is 199.8 kN (44,800 lbs.) at a cold inflation pressure of 1,034 kPa (150 psi). The test load for this study was 100 kN (22,500 lbs.) at the rated tire pressure. The aircraft tire was used on Section 513RF.

There are important differences between the four tire/wheel types included in the study that should be expected to impact rutting performance. Assuming constant temperature, traffic wander, and wheel speed, rutting would be expected to occur under conditions of larger inflation pressures and larger loads. Larger inflation pressures and loads should be expected to increase the shear stresses at the edges of the tire, which cause permanent deformation.

The ranking of inflation pressures from lowest to highest is: dual/bias-ply, dual/radial, wide-base single, aircraft. Rutting performance would be expected to be worst for the aircraft tire and best for the dual/bias-ply. With respect to load, the aircraft tire load of 100 kN would be expected to produce ruts faster than the other three tires, all of which were trafficked at 40 kN.

2.2.3 Wheel Speed and Direction

All of the rutting test sections were trafficked in the unidirectional mode, except for Section 513RF (aircraft tire) which was trafficked bi-directionally. In the unidirectional mode, the HVS wheel travels the 8-m long section loaded in one direction. It rolls up a short ramp at the end of the section, which locks it in a position in which the wheel is not in contact with the pavement. The wheel is then pulled back to the beginning of the section, where it is placed in contact with the pavement for the next cycle. In the bi-directional mode of loading, the wheel travels loaded in both directions. The bi-directional mode was not used for the aircraft wheel because the ramp did not work well with that wheel. Only loaded passes were counted as load repetitions in the results presented in this report, regardless of whether the trafficking was unidirectional or bi-directional.

The wheel speed in the loaded direction of the unidirectional mode was measured to be between 7.0 and 7.8 km/hr (4.3 to 4.8 mph), averaging 7.5 km/hr (4.7 mph). In the bi-directional mode the wheel speed in one direction is the same as that of the unidirectional mode, and averaged 6.8 km/hr (4.2 mph) in the other direction.

The wheel speed of the HVS is much slower than typical, free flowing highway traffic. Because slower speeds and the corresponding longer loading times result in more rutting than do typical highway traffic conditions, the HVS testing was performed under more severe conditions than would be expected on a free flowing highway. The HVS wheel speed is more typical of traffic on traffic jam on an urban freeway, or congested traffic on a highway or city street.

Tire contact area information from a previous study completed for CAL/APT by CSIR was used to calculate the contact load duration for each of the tire types used in the study. The calculations were made using the average speed in the loaded direction , and are shown in Table 12.

Table 12 Calculated surface contact durations for tire/wheel types included in study, assuming average unidirectional wheel speed. (18)

Tire/ Wheel Type	Load* (kN)	Inflation Pressure (kPa)	Contact width* (mm)	Contact length** (mm)	Contact Duration (seconds)
Dual bias-ply	41	620	200	306	0.15
Dual radial	41	720	200	300	0.14
Wide-base single	40	758	330	227	0.11
Aircraft	106	1040	290	380	0.18

* for dual tires, load and width of one tire
** wide-base single interpolated from other loads and pressures).

With respect to contact duration time, the expected rutting performance ranking, from best to worst, is: aircraft, dual/radial and dual/bias-ply similar, wide-base single.

2.2.4 Instrumentation and Data Collection

Instrumentation of the test sections was minimal due to time constraints and the need to minimize interference of instrumentation with the performance of the pavements. Instrumentation and data collections consisted of thermocouples to measure and control pavement temperatures, and laser profilometer readings to measure the surface profiles of the test sections.

In the two years after HVS trafficking of the rutting test sections was completed, cores were taken and trenches were dug to evaluate the performance of the test sections. The test sections were not subjected to any traffic, high temperatures, or water between the time trafficking was completed and coring and trenching were finished.

Locations of thermocouples, profilometer locations and trenching and coring locations are shown in Figure 4.

2.2.4.1 Thermocouples

Sets of three to five Type K thermocouples were installed just outside of the wheelpath at one or two locations on each side of the section. The locations were offset along the length of the section (Figure 4). The thermocouples in each set were placed at different depths between the surface and bottom of the asphalt treated layers, including the ATPB where applicable. Thermocouple depths and temperature data are included in Appendix Temperature.

To install the thermocouples, a 10-mm diameter hole was drilled in the asphalt concrete. The thermocouples were wrapped around a wooden dowel and taped in place. They were then placed in the hole, and back filled with hot asphalt.

2.2.4.2 Profilometer and Straight Edge

The laser profilometer and data acquisition system developed by CSIR was used to measure surface profile at various times as rutting developed. The laser profilometer is described in detail in Reference (5).

Profiles were taken transverse to the wheelpath, at locations 0.5 m apart along the wheelpath (Figure 4). Maximum rut depth from the profiles obtained from the laser profilometer was defined as the difference between the highest point in the profile and lowest point. On all sections, "humps" of material developed at the sides of the wheelpath as trafficking progressed. On the sections tested with dual wheels, humps also developed between the tires.

A straight edge was used in the early stages of the experiment to measure maximum rut depth, as an independent check of the laser profilometer. It was found that the maximum rut depth found using both instruments was quite similar, and use of the straight edge was abandoned.

2.2.4.3 Trenches and Cores

After completion of all of the HVS rutting tests on the overlays, a trench was dug across the wheelpath at one location on each test section (Figure 4). The first stage of trenching was to cut the trench edges using a water-cooled saw. The trenches were cut wide enough so that they included sections of the pavement not influenced by the HVS loading, the humps at the sides of the wheelpath, and the wheelpaths. After waiting several weeks to permit the sections to dry out, the asphalt bound layers were removed in slabs. The slabs were saved to provide material for additional cores if needed. The thickness of the asphalt bound layers, including the overlays and

both lifts of Goal 1 asphalt concrete, were measured on the cut face at the sides of the trench at 25-mm intervals.

Photographs were taken of the trench with the asphalt bound layers removed. The laser profilometer was then placed in the trench on the exposed surface of the aggregate base layer, and the profile of the base was taken. The aggregate base was then excavated to the top of the aggregate subbase, and the thickness of the aggregate base was measured at various transverse points across the trench.

Cores were taken at several locations along the wheelpath (Figure 4). Cores were taken outside the heated area of the HVS test, within the heated area but outside the area influenced by the HVS trafficking, in the humps, and in the wheelpath. Cores were taken in all three humps and both wheelpaths on the dual wheel sections.

2.2.4.4 Data Collection Schedule

Air and pavement temperatures were recorded hourly. Temperatures included in this report are only those recorded when the HVS was trafficking. Profiles were recorded at different intervals, depending upon how quickly rutting was developing on each section.

2.2.5 Heating and Temperature Control

Target temperatures for each test section were shown in Table 2. To heat the test section pavements to the target temperatures a set of banked reflectors fitted with infrared lamps and resistance heating elements was used. A kerosene fired air heater was also used for a few hours at the beginning of each test to bring the air temperature from ambient conditions to just below

the target temperature. HVS trafficking was not begun until temperatures had stabilized throughout the asphalt concrete layer, as determined from thermocouples. In some cases, heating continued for more than 12 hours before trafficking was begun.

Once the target temperature was reached, it was maintained by a control system that turned the lamps and heating elements on or off whenever the temperature measured by the thermocouple at 50 mm depth was more than 2°C from the target. The curved shape of the reflectors and channelized traffic pattern, which precluded side-shift movement of the beam, created an enclosed space over the test section that helped to maintain heat in the pavement (Figure 9).

Figures 9a and 9b. Aluminum reflector with resistance-heating element and infrared lamps.

3.0 HEAVY VEHICLE SIMULATOR TEST RESULTS

Comparisons of rutting performance for single variables included in the experiment design can be determined from comparison of HVS test section results as shown in Table 13.

Table 13. Comparison of single variables from HVS test section results.

Variable Comparison	HVS Test Sections (fixed variables)
Overlay Type: DGAC, 38 mm ARHM-GG, 62 mm ARHM-GG	510RF, 509RF, 506RF (radial tire/dual wheel, 50 C)
Overlay Type: DGAC, 38 mm ARHM-GG, 62 mm ARHM-GG	511RF, 508RF, 507RF (wide-base single, 50 C)
Tire Type: Dual/Radial, Dual/Bias-Ply, Wide-base Single, Aircraft	507RF, 505RF, 507RF, 513RF (DGAC, 50 C)
Tire Type: Dual/Radial, Wide-base Single	510RF, 511RF (38 mm ARHM-GG, 50 C)
Tire Type: Dual/Radial, Wide-base Single	509RF, 508RF (62 mm ARHM-GG, 50 C)
Pavement Temperature: 40 C, 50 C	507RF, 512RF (DGAC, wide-base single)
DGAC Type: Goal 1 mix, Goal 3 mix	504RF (Goal 1 mix, 45 C), 507RF (Goal 3 mix, 50 C), 512RF (Goal 3 mix, 40 C), all wide-base single

3.1 Pavement Temperatures

Temperature data for each test section are summarized in Table 14, including the average temperature at each depth, the layer in which the thermocouples were located, and the average standard deviation for each depth in each section.

The temperature data show that the target temperature of 50°C at 50 mm depth was matched within ± 2 C by the average temperatures at that depth on Sections 505, 506, 507, 508, 509, 510, 511 and 513. The target temperature of 40°C at 50 mm depth was met on Section 512. Average standard deviations of temperature at depths of less than 100 mm were typically less than 3.0°C. Section 508 had much greater variability near the surface than the other sections.

Table 14 Summary of pavement temperatures and thermocouple depths during HVS trafficking.

	Level 1 Thermocouple			Level 2 Thermocouple			Level 3 Thermocouple			Level 4 Thermocouple			Level 5 Thermocouple		
Section	**Avg. (Std. Dev.)**	**Depth in mm**	**Layer**	**Avg. (Std. Dev.)**	**Depth in mm**	**Layer**	**Avg. (Std. Dev.)**	**Depth in mm**	**Layer**	**Avg. (Std. Dev.)**	**Depth in mm**	**Layer**	**Avg. (Std. Dev.)**	**Depth in mm**	**Layer**
504	49 (4.9)	0	AC1	41 (5.4)	76	AC1 AC2	36 (6.3)	137	AC2						
505	52 (2.6)	0	DG	50 (2.0)	50	DG	47 (0.4)	100	AC1	44 (4.5)	165	AC2	44 (4.4)	237	AT PB
506	53 (3.0)	0	DG	50 (2.2)	50	DG	47 (2.1)	76	DG AC1	44 (2.0)	138	AC1	41 (2.7)	214	AC2
507	54 (3.3)	0	DG	49 (2.4)	50	DG	48 (2.2)	76	DGAC 1	46 (2.2)	138	AC1	43 (2.1)	214	AC2
512	42 (1.2)	0	DG	41 (1.0)	50	DG AC1	40 (1.0)	76	AC1	39 (0.9)	145	AC2	37 (0.9)	230	AT PB
513	51 (2.1)	0	DG	48 (1.9)	50	DG	45 (1.9)	76	DGAC 1	40 (3.2)	138	AC1	37 (3.8)	214	AC2
508	54 (5.6)	0	AR	51 (5.0)	50	AR	49 (4.9)	61	AR	46 (4.5)	137	AC1	44 (4.4)	213	AC2
509	56 (2.4)	0	AR	52 (1.5)	50	AR	51 (1.2)	61	AR	46 (1.8)	137	AC1	46 (1.2)	213	AC2
510	53 (2.2)	0	AR	51 (3.0)	37	AC1	50 (1.6)	50	AC1	48 (2.8)	112	AC2	45 (1.8)	187	AT PB
511	51 (1.6)	0	AR	50 (1.2)	37	AC1	50 (1.0)	50	AC1	47 (0.9)	112	AC2	44 (1.0)	187	AT PB

Notes: Avg. is the average temperature at that depth across the thermocouple sets
Std. Dev. is the average standard deviation for the thermocouple sets on a section
Depth in mm is the depth of the thermocouple location
Layer is the layer that the thermocouple is in: AR=ARHM-GG overlay, DG=DGAC overlay, AC1=top lift of Goal 1 asphalt concrete, AC2=bottom lift of Goal 1 asphalt concrete, ATPB=asphalt treated permeable base.

Typically, there was larger variability in temperatures at depths greater than 100 mm. This is primarily due to continued heating of the lower asphalt bound layers during the duration of the trafficking, since trafficking was begun as soon as temperatures nearer to the surface had stabilized.

The average temperature met the target temperature of 50°C at the surface of Section 504. Temperature variability is quite high on this section, which was used to develop the temperature control equipment and procedures.

The thermocouple depths were designed to provide temperatures throughout all the asphalt bound layers. Profiles of average temperature versus depth are shown in Figure 10. Complete temperature data for each test is included in Appendix E.

The temperature profiles of the sections are fairly linear for all sections except the bottom sensor of Section 509RF. The primary non-linearity in the profiles typically occurs near the interface between the overlays and the top lift of Goal 1 asphalt concrete. This is likely an artifact of thermocouple location near the interface, and because commencement of HVS trafficking was determined by temperature stability near the 50-mm depth. The temperature gradients (°C/mm) for each section are generally similar assuming a linear temperature profile between the top and bottom thermocouples, except for Sections 504RF and 512RF (Table 15). The average gradient for the test sections with target temperatures of 50°C at 50-mm depth is –0.049 C/mm.

Comparison of average temperature profiles for the three overlays (DGAC, 38-mm ARHM, 62 mm ARHM) under dual-radial wheel loading (Figure 11) shows that they are similar,

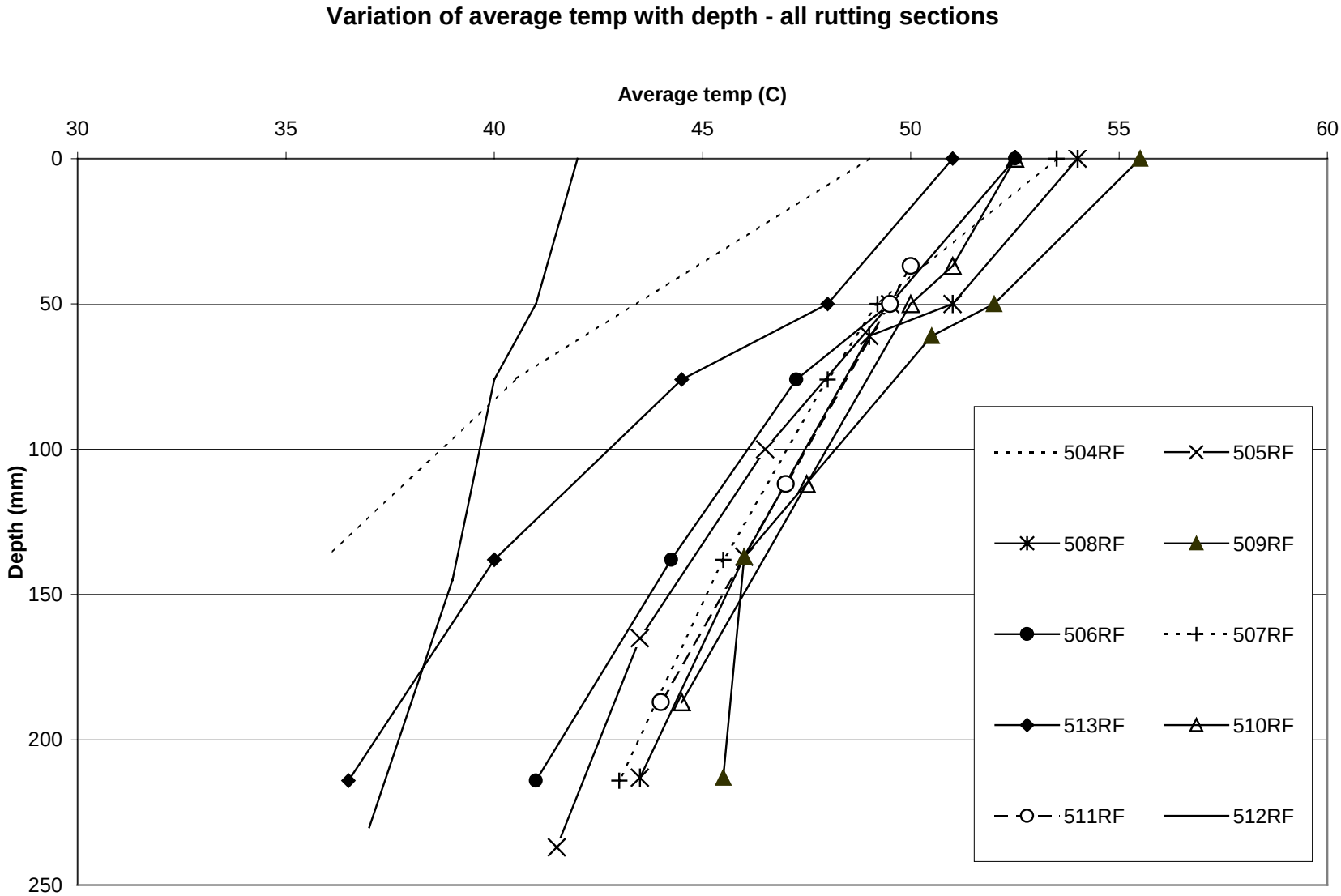

Figure 10. Average pavement temperature profiles during HVS trafficking.

Table 15 Temperature gradients in asphalt bound layers, assuming linear gradient between top and bottom thermocouples.

Section	504	505	506	507	512	513	508	509	510	511
Average Temp at 50 mm (°C)	43	50	50	49	41	48	51	52	50	50
Linear Gradient (°C/mm)	-0.095	-0.048	-0.054	-0.049	-0.022	-0.068	-0.049	-0.047	-0.043	-0.037

with the DGAC overlay about 2.5°C cooler than the ARHM-GG overlays. The average temperature profiles for the sections comparing the three overlays under wide-base single wheel loading are nearly identical (Figure 12). Of the four sections comparing tire type, the temperature profiles of the highway vehicle tires are nearly identical, while that of the aircraft tire is cooler, particularly below 75 mm depth (Figure 13). A desired large difference in temperature profile between Sections 507RF and 512RF was achieved, with a difference of 12°C at the surface and about 6°C near the bottom of the Goal 1 asphalt concrete (Figure 14).

3.2 Rutting Results

The development of average maximum rut depth versus load repetitions is shown for all sections in Figure 15. The development of average transverse profile versus load repetitions is shown for each test section in Appendix F. For sections with two wheelpaths from a dual wheel, the maximum rut depth is the largest of the two. The profiles show that in addition to a downward rut in the wheelpath(s), each test section also had significant humps develop at the sides of the wheelpath. As noted previously, the maximum rut depth is defined for this study as the vertical distance between the bottom of the wheelpath and the highest of the adjacent humps.

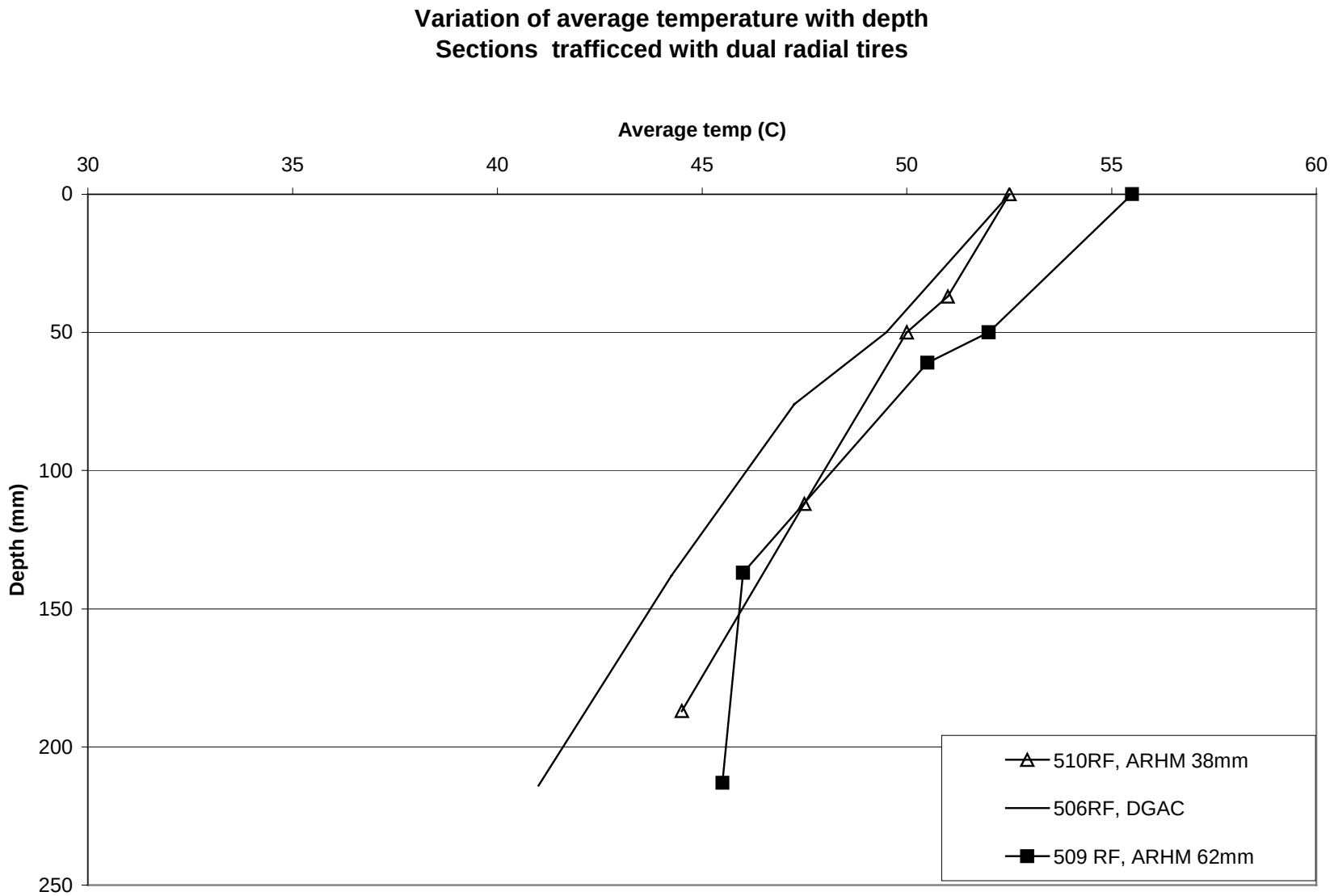

Figure 11. Average pavement temperature profiles during HVS trafficking for three overlays under dual-radial wheel.

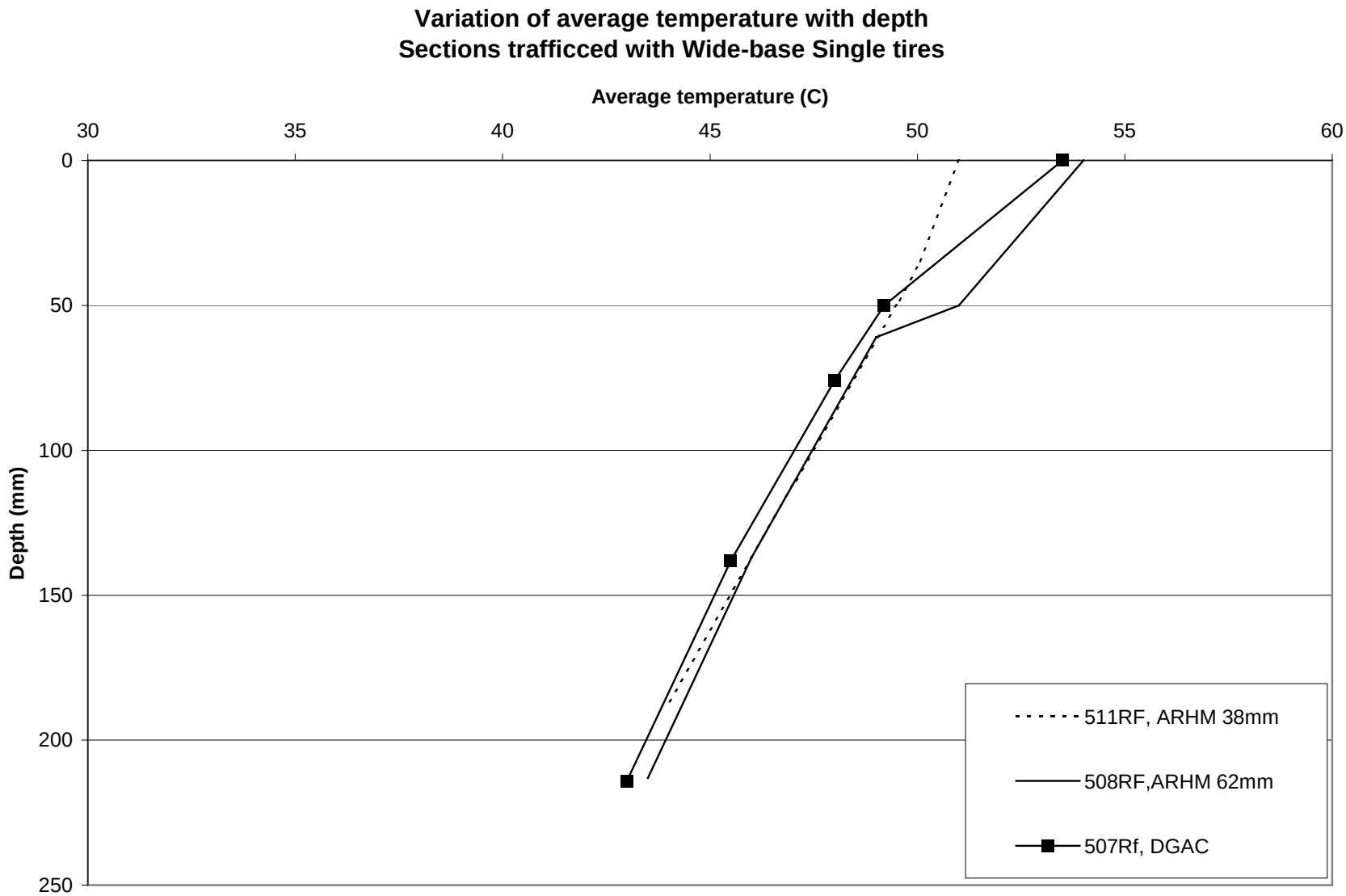

Figure 12. Average pavement temperature profiles during HVS trafficking for three overlays under wide-base single wheel.

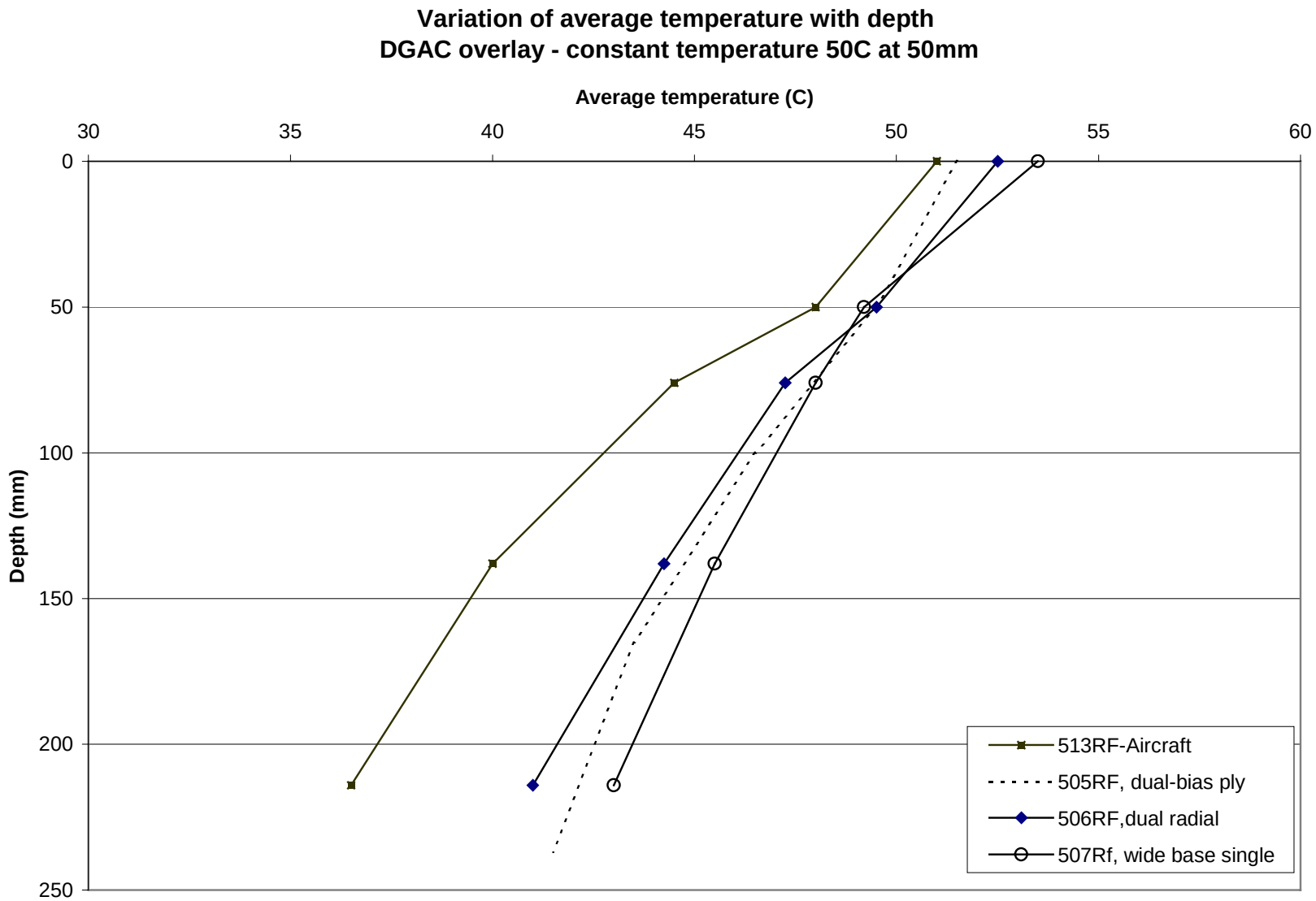

Figure 13. Average pavement temperature profiles during HVS trafficking for four tire types on DGAC overlay.

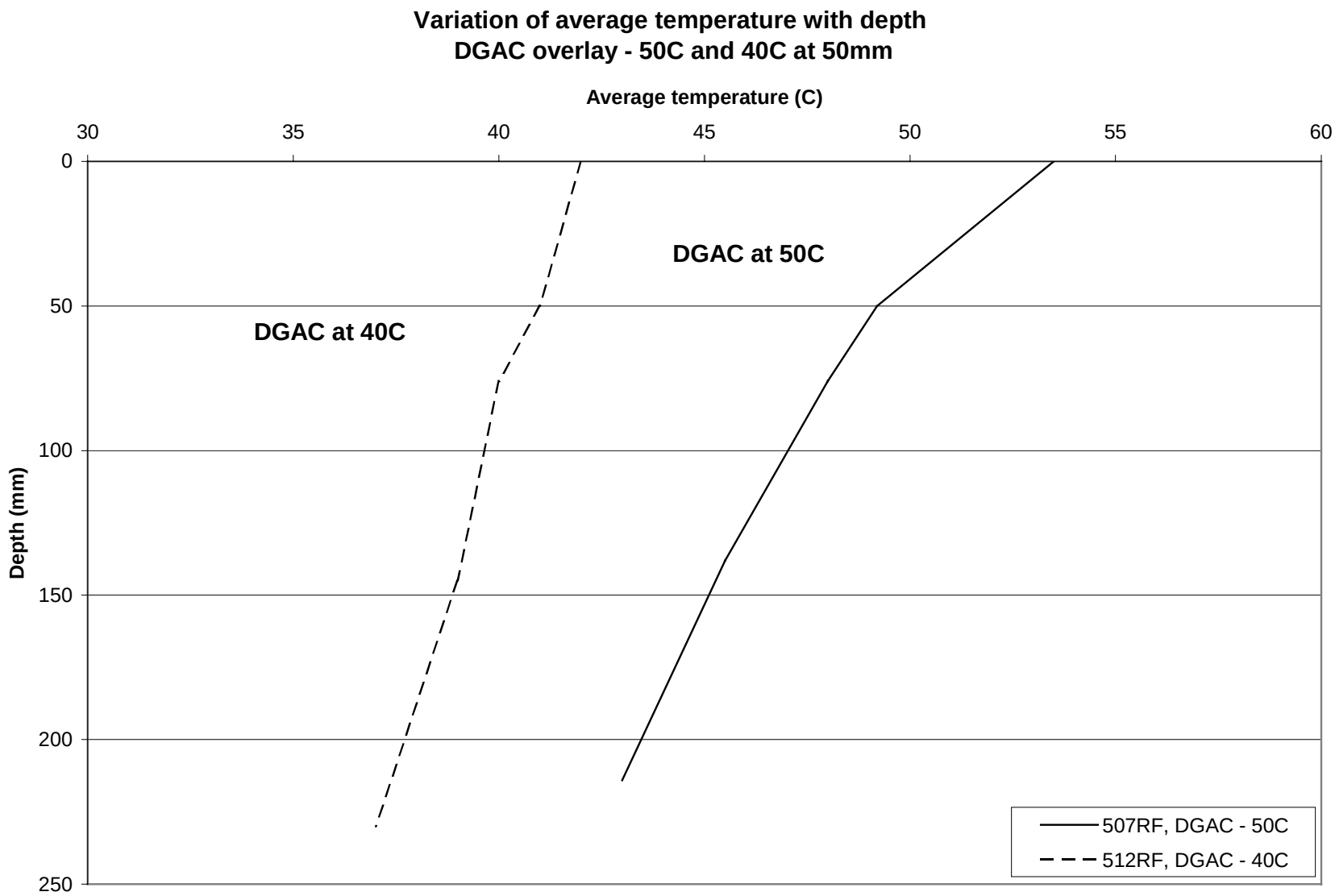

Figure 14. Average pavement temperature profiles during HVS trafficking for two temperatures, wide-base single wheel, DGAC overlay.

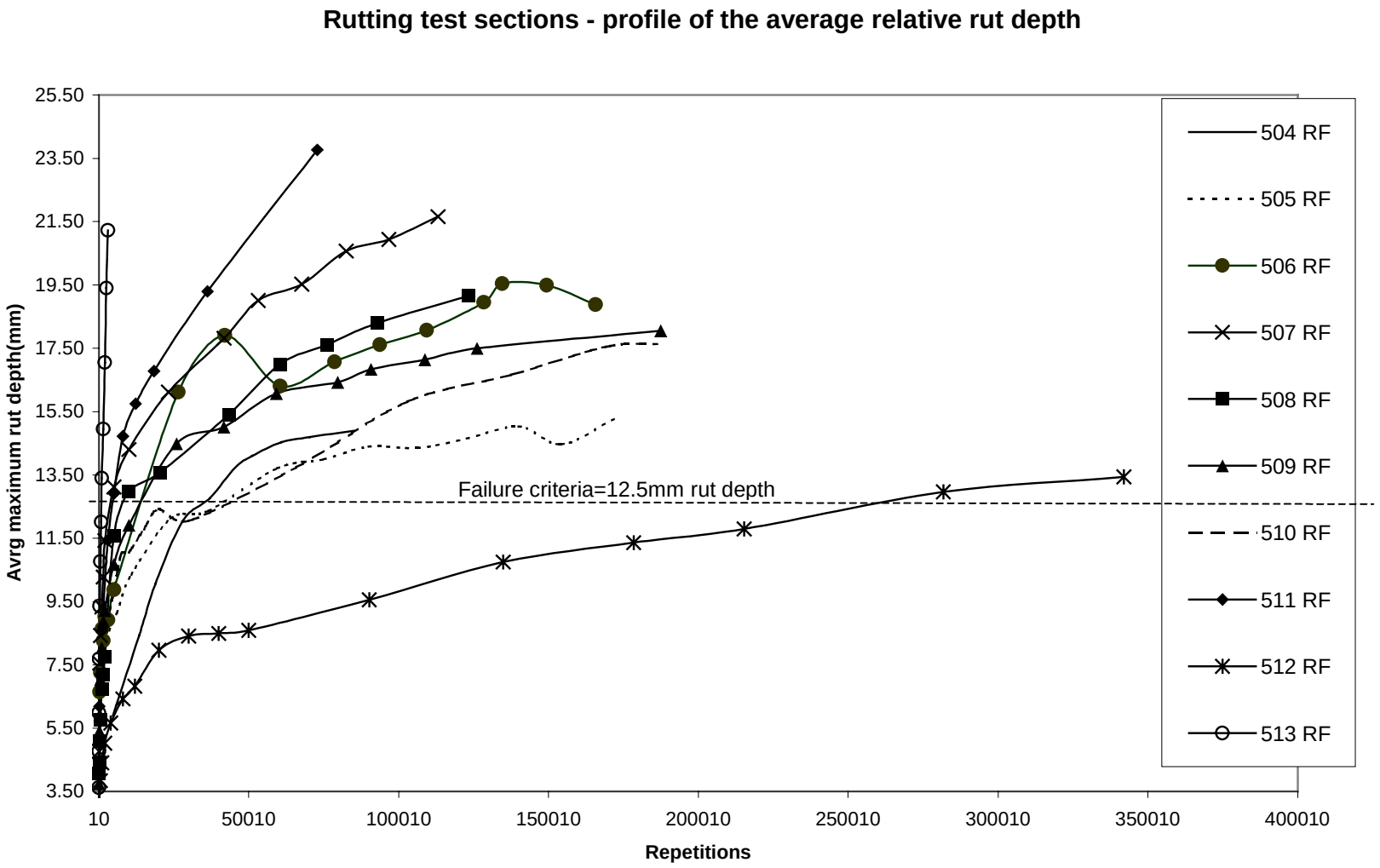

Figure 15. Plot of average maximum rut depth versus load repetitions for all test sections.

On many of the test sections, HVS trafficking was continued well beyond the failure rut depth of 12.5 mm. Final rut depths ranged between 15 and 24 mm (Table 16). Figure 15 indicates all of the sections subjected to trafficking by highway wheels/tires had an initial period of rapid rut development, followed by a second period with a reduced rate of rutting that continued until trafficking was stopped. The aircraft wheel test section (513RF) had a slight reduction in rut rate as trafficking progressed, but much less than that of the other test sections. None of the test sections showed any evidence of a "tertiary" period of rut development in which the rate of rut development increases again after the second period of reduced rutting rate. The lack of a tertiary rutting period, despite final ruts of 15 to 24 mm, suggests that this is either:

- A phenomenon that occurs only in the laboratory during triaxial repeated load testing,
- A phenomenon that occurs in the field when temperatures or loads exceed those previously experienced by the mix, or
- A phenomenon that only occurs when rut depths have already exceeded 24 mm.

Table 16 Average maximum rut depth and load repetitions at completion of HVS trafficking.

Section	Final Load Repetitions	Final Average Maximum Rut Depth (mm)
504 RF	85,043	14.9
505 RF	172,529	15.3
506 RF	165,734	18.9
507 RF	113,176	21.7
512 RF	341,976	13.4
513 RF	3,033	21.2
508 RF	123,426	19.2
509 RF	187,478	18.1
510 RF	186,308	17.6
511 RF	72,837	23.8

Results of trenching and profilometer measurements at the top of the base indicate that less than 5 mm of the final average maximum rut depth occurred at the surface of the aggregate base on any of the test sections. The measurements are not precise because of noise caused by individual particles at the surface of the base. Disturbance at the surface of the base was minimized during sawing and slab removal, although some disturbance was inevitable due to penetration of the prime coat into the base and adhesion of particles of the base to the asphalt layers when the slabs were removed.

The number of load repetitions to reach the failure criterion of a maximum rut depth of 12.5 mm varied depending upon overlay type, tire type, and temperature. The number of repetitions to reach an average maximum rut depth of 6.25 mm, and to failure (12.5 mm), for each test section is shown in Table 17. The values shown are averages of the transverse profiles taken at 0.5-m intervals along the middle 6 m of the 8-m long test sections. Also shown is the standard deviation of the rut depth along the section at that number of load repetitions.

All of the test sections except 510RF have relatively uniform rut depths along the test section, as can be seen from the standard deviations of maximum rut depth in Table 17.

The ranking of rutting performance based on load repetitions to the failure rut depth is as follows:

1. DGAC overlay at target temperature of 40 C (Section 512RF),

2.a. 38 mm ARHM-GG overlay with dual radial tires (Section 510RF),

2.b. DGAC overlay with dual bias-ply tires (Section 505RF),

3.a. DGAC overlay with dual radial tires (Section 506RF),

3.b. 62 mm ARHM-GG overlay with dual radial tires (Section 509RF),

4. 62 mm ARHM-GG overlay with wide-base single tire (Section 508RF),

5. 38 mm ARHM-GG overlay with wide-base single tire (Section 511RF),

6. DGAC overlay with wide-base single tire (Section 507RF), and

7. DGAC overlay with aircraft tire (Section 513RF).

Table 17 Load repetitions to 6.25 mm and 12.5 mm average maximum rut depth.

Section	Tire type	Overlay type	Average Temperature at 50 mm (C)	Reps to 6.25-mm rut	Standard Deviation at 6.25 mm (mm)	Reps to 12.5-mm rut	Standard Deviation at 12.5 mm (mm)
505 RF	dual bias-ply	DGAC	50	1,513		38,973	2.1
506 RF	dual radial	DGAC	50	235		14,051	2.3
507 RF	wide-base single	DGAC	49	180	2.5	1,817	2.4
512 RF	wide-base single	DGAC	41	7,068	0.9	255,254	1.5
513 RF	Aircraft	DGAC	48	58	1.7	838	3.8
508 RF	wide-base single	ARHM 62mm	51	750	0.6	8,307	1.5
509 RF	dual radial	ARHM 62mm	52	323	0.4	13,673	0.9
511 RF	wide-base single	ARHM 38mm	50	218	0.8	4,441	1.6
510 RF	dual radial	ARHM 38mm	51	617	1.0	39,697	1.4

3.2.1 Comparison of Tire/Wheel Types

The ranking of the tire/wheel types was consistent across the three overlay types with respect to rate of rut development (Table 17, Figure 16).

All four tire/wheel types were compared on the DGAC overlay at a 50 C target temperature at 50 mm depth. The ranking from best to worst and the relative number of repetitions compared to the best performing type is as follows:

Ranking	**Type**	**Relative Repetitions to 12.5 mm Rut**
1	Dual/bias-ply	1.00
2	Dual/radial	0.36
3	Wide-base single	0.05
4	Aircraft	0.02

The dual/radial and wide-base single types were compared on both the 38-mm and 62-mm thick ARHM-GG overlays. The rankings from best to worst and the relative number of repetitions compared to the best performing type on those overlays are as follows:

		Relative Repetitions to 12.5 mm Rut	
Ranking	**Type**	**38 mm ARHM-GG**	**62 mm ARHM-GG**
1	Dual/radial	1.00	1.00
2	Wide-base single	0.11	0.61

The performance of the different tire types follows expectations if it is assumed that greater tires pressures result in larger shear stresses, and faster rut development. The combination of very high tire inflation pressure, heavier load, and bi-directional loading help explain the very fast rutting that developed under the aircraft tire. Pavement temperatures were nearly identical on of these eight test sections.

One factor that likely contributed to poorer performance by the wide-base single tires is larger air-void contents on the test sections compared to air-void contents on sections tested with

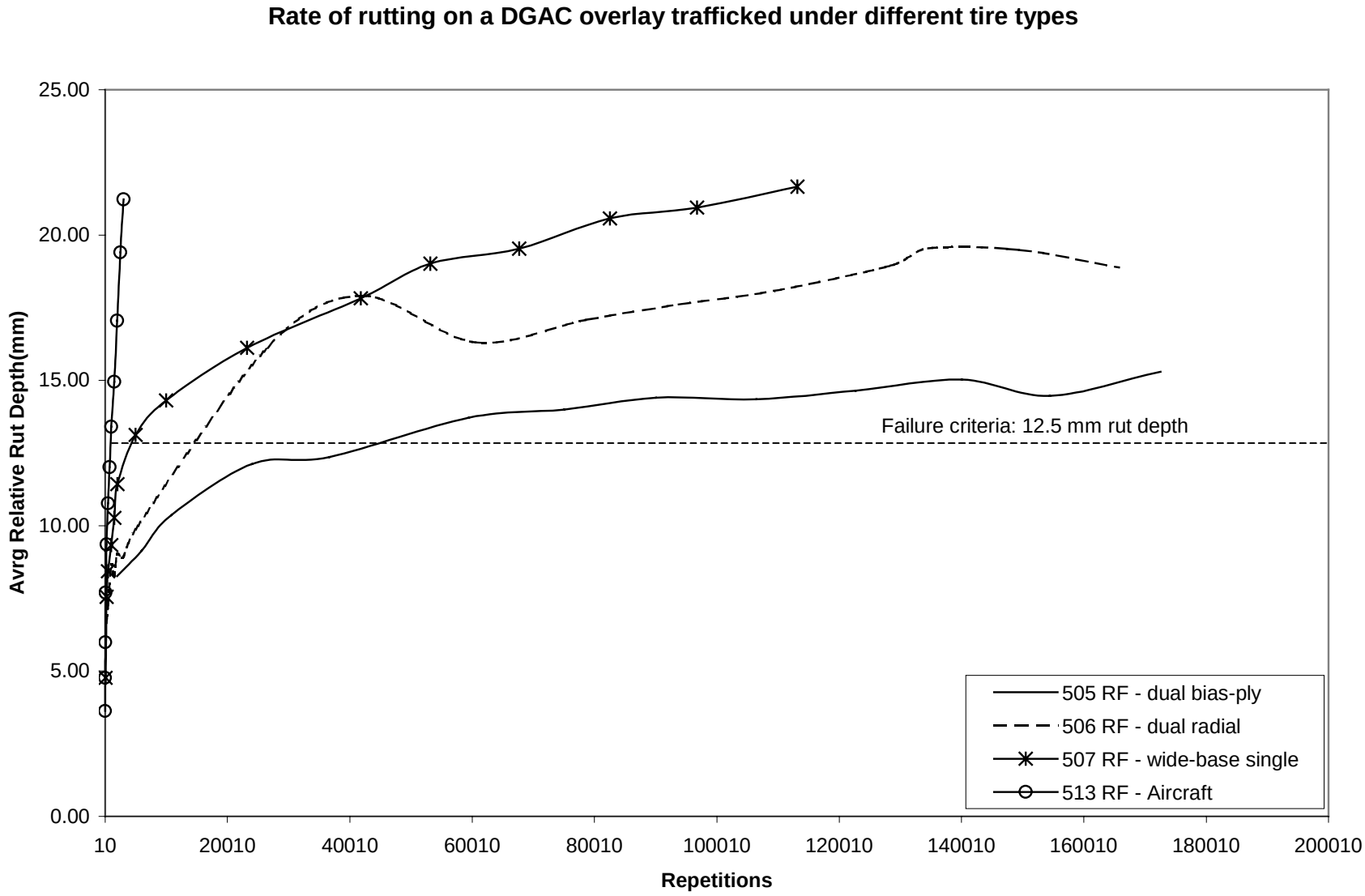

Figure 16. Plot of average maximum rut development versus load repetitions for four tire/wheel types on DGAC overlay.

other wheel/tire types. On the DGAC overlay, the average initial air-void content under the wide-base single was 7.9 percent, compared to 5.8 and 4.7 percent under the dual/bias-ply and dual/radial wheels, respectively. On the ARHM-GG overlays, the average air-void contents under the wide-base single were 12.5 and 17.9 percent, compared to 9.9 and 15.2 percent under the dual/radial. While the differences in air-void content are not so different that they would be expected to reverse the rankings, they likely increased the rut development under the wide-base single.

3.2.2 Comparison of Overlay Types

The ranking of the three overlay types/thicknesses was not consistent for the two types of wheels they were tested with (Table 17, Figures 17,18).

The ranking of the overlays and the relative number of repetitions compared to the best performing overlay under each wheel is as follows:

Dual/Radial Tires			Wide-base Single Tire		
Ranking	Overlay	Relative Reps.	Ranking	Overlay	Relative Reps.
1	38 mm ARHM-GG	1.00	1	62 mm ARHM-GG	1.00
2a	DGAC	0.35	2	38 mm ARHM-GG	0.53
2b	62 mm ARHM-GG	0.34	3	DGAC	0.22

Average pavement temperatures at 50 mm depth during each test were quite similar. These results suggest that in general, the performance of both thicknesses of the ARHM-GG overlay is not that different from that of the DGAC, and might be considered superior.

Two factors must be considered in evaluating this observation. First, the binder content of the ARHM-GG overlay was on average one percent less than the target binder content, while

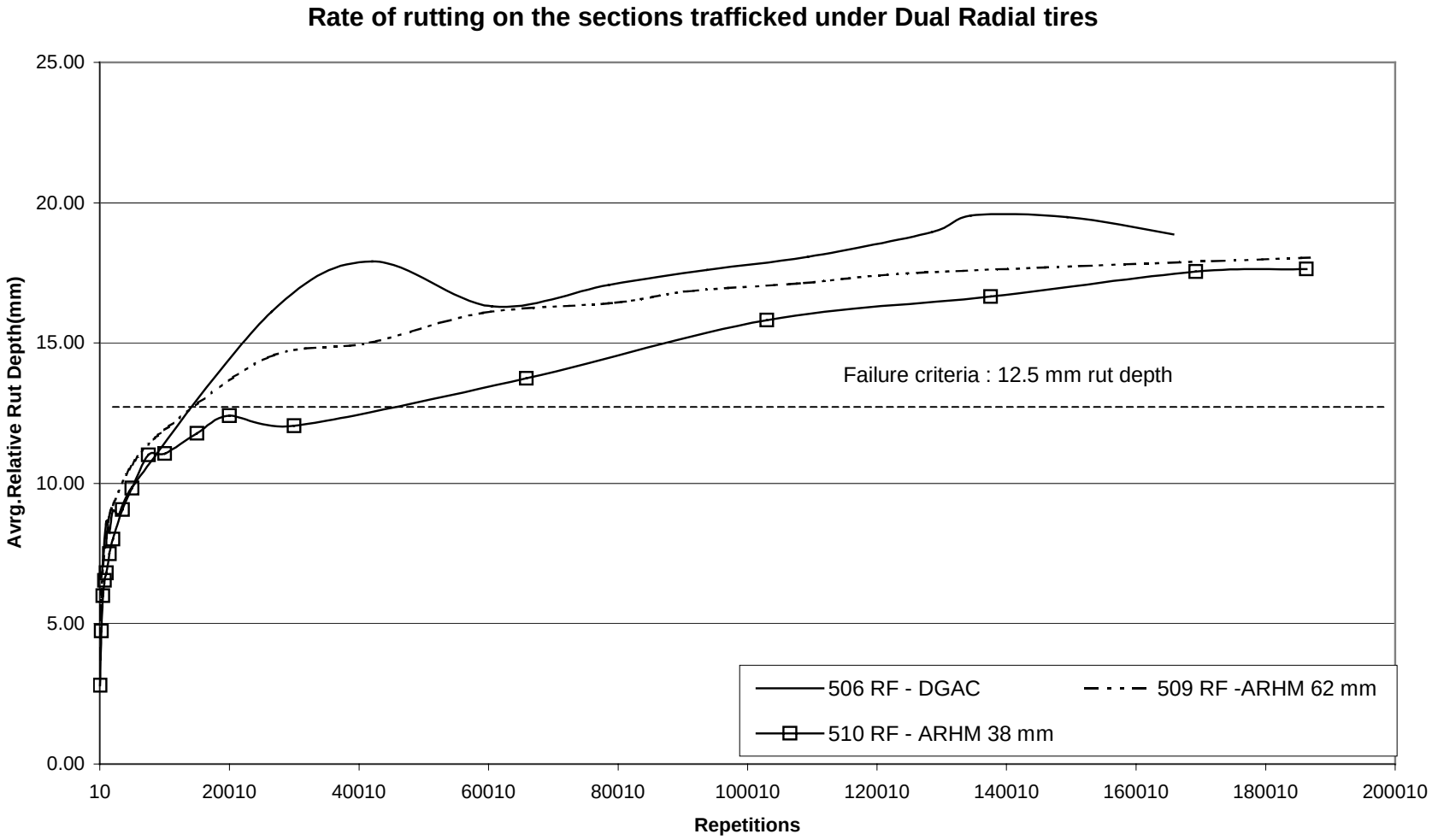

Figure 17. Plot of average maximum rut development versus load repetitions for DGAC, 38 mm ARHM-GG and 62 mm ARHM-GG overlays under dual/radial tires.

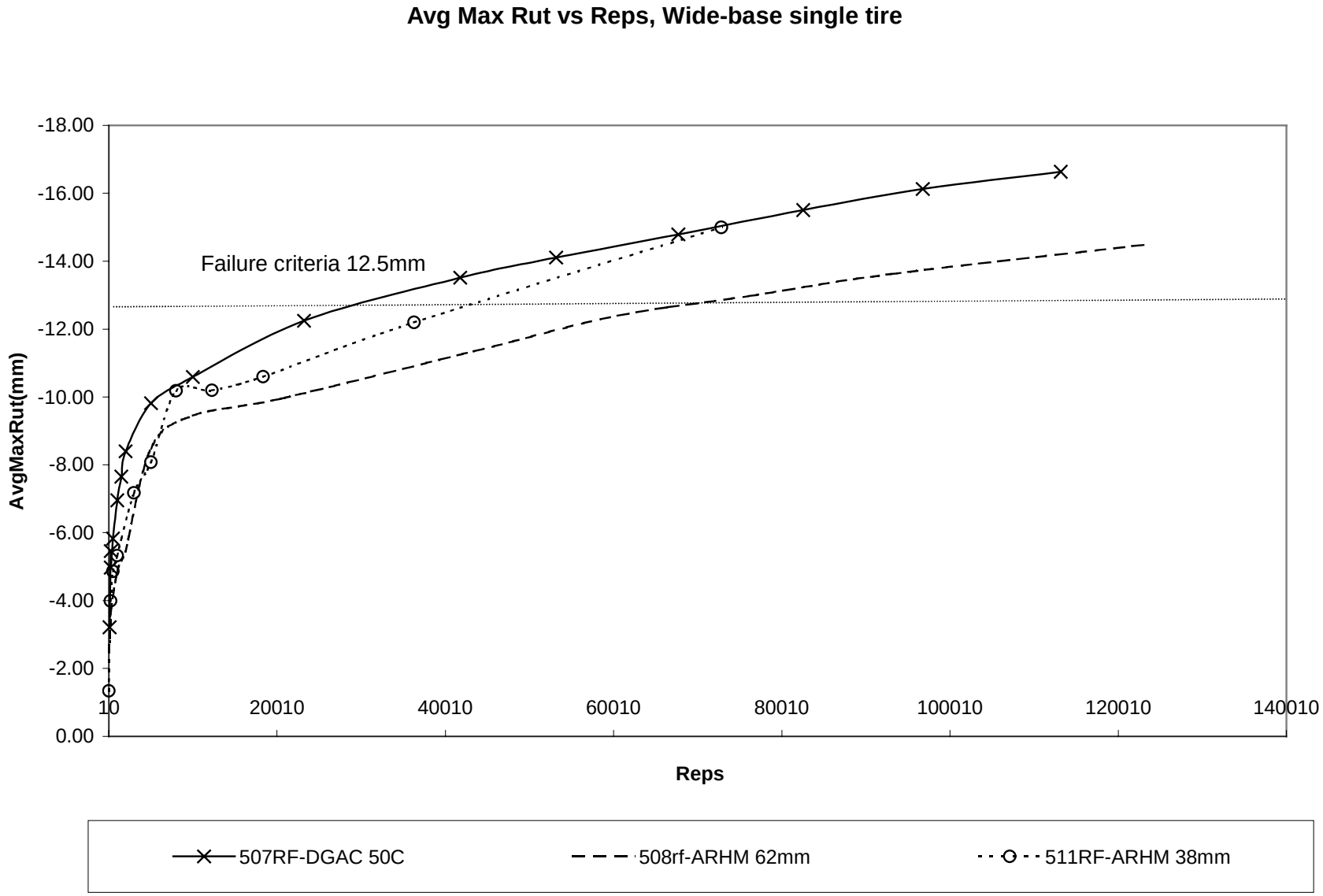

Figure 18. Plot of average maximum rut development versus load repetitions for DGAC, 38 mm ARHM-GG and 62 mm ARHM-GG overlays under wide-base single tire.

the binder content of the DGAC overlay was within the target range. This would tend to improve the rutting performance of the ARHM-GG overlay compared to that of the DGAC. On the other hand, the air-void contents of the ARHM-GG overlay are considerably greater than those of the DGAC, particularly the sections with a 38-mm ARHM-GG thickness. The poorer compaction of the ARHM-GG overlay would be expected to result in poorer rutting performance. The net effect of these two differences from design targets on rutting performance must be further evaluated through laboratory testing.

The fact that the performance of the overlaid structures is similar can be attributed in part to the presence of the same Goal 1 dense graded asphalt concrete layers underlying each test section. As will be seen, a portion of the rutting in each section occurred in the underlying asphalt concrete layers, as well as in the overlays.

3.2.3 Comparison of Pavement Temperature

As would be expected, reducing pavement temperature significantly improves rutting performance (Table 17, Figure 19). The difference of 8°C in average temperature between Sections 507RF and 512RF resulted in a ratio of load repetitions to reach 12.5 mm rut depth of 140:1. These results strongly indicate that mix design procedures should account for expected pavement temperatures at a project location when selecting binder content and evaluating the expected rutting performance.

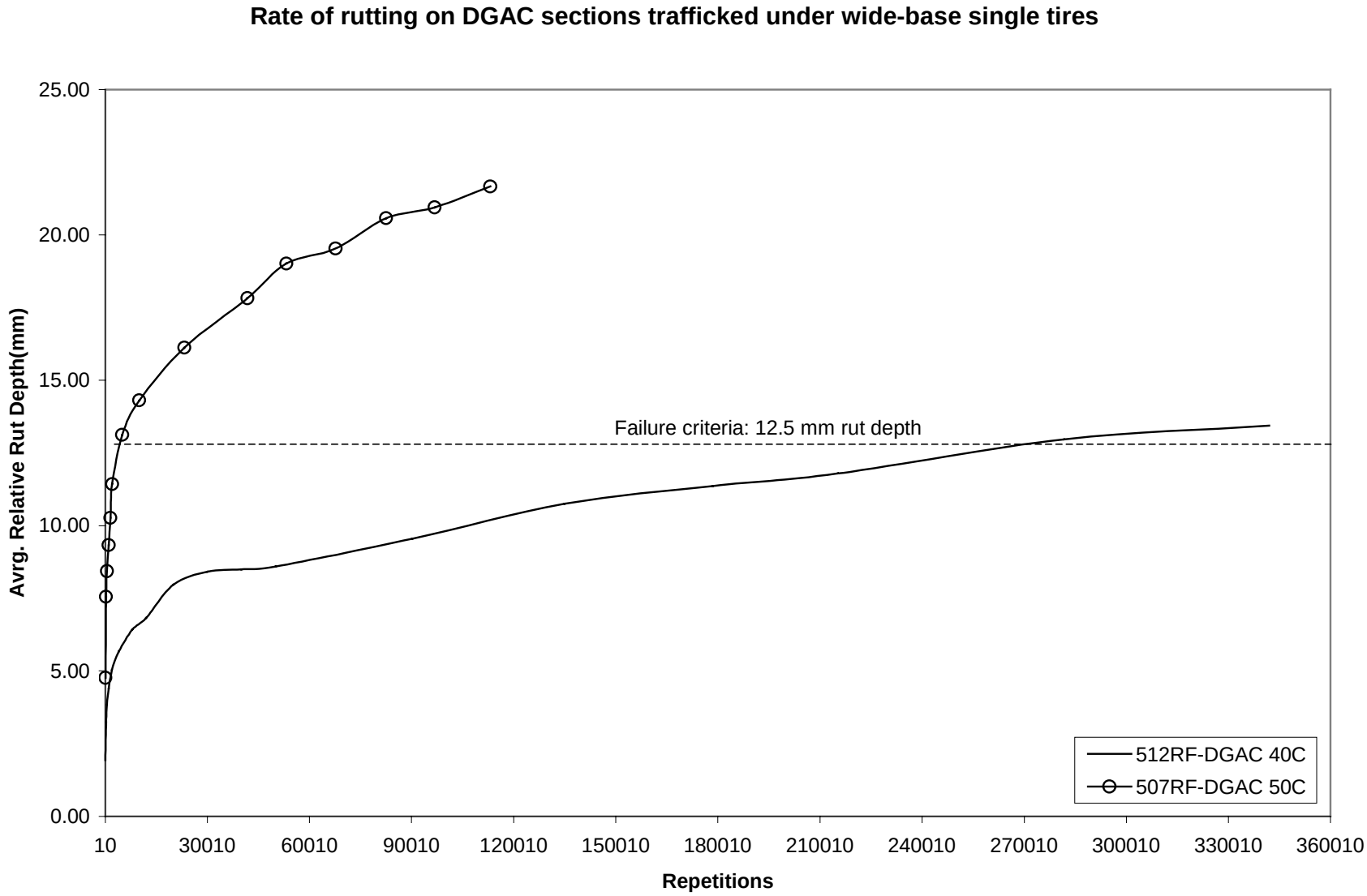

Figure 19. Plot of average maximum rut development versus load repetitions for DGAC overlay at two different temperatures.

3.3 Contribution to Rutting of Shear and Densification of Different Layers

Rutting occurred in all of the asphalt-bound layers. Rutting in each layer can be divided between permanent reduction in volume (densification), permanent movement of material at constant volume (shear or shape change), or a combination of both. The relative amounts of rutting occurring in each layer, and the relative proportions of rut depth that can be attributed to densification and shear were evaluated through analysis of:

- layer thicknesses from slabs taken in the trenches,
- layer thickness from cores,
- volumes of material in the humps and wheelpath measured from the transverse profilometer profiles, and
- air-void contents of the cores.

It is important to measure and understand the relative contributions of densification and shear in order to develop mix design methods that effectively reduce the risk of premature rutting.

3.3.1 Profile changes

Humps would not appear at the edges of the wheelpath if rutting in asphalt concrete layers was solely caused by densification (or reduction in air-void content) from compaction under the repeated wheel loads. The development of upheavals of asphalt concrete is apparent in the humps at the edge of the wheelpath seen in the surface profile plots from the laser profilometer in Appendix F. The surface profiles also indicate a downward movement of the

surface in the wheelpaths, which is due to a combination of shear flow of material to the humps, and densification of the material in the wheelpath.

The surface profiles indicate that the humps are sometimes equal on each side of the wheelpath(s) and sometimes not. The humps are particularly large on the sections with 38-mm ARHM-GG overlays (510RF, 511RF), and are small under the aircraft wheel (513RF).

The thicknesses of the asphalt concrete layers on transverse cross sections measured on slabs taken during trenching are plotted in Appendix G. The plots assume no rutting of the base. The plots indicate some development of humps in nearly all sections. Humps are particularly noticeable between dual tires, and in the Goal layers under the 38-mm ARHM-GG overlay sections.

The surface of the top lift of Goal 1 asphalt concrete typically shows some rutting, except for the section tested at 40°C (512RF). The rutting at the top of the Goal 1 AC is typically less than that at the surface, except under the 38-mm ARHM-GG overlays, which show considerable rutting in the surface of both the top and bottom lifts of Goal 1 AC. The presence of large humps at the surface and considerable rutting of the Goal 1 AC layers on the 38-mm ARHM-GG sections indicates that shear movement can occur at the same time as densification, and in mixes with high air-void contents. The average air-void content of those sections (510RF, 511RF) prior to trafficking was 16.6 percent.

3.3.2 Air-void content changes

Average air-void contents in the wheelpath and humps from cores taken after trafficking are shown for each test section in Table 18. There is inherent variability in the comparison of

cores from before traffic and after, since the two measurements must be taken on two cores from different locations. As was seen in Figure 4, the cores were taken as near as possible at the same transverse location along the wheelpath.

Table 18 Air-void contents before and after HVS trafficking, from cores.

Section	Average Air-Void Content (percent)				
	Before Traffic	First* Wheelpath	Second Wheelpath	Edge* Hump	Middle Hump**
504RF – Top Lift	5.2	4.5		6.0	
Bottom Lift	4.6	2.7		2.6	
505RF – DGAC Overlay	5.8	5.0	4.4	6.8	
Top Lift	5.5	4.7	4.0	4.5	
Bottom Lift	2.9	3.2	2.3	2.0	
506RF – DGAC Overlay	4.7	4.0	4.5	5.0	6.2
Top Lift	4.6	3.7	3.3	3.5	3.2
Bottom Lift	4.7	3.5	4.4	4.0	4.0
507RF – DGAC Overlay	7.9	4.3		7.6	
Top Lift	4.1	3.0		4.4	
Bottom Lift	4.1	2.7		5.7	
512RF – DGAC Overlay	10.3	6.1		9.9	
Top Lift	6.7	5.6		8.7	
Bottom Lift	3.0	5.3		3.1	
513RF – DGAC Overlay	7.1	4.1			
Top Lift	6.2	5.0			
Bottom Lift	4.7	4.3			
508RF – ARHM 62 mm Overlay	12.5	8.3		10.3	
Top Lift	6.4	6.7		6.5	
Bottom Lift	3.5	2.5		3.2	
509RF – ARHM 62 mm Overlay	10.0	7.4	9.1	10.1	
Top Lift	8.7	5.0	6.0	8.1	
Bottom Lift	4.9	3.8	3.5	4.7	
510RF – ARHM 38 mm Overlay	15.2	9.7		11.9	11.6
Top Lift	4.7	3.6		5.6	4.2
Bottom Lift	6.5	2.7		4.3	2.4
511RF – ARHM 38 mm Overlay	17.9	12.8		15.9	
Top Lift	6.4	3.0		5.4	
Bottom Lift	3.3	3.3		3.1	

The results indicate that some densification occurred in the wheelpath of each section. Larger changes in air-void content occurred in the overlays of sections that had larger air-void contents to begin with (510RF, 511RF, 512RF), regardless of mix type. Greater densification occurred in the top and bottom lifts of Goal 1 AC on sections where air-void contents before trafficking were high, as well. None of the layers in any section had air-void contents in the wheelpaths below 2.3 percent after trafficking, and that layer (bottom lift, Section 505RF) had an air-void content of 2.9 percent before trafficking.

Air-void contents in the humps appear to typically fall between those of the untrafficked areas and the wheelpaths, and show no other clear pattern across all sections. During trenching in some sections, it was observed that the material in the top 10 mm of the hump appeared to have a different gradation and air-void content compared to the material below it. There was no method available to sample such a small volume for air-void content and gradation, and the air-void contents measured from the hump cores are averages over the entire height of the overlay layer.

Summary wheelpath air-void contents for each asphalt concrete layer are shown in Table 19, before and after trafficking. The results indicate that the mixes that were poorly compacted to begin with, such as the ARHM-GG overlays, underwent the most densification. The dense graded mixes (DGAC overlay and Goal 1 AC layers) which had good compaction during construction, did not experience much densification despite the hot temperature conditions, heavy loads, and channelized traffic of the HVS. This indicates that good construction compaction helps reduce the amount of densification that occurs under trafficking and reduces the amount of rutting caused by densification.

Comparison of final wheelpath air-void contents (Tables 18, 19) for the same pavement structures and different tire/wheel types indicates that there was not much difference in the densification of any layer under the different tire/wheel types. This indicates that the large differences in rutting performance under the different tire/wheel types can largely be attributed to differences in shear rather than differences in densification.

Table 19 Final wheelpath air-void contents by tire/wheel type and layer type.

Layer	Before Trafficking Average (percent)	Average Final in Wheelpath* (percent)	Minimum Final in Wheelpath* (percent)	Maximum Final in Wheelpath* (percent)
DGAC overlay	7.2	4.6	3.9	6.2
ARHM 62 mm	11.2	8.3	7.4	8.3
ARHM 38 mm	16.6	11.3	9.7	12.7
Top Lift	6.0	4.5	3.0	6.7
Bottom Lift	4.2	3.4	2.3	5.3
Single – Overlay	12.7	8.4		
Single – Top Lift	5.8	4.2		
Single – Bottom Lift	3.8	3.5		
Dual/Radial – Overlay	10.0	7.0		
Dual/Radial – Top Lift	6.0	4.1		
Dual/Radial – Bottom Lift	5.4	3.3		

* largest change of two wheelpaths for dual tires

The change in air-void content in cores taken from the humps indicates that the material in the humps probably did not incur significant densification, nor dilation (Table 20). This indicates shear flow at constant volume. The ARHM-GG overlay sections appeared to have undergone some densification, before material flowed to the humps. Those sections had very large initial air-void contents.

The air-void content of the ATPB layer in Section 510RF was measured before (outside the wheelpath) and after trafficking (inside the wheelpath), and was found to have changed from 31 percent to 25 percent. This indicates that some densification may have occurred in the ATPB.

Table 20 Final hump air-void contents by tire/wheel type and layer type.

Layer	Before Trafficking Average (percent)	Average Final in Hump* (percent)	Minimum Final in Hump* (percent)	Maximum Final in Hump* (percent)
DGAC overlay	7.2	7.6	6.2	10.0
ARHM 62 mm	11.2	8.7	7.1	10.3
ARHM 38 mm	16.6	13.9	11.9	15.9
Top Lift	6.0	5.8	3.2	8.7
Bottom Lift	4.2	4.3	2.0	7.8
Single – Overlay	12.7	11.3		
Single – Top Lift	5.8	5.4		
Single – Bottom Lift	3.8	4.0		
Dual/Radial – Overlay	10.0	8.4		
Dual/Radial – Top Lift	6.0	5.7		
Dual/Radial – Bottom Lift	5.4	5.4		

* largest change in two or three humps in each section

3.3.3 Thickness Changes

Asphalt concrete layer thicknesses from trench slabs are summarized in Table 21. The maximum hump thickness is the largest of the two humps for single wheels and of the three humps for dual wheels. The minimum wheelpath thickness is the smallest of the two wheelpaths for dual wheels. Average layer thicknesses from cores are summarized in Table 22. Limited numbers of measurements of ATPB thickness before and after trafficking are summarized in Table 23.

The few measurements shown in Table 23 indicate that some small decreases in thickness may have occurred in the ATPB layer.

Evaluation of relative rutting in different layers from core and slab thicknesses is somewhat difficult because measurement precision is too close to the size of some of the changes in layer height, and because of differences in height across transverse profiles from construction

Table 21. Thicknesses before and after HVS trafficking, from slabs.

Section	Thickness (mm)		
	Before Traffic	Minimum Wheelpath	Maximum Hump
504RF – Top Lift	78	71	80
Bottom Lift	81	74	81
505RF - DGAC Overlay	54	55	62
Top Lift	72	62	73
Bottom Lift	77	82	83
506RF – DGAC Overlay	78	71	83
Top Lift	80	72	78
Bottom Lift	81	74	76
507RF – DGAC Overlay	76	62	77
Top Lift	76	75	81
Bottom Lift	74	71	77
512RF – DGAC Overlay	49	43	54
Top Lift	65	63	67
Bottom Lift	77	80	76
513RF – DGAC Overlay	80	69	81
Top Lift	72	65	72
Bottom Lift	78	81	82
508RF – ARHM 62 mm Overlay	73	66	75
Top Lift	76	66	75
Bottom Lift	75	72	76
509RF – ARHM 62 mm Overlay	75	65	80
Top Lift	74	64	70
Bottom Lift	72	73	74
510RF – ARHM 38 mm Overlay	35	22	34
Top Lift	64	52	67
Bottom Lift	83	80	81
511RF – ARHM 38 mm Overlay	35	30	35
Top Lift	66	64	76
Bottom Lift	77	74	88

Table 22 Thicknesses before and after HVS trafficking, from cores.

Section	Average Thickness (mm)				
	Before Traffic	First* Wheelpath	Second Wheelpath	Edge* Hump	Middle Hump**
504RF – Top Lift	76	66		76	
Bottom Lift	82	80		82	
505RF - DGAC Overlay	61	51	55	60	60
Top Lift	75	68	68	74	74
Bottom Lift	75	74	64	73	72
506RF – DGAC Overlay	78	70	66	79	82
Top Lift	79	72	72	75	74
Bottom Lift	78	72	72	75	74
507RF – DGAC Overlay	78	68		78	
Top Lift	76	73		78	
Bottom Lift	76	72		74	
512RF – DGAC Overlay	52	45		52	
Top Lift	69	64		69	
Bottom Lift	72	73		70	
513RF – DGAC Overlay	77				
Top Lift	67				
Bottom Lift	78				
508RF – ARHM 62 mm Overlay	66	64		70	
Top Lift	75	66		75	
Bottom Lift	82	73		77	
509RF – ARHM 62 mm Overlay	70	68	72	70	
Top Lift	70	67	71	71	
Bottom Lift	70	72	70	68	
510RF – ARHM 38 mm Overlay	34	30		38	37
Top Lift	61	55		64	64
Bottom Lift	74	78		76	79
511RF – ARHM 38 mm Overlay	38	34		39	
Top Lift	69	62		69	
Bottom Lift	83	78		82	

Table 23 Thickness of ATPB before and after HVS trafficking, from cores.

Section	Average ATPB Thickness (mm)				
	Before Traffic	First* Wheelpath	Second Wheelpath	Edge* Hump	Middle Hump**
505RF	73	66	77	71	70
512RF	70	69		74	
510RF	75	68		72	62
511RF	81			74	

prior to HVS trafficking. However, some patterns can be discerned from the results of Tables 21 and 22, and averages taken across the different experiment variables and summed in Table 24.

Across all sections (Table 24), most of the change in layer thickness in the wheelpaths occurred in the overlay and top lift of Goal 1 AC. Some reductions in thickness occurred in the bottom lift of Goal 1 AC, however they were typically much less than those of the other two layers. Similarly, most increase in thickness in the humps occurred in the overlays.

The DGAC and 62-mm ARHM-GG overlays were of similar thickness, and percentage changes of thickness in these sections result in similar changes of rut depth (Table 24). In general, both overlays show similar percentage decreases in thickness in the wheelpath in the three layers. The percentage increases in thickness in the humps in the three layers are not clear from the core and slab data, except to indicate that there was not much hump development in the bottom lift of Goal 1 AC.

The 38-mm ARHM-GG overlay shows somewhat greater percentage decreases in thickness in the wheelpaths compared to the other two overlays (Table 24). The 38-mm ARHM-GG overlay had the poorest compaction, which should result in more densification and less shear resistance. The small thickness of this layer would also result in a greater concentration of large shear stresses and hotter temperatures in the overlay compared to the structures with thicker overlays.

The dual/radial and wide-base single tires show similar trends with respect to the percentage thickness changes in each layer (Table 24).

Table 24 Summary averages for percent change in thickness of asphalt concrete layers under HVS trafficking.

		Percent Change in Thickness (cores)			Percent Change in Thickness (slabs)		
	Location*	**OL**	**TL**	**BL**	**OL**	**TL**	**BL**
All	wheelpath	-9	-8	-5	-14	-9	-1
	hump	3	1	-3	5	3	3
DGAC	wheelpath	-11	-7	-7	-10	-7	0
	hump	1	-2	-3	7	2	2
ARHM 62	wheelpath	-2	-7	-5	-11	-13	-1
	hump	3	1	-4	5	-3	2
ARHM 38	wheelpath	-12	-10	0	-26	-11	-4
	hump	5	4	1	-1	10	6
Single	wheelpath	-8	-7	-7	-14	-6	-4
	hump	1	2	-3	2	7	7
Dual/radial	wheelpath	-9	-8	0	-20	-14	-3
	hump	5	-1	-2	4	-1	-2

* calculated from maximum hump thickness and minimum wheelpath thickness on each section; OL – overlay, TL – top lift Goal 1 AC, BL – bottom lift Goal 1 AC).

Section 504RF, in which trafficking occurred on the surface of the Goal 1 AC, indicated rutting in both the top and bottom lifts, although core measurements indicate more in the top lift than the bottom lift than do slab measurements (Tables 21, 22). The aircraft wheel (513RF) results show that rutting occurred in the DGAC overlay and top lift of Goal 1 AC, and not in the bottom lift of Goal 1 AC. The results of Sections 507RF and 512RF indicate that the 8°C difference in temperature did not affect the locations where rutting occurred, although it dramatically affected the rate at which it occurred. Most of the rutting and hump development in both sections occurred in the overlay.

3.3.4 Identification of Shear and Densification

A one-percent change in air-void content indicates a one-percent change in the volume of the mix. If it is assumed that volume change occurs in the vertical direction only, then a one percent change in air-void content of a layer should result in a one percent change in height of that layer. At the other extreme, if it is assumed that densification occurs equally in all three principal directions, then a one percent change of air-void content would result in a change in height of 0.33 percent.

One method to evaluate whether rutting in the HVS test sections is primarily due to densification or shear is to evaluate the relationship between changes in air-void content and thickness caused by trafficking. The percent changes in thickness for each layer of each section from the slab and core measurements are included with the change in air-void contents measured from the cores in Table 25.

The percent changes in thickness and air-void content from trafficking were plotted against each other for the wheelpath samples (Figure 20) and hump samples (Figure 21). Included in both figures is a solid line indicating a 1:1 ratio between thickness changes and air-void content changes. If densification in the vertical direction were solely responsible for rutting, then the points in the figure would fall along the 1:1 line. If densification occurs horizontally (both directions) as well as vertically, then the points should fall above the 1:1 line, and if shear flow as well as densification occurs, then the points should fall below the 1:1 line.

The results from the wheelpath samples (Figure 20) indicate that most of the layers had a greater reduction in thickness than densification alone can explain. Although there is some trend

Table 25 Percent change of layer thickness from slabs and cores, and change of air-void content from cores at end of HVS trafficking.

Section	Percent Change of Thickness				Change of Air-Void Content (percent)	
	Wheelpath Cores	Wheelpath Slabs	Hump Cores	Hump Slab	Wheelpath Cores	Hump Cores
504RF – Top Lift	-13	-9	1	2	-0.7	0.8
Bottom Lift	-2	-8	0	0	-1.9	-2.1
505RF – DGAC Overlay	-10	2	-2	16	-1.5	1.0
Top Lift	-9	-13	-1	2	-1.5	-1.0
Bottom Lift	-15	6	-3	8	-0.6	-0.9
506RF – DGAC Overlay	-10	-9	5	7	-0.8	1.5
Top Lift	-10	-10	-7	-3	-0.9	-1.4
Bottom Lift	-8	-9	-5	-6	-1.3	-0.7
507RF – DGAC Overlay	-13	-18	1	1	-3.6	-0.3
Top Lift	-3	-1	3	7	-1.7	-0.3
Bottom Lift	-4	-3	-2	5	0.1	1.1
512RF – DGAC Overlay	-14	-37	1	-3	-4.1	-0.3
Top Lift	-8	-18	-1	6	-1.1	2.1
Bottom Lift	1	-4	-3	-2	2.3	1.4
513RF – DGAC Overlay		-14		0	-3.0	
Top Lift		-3		15	-1.2	
Bottom Lift		-4		14	-0.4	
508RF – ARHM 62 mm Overlay	-2	-13	6	10	-4.1	-2.2
Top Lift	-11	-3	1	3	0.3	0.1
Bottom Lift	-11	4	-6	-1	-1.0	-0.4
509RF – ARHM 62 mm Overlay	-2	-13	0	2	-2.6	-2.8
Top Lift	-4	-9	1	0	-3.7	-0.6
Bottom Lift	2	3	-3	5	-1.0	2.9
510RF – ARHM 38 mm Overlay	-14	-9	9	3	-5.6	-3.4
Top Lift	-10	-13	4	-1	-1.1	0.9
Bottom Lift	5	-4	2	1	-3.8	-2.2
511RF – ARHM 38 mm Overlay	-10	-13	2	7	-5.2	-2.0
Top Lift		-13		-5	-3.4	-1.0
Bottom Lift	-6	2	-1	3	0.0	-0.2

between decreases in air-void content and thickness, most of the data falls below the percent change in thickness corresponding to a 1:1 ratio between densification and thickness change. This indicates that shear flow must be responsible for movement of material out of the wheelpath and into the humps at the sides of the wheelpath. Most of the points that fall above the 1:1 line are for sample that had little change in air-void content or thickness.

The material moved by shear from the wheelpath to the humps appears to undergo the potential for densification, dilation, and no change (Table 25, Figure 21). Air-void content in the humps of all layers typically appears to be distributed within zero to three percent of air-void contents taken in untrafficked areas, which would indicate that the shear flow occurs at close to constant volume. The largest changes in air-void content in the humps occurred in the poorly compacted ARHM-GG overlay layers, indicating that some densification and shear flow occurred to the humps in those sections.

The volume of empty space in the rutted wheelpath below the original surface profile was compared to the volume of material in the hump to evaluate the relative contributions of densification and shear to rut development. The volume of space in the hump is attributable to both reduced density of the material in the wheelpath, and removed volume of material pushed out of the wheelpath and into the humps. Assuming that the material in the humps was moved at constant volume (no densification) by shear, then the ratio of the volume of the humps to the volume of space in the rutted wheelpath is the proportion of the rut attributable to shear. The proportion of rut volume not attributable to shear is attributable to densification.

The calculations were performed using the surface profiles averaged across all data acquisitions performed during HVS trafficking (Table 26), and at a 12.5-mm average maximum

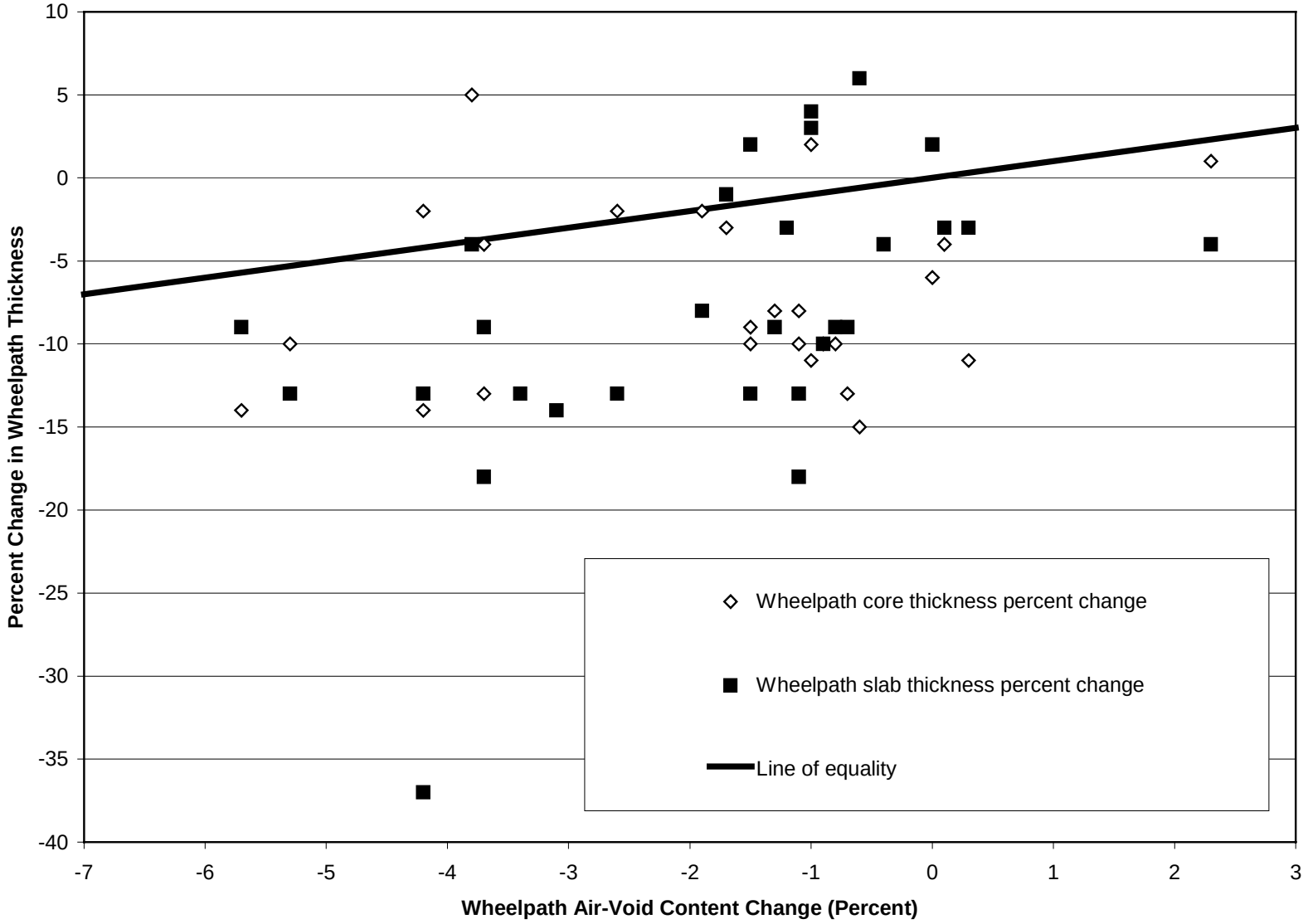

Figure 20. Percent change in layer thickness versus air-void content change from HVS trafficking in the wheelpath.

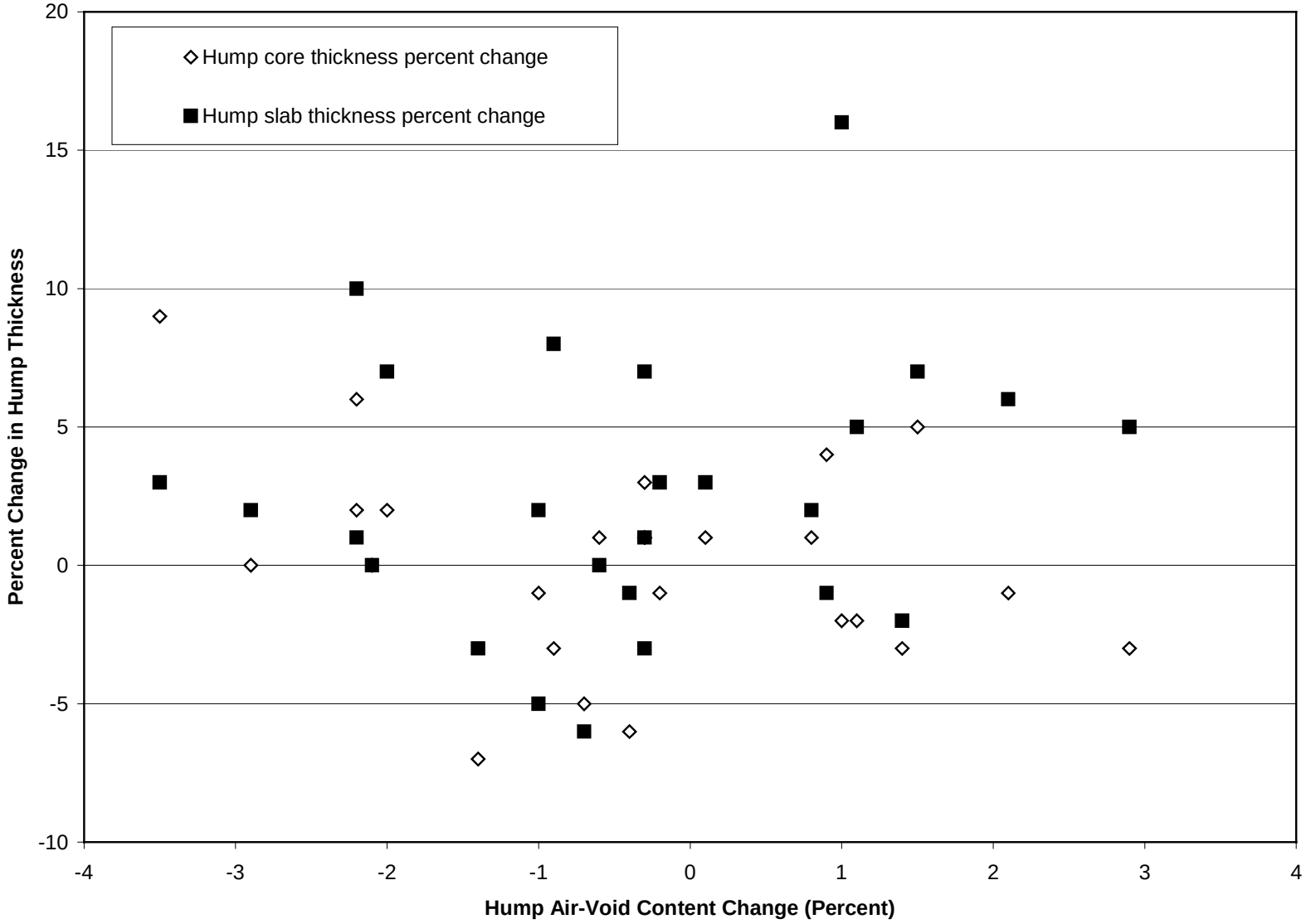

Figure 21. Percent change in layer thickness versus air-void content change from HVS trafficking in the wheelpath.

rut depth (Table 27) for each section, using the laser profilometer data. The results in Tables 26 and 27 indicate that the proportion of rut volume attributable to shear and densification at 12.5 mm is fairly typical of the proportion across all HVS trafficking.

Table 26 Volume of wheelpaths and humps, percent of rut volume attributed to shear (ratio of hump to wheelpath volume) and densification (1-shear), average across all data acquisitions during HVS trafficking.

Section	Final Rut Depth (mm)	Volume Change Along 5 m Section (m^3)					Percent of Wheelpath Rut Volume	
		First Hump	First Wheelpath	Middle Hump	Second Wheelpath	Second Hump	Shear	Densification
505 RF	15.3	0.0016	0.0100	0.0006	0.0084	0.0014	19	81
506 RF	18.9	0.0028	0.0081	0.0010	0.0061	0.0028	47	53
507 RF	21.7	0.0027	0.0139			0.0025	38	62
512 RF	13.4	0.0010	0.0081			0.0010	24	76
513 RF	21.2	0.0012	0.0140			0.0022	24	76
508 RF	19.2	0.0025	0.0098			0.0029	56	44
509 RF	18.1	0.0014	0.0070	0.0008	0.0067	0.0025	34	66
510 RF	17.6	0.0031	0.0051	0.0017	0.0042	0.0024	77	23
511 RF	23.8	0.0053	0.0096			0.0043	100	0

Table 27 Volume of wheelpaths and humps, percent of rut volume attributed to shear (ratio of hump to wheelpath volume) and densification (1-shear), at 13 mm rut depth.

Section	Reps to 13-mm rut depth	Volume Change Along 5 m Section (m^3)					Percent of Wheelpath Rut Volume	
		First Hump	First Wheelpath	Middle Hump	Second Wheelpath	Second Hump	Shear	Densification
505 RF	47,450	0.0023	0.0122	0.0009	0.0105	0.0018	22	78
506 RF	15,773	0.0057	0.0180	0.0020	0.0133	0.0069	47	53
507 RF	1,965	0.0019	0.0132			0.0021	31	69
512 RF	286,079	0.0020	0.0147			0.0019	26	74
513 RF	928	0.0015	0.0193			0.0030	23	77
508 RF	10,498	0.0036	0.0132			0.0038	56	44
509 RF	16,765	0.0030	0.0122	0.0018	0.0118	0.0055	42	58
510 RF	50,239	0.0073	0.0112	0.0040	0.0091	0.0056	83	17
511 RF	5,142	0.0066	0.0106			0.0054	114	-14

The heavily loaded, high pressure aircraft tire produced the most densification and least shear. The wide-base single test on the DGAC overlay at 40°C produced a similar low ratio of shear to densification. The section with the greatest shear, which resulted in little or no net densification in the wheelpath, was the 38-mm ARHM-GG overlay tested by the wide-base single tire (511RF). The other 38-mm ARHM-GG overlay had the next greatest proportion of shear to densification (510RF).

Summary averages of shear and densification proportions are included in Table 28. The DGAC mix had the least proportion of shear, followed by the 62-mm ARHM-GG overlay, and the 38-mm ARHM-GG overlay, on average across tire/wheel types and test temperature. The 38-mm ARHM-GG overlay had the largest air-void content, followed by the 62-mm ARHM-GG overlay and the DGAC overlay. This indicates that poor compaction results in poor shear resistance, which can be responsible for much of the rutting occurring under traffic.

Table 28 Summary averages of percent of rut volume attributed to shear and densification.

	At 12.5 mm average maximum rut depth		**Average across all data acquisitions**	
	Shear	**Densification**	**Shear**	**Densification**
DGAC	30	70	30	70
ARHM 62	49	51	45	55
ARHM 38	99	1	89	11
Wide single	67	33	64	36
Dual radial	57	43	53	47

The wide-base single appeared to have a larger proportion of shear to densification compared to the dual/radial tire.

Plots in Appendix H of wheelpath rut volume, hump volume, and the volume in the wheelpath attributable to densification indicate that densification and shear flow are not

processes that continue simultaneously with a constant ratio between them. Instead, the plot indicate that for nearly all tests there is an initial period of both densification and shearing, followed by alternating periods where either densification or shearing is predominant. The poorly compacted 38-mm ARHM-GG test sections (510RF and 511RF) showed initial densification, followed by several periods of a net increase in volume (dilation).

3.4 Rutting in the Underlying Layers

Transverse profiles were taken on the surface of the aggregate base using the laser profilometer after HVS trafficking was completed. The profiles were obtained by sawing and removing transverse section of the asphalt bound layers, and placing the profilometer in the resulting trench. The transverse profiles are included in Appendix I. The final profiles taken on the surface of the asphalt bound layers are superimposed on the profiles of the aggregate base to show the approximate width of the surface ruts, and therefore the locations in the aggregate base where rutting of the underlying layers should have occurred.

It is difficult to make precise measurements of rutting in the underlying layers from the aggregate base surface profiles because of irregularities in the profiles caused by adhesion of aggregate base to the asphalt bound layers during removal of the slabs, due to the prime coat. There also appear to be small differences in cross slope between the aggregate base and the surface. However, some observations can be made regarding the assumption of the experiment design that no rutting would occur in the aggregate base and below.

The sections with DGAC overlays trafficked at 50°C with the three tire/wheel types appears to have no rutting in the unbound layers (505RF, 506RF, 507RF). The section overlaid

with DGAC and trafficked at 40°C (512RF) also appears to have no rutting in the unbound layers. The section overlaid with DGAC and trafficked with the aircraft wheel appears to have about 5 mm of rut at the top of the aggregate base. This indicates that the 200 mm of asphalt concrete did not provide adequate protection from the high pressure, heavy load aircraft wheel at 50°C, and rutting occurred in the unbound layers after only 3,033 repetitions.

Of the four sections overlaid with ARHM-GG, the two sections trafficked with the dual radial tire/wheel appear to have no rutting in the unbound layers (509RF, 510RF), regardless of the thickness of the ARHM-GG overlay. The two sections trafficked with the wide-base single tire/wheel appear to have some rutting in the unbound layers. The section with the 38-mm ARHM-GG overlay (511RF) appears to have about 4 mm of rut at the top of the aggregate base, and the section with the 62-mm ARHM-GG overlay (508RF) appears to have 1 to 2 mm of rut. Fewer repetitions were placed with the wide-base single than with the dual radial on these sections (Table 16).

The results indicate that at 50°C, the ARHM-GG overlays do not provide as much protection to the unbound layers as do the thicker DGAC overlays for similar load repetitions and the same load. This is to be expected since the ARHM-GG overlays are not as thick, nor as stiff as the DGAC.

The results also indicate that the wide-base single may be more severe for rutting of the unbound layers, as well as for the asphalt bound layers.

3.5 Late Bonding of Layers

As reported in References (5-9), the test pavement constructed at the Pavement Research Center was observed to have no bond between asphalt concrete layers. The test pavement was constructed following the Caltrans Method Specification, which does not require a tack coat between lifts except under special circumstances or if the resident engineer requests it. The conditions under which the HVS test sections were constructed were ideal for bonding between lifts without the use of a tack coat – there was no exposure to dust or rain, and because the sections were constructed inside a building, the lifts retained plenty of heat and should have formed an excellent bond.

Cores taken from just outside the wheelpath of the rutting test sections showed no bond between asphalt lifts. However, after HVS trafficking during rutting tests, some cores taken from inside the wheelpath these sections showed that a bond between asphalt layers had indeed been formed. This bond was likely due to the high temperature of the pavement, the stress under the HVS wheel load, and possibly some "kneading" action caused by the permanent deformation and material flow taking place during the test.

Caltrans field representatives have often reported observing a bond between asphalt lifts even when no tack coat was used between successive lifts during their construction. This observation has been suggested as a rationale for the Caltrans Method Specification, which in most cases does not require a tack coat. Given that no such bond was observed on the untrafficked HVS test sections, which were also constructed without use of a tack coat, but which were constructed under ideal conditions to enable a bond to form (e.g., high temperature, no wind, no exposure to dust or water), it is suggested that the bond observed in the field may only form after exposure to traffic and high temperatures.

Before this bond between layers forms, a period may exist during which a bond is not present and the bottom of the top lift experiences strains which may lead to preventable fatigue cracking and which could be mitigated by the use of a tack coat between lifts. References (5-9) provide an in-depth discussion of how a bond between layers can significantly increase the fatigue life of asphalt pavements.

4.0 CONCLUSIONS AND RECOMMENDATIONS

4.1 Conclusions

The following conclusions were drawn from the results presented in this report:

1. ARHM-GG cools very quickly after placement, particularly when placed in 38-mm lifts, as opposed to 62-mm lifts. Average air-void contents of 16.6 and 12.2 percent were found for the thin and thick ARHM-GG overlays on this project prior to construction. Extra attention must be placed on temperature control of this material during compaction to obtain good compaction.

2. Overall, the 62-mm ARHM-GG and 50- to 75-mm DGAC overlays had similar performance, and the 38-mm ARHM-GG overlay had superior performance, under dual/radial loading. Both ARHM-GG overlays had better performance than the DGAC overlay under wide-base single loading. The rutting performance of the ARHM-GG was therefore concluded to be generally similar to that of the DGAC, after consideration of as-built binder contents and compaction.

3. Low Hveem stabilometer values obtained for the ARHM-GG mix were not reflected by the performance of the mix under HVS loading. Better methods of characterizing rutting performance of ARHM-GG mixes are needed.

4. The ranking of repetitions to a 12.5-mm rut failure on the DGAC overlay was (best to worst): dual/bias-ply, dual/radial, wide-base single, aircraft. The ranking on the ARHM overlays was dual/radial, wide-base single. The wide-base single had 0.05 to 0.61 times the repetitions to failure of the dual/radial, depending upon the overlay type and thickness.

These results indicate that rutting damage will increase if the use of wide-base single tires becomes more widespread.

5. The temperature difference of 8°C at a 50-mm depth between two otherwise similar tests resulted in 140 times more load repetitions being applied before rutting failure on the cooler section compared to the hotter section. The results emphasize the need to account for local project pavement temperatures in the mix design process.

6. Air-void contents of cores taken in the wheelpath after trafficking showed relatively little densification, except when the overlays were poorly compacted, despite final rut depths of 15 to 24 mm. The average proportion of rut depth attributable to shear flow as opposed to densification varied between 19 to 100 percent, depending on the overlay type. The greatest shear flow occurred on the 38-mm ARHM-GG sections, and the least on the DGAC sections. These results indicate that rutting did not consist of a process of densification to a very low air-void content followed by rapid shear flow. Instead, it appears that rutting consists of simultaneous densification and shear flow, with the rates of shearing and densification varying at different periods of rut development. The performance of the poorly compacted ARHM-GG mixes indicates that considerable shear flow occurs at high air-void contents.

7. The protection against rutting provided to the underlying layers at elevated temperatures by the ARHM-GG overlays appears to be less than that provided by the DGAC overlays. This is expected due to the greater thickness and stiffness of the DGAC overlays. The 2:1 structural equivalence ratio between ARHM-GG and DGAC for overlays should not be extended to the unbound layers rutting distress mechanism.

4.2 Recommendations

The following recommendations are based on the results and conclusions presented in this report:

1. The use of ARHM-GG overlays up to at least 62 mm thick does not appear to incur a greater risk of rutting of the pavement surface at elevated temperatures. The limitation of use of ARHM-GG in hot environments does not appear to be warranted, provided that the overlay is designed to adequately resist rutting.

2. The implementation of a better method for mix design of ARHM-GG is warranted. The use of the Repeated Simple Shear Test at Constant Height (RSST-CH) is being investigated as part of this project. If those results indicate that the RSST-CH and the mechanistic-empirical procedure used to predict rutting from its results are applicable for this project, its implementation for ARHM-GG mix design should be considered.

3. Implementation of mechanistic-empirical mix design procedures that incorporate the effects of project temperature should be implemented. A difference of only 8°C resulted in a significant difference in rutting performance. Use of a single evaluation temperature in the current Caltrans procedure is likely producing over-conservative mixes for cooler regions, thus increasing the probability of cracking. The current criteria may not be adequate for very hot desert regions of California.

4. The method specification for compaction of ARHM-GG can result in very high air-void contents. Improvement of ARHM-GG compaction will result in better performance for both rutting and cracking. Quality Control/Quality Assurance (QC/QA) procedures for ARHM-

GG should be implemented. As a preliminary step, use of end-result specifications for ARHM-GG compaction should be implemented immediately.

5. Caltrans should closely monitor use of wide-base single tires on California highways. Increased use poses a risk of increased rutting.

6. Caltrans should monitor tire pressures, as well as loads, on the truck fleet using California highways. The increased rutting under the wide-base single and the aircraft wheel found in this study indicate that increased tire pressures will increase the risk of rutting. Rational adjustment of mix design criteria should be evaluated periodically as tire pressures continue to increase.

7. The ARHM-GG structural equivalencies for fatigue and reflection cracking should not be used for pavement design for the design criterion of rutting of the unbound layers.

5.0 REFERENCES

1. Shatnawi, S. 1999. *Performance of Asphalt Rubber Mixes in California*. Submitted to the International Journal of Pavement Engineering, July.

2. Maintenance Program, Pavement Management Information Branch. *1995 State of the Pavement*. California Department of Transportation, Sacramento, November.

3. Office of Office Engineer, Division of Construction. *1993 Contract Cost Data*. California Department of Transportation, Sacramento.

4. *Standard Tests*, California Department of Transportation, Sacramento, 1995.

5. Harvey, J., L. du Plessis, F. Long, S. Shatnawi, C. Scheffy, B. Tsai, I, Guada, D. Hung, N. Coetzee, M. Reimer, and C. L. Monismith, Initial CAL/APT Program: Site Information, Test Pavement Construction, Pavement Materials Characterizations, Initial CAL/HVS Test Results, and Performance Estimates, Pavement Research Center, CAL/APT Program, Institute of Transportation Studies, University of California, Berkeley, June 1996.

6. Harvey, J., L. du Plessis, F. Long, J. Deacon, I, Guada, D. Hung, and C. Scheffy, CAL/APT Program: Test Results from Accelerated Test on Pavement Structure Containing Asphalt Treated Permeable Base (ATPB)—Section 500RF, Pavement Research Center, CAL/APT Program, Institute of Transportation Studies, University of California, Berkeley, June 1997.

7. Harvey, J., J. Prozzi, J. Deacon, D. Hung, I. Guada, L. du Plessis, F. Long and C. Scheffy, CAL/APT Program: Test Results from Accelerated Pavement Test on Pavement Structure Containing Aggregate Base (AB) - Section 501RF, Report for the California Department of Transportation, Institute of Transportation Studies, University of California, Berkeley, April, 1999 (Draft submitted September, 1997).

8. Harvey, J., I, Guada, C. Scheffy, L. Louw, J. Prozzi, and D. Hung, CAL/APT Program: Test Results from Accelerated Pavement Test on Pavement Structure Containing Asphalt Treated Permeable Base—Section 502CT, Draft Report, Pavement Research Center, CAL/APT Program, Institute of Transportation Studies, University of California, Berkeley, February 1998.

9. Harvey, J., D. Hung, J. Prozzi, L. Louw, C. Scheffy, and I. Guada, CAL/APT Program: Test Results from Accelerated Pavement Test on Pavement Structure Containing Untreated Aggregate Base—Section 503RF, Draft Report, Pavement Research Center, CAL/APT Program, Institute of Transportation Studies, University of California, Berkeley, December 1997.

10. University of California Berkeley Pavement Research Center; Dynatest Consulting, Inc.; Division of Roads and Transport Technology, CSIR. 1997. *Test Plan for CAL/APT Goal 3.* Test Plan prepared for the California Department of Transportation, 1997.

11. Harvey, J., N. Coetzee and L. Louw, Design and Construction of CAL/APT Goal 3 DGAC and ARHM-GG Overlays, and Review of Caltrans Design and Construction Methods, Draft Report prepared for California Department of Transportation. CAL/APT Program, Pavement Research Center, Institute of Transportation Studies, University of California, Berkeley, December, 1999.

12. Dynatest Consulting, Inc. ELMOD Version 3.0 1988, Version 4.0 1999, Ojai, California.

13. *Standard Specifications*, California Department of Transportation, Sacramento, July, 1995.

14. Asphalt Institute Research Center, *Superpave Asphalt Mixture Analysis, Advanced Course Text for the National Asphalt Training Center II*, Prepared for Federal Highway Administration Office of Technology Applications, Washington, D. C., January, 1996.

15. Rust, F., L. Du Plessis, B. Verhaeghe, and J. Grobler. "Heavy Vehicle Simulator Testing of Trial Sections for Caltrans," Report prepared for Caltrans, DPVT C/255, CSIR, Pretoria, South Africa, October 1993.

16. Ardila-Coulson, M., D. Coulson, and P. Sebaaly, Extent of Use and Performance Traits of Super-Single Tires, Draft report prepared for National Cooperative Highway Research Program, University of Nevada, Reno, February, 1998.

17. Bell, C. and S. Randhawa, Truck Tire Issues: Evaluation of Impacts of High Pressure Tires and Single-Tired Axles in Oregon, Transportation Research Report 92-17, Transportation Research Institute, Oregon State University, Corvallis, November, 1992.

18. de Beer, M. and C. Fisher, Contact Stresses of Pneumatic Tires Measured with the Vehicle-Road Surface Pressure Transducer Army (VRSPTA) System for the University of California at Berkeley (UCB) and The Nevada Automotive Test Center (NATC). Vols. 1 and 2., Transportek, CSIR, South Africa, June 1997.

APPENDIX A: CALTRANS ARHM-GG/DGAC THICKNESS EQUIVALENCIES

Table A-1 California Structural Equivalencies.

Lift Thickness (mm)		
Dense Graded Asphalt Concrete (DGAC)	**Asphalt Rubber Hot Mix, Gap Graded (ARHM-GG)***	**Asphalt Rubber Hot Mix, Gap Graded with Stress Absorbing Material Interface (ARHM-GG/SAMI)**
45	30**	-
60	30	-
75	45	30
90	45	30
105	60	45
120	60	45
135	45†	60
150	45‡	60
165	60†	45†
180	60‡	45‡

Notes:
* The maximum allowable non-experimental equivalency for ARHM-GG is 2:1.
** The minimum allowable ARHM-GG lift thickness is 30 mm.
† Place 45 mm of new DGAC first.
‡ Place 60 mm of new DGAC first.

Table A-2 California Reflective Crack Retardation Equivalencies.

Lift Thickness (mm)		
Dense Graded Asphalt Concrete (DGAC)	**Asphalt Rubber Hot Mix, Gap Graded (ARHM-GG)***	**Asphalt Rubber Hot Mix, Gap Graded with Stress Absorbing Material Interface (ARHM-GG/SAMI)**
45	30*	-
60	30	-
75	45	-
90	45	-
105**	45†	30‡

Notes:
* The minimum allowable ARHM-GG lift thickness is 30 mm.
** A DGAC thickness of 106 mm is the maximum thickness recommended by Caltrans for mitigation of reflection cracking.
† Use 45 mm if the crack width is less than 3 mm and 60 mm if the crack width is equal to or greater than 3 mm.
‡ Use if the crack width is equal to or greater than 3 mm. If less than 3 mm, use another strategy.

APPENDIX B: THICKNESS DATA FROM CORES AND TRENCH SLABS

The following key applies to all tables in this Appendix:

Specimen Labeling:
[Test Section]-[Point Location]-[Transverse Location]-[Bonding]
Test Section – Test number (e.g. 503, 514)
Point Location – Test Section Measuring Points (0 - 16, for most sections)
Transverse Location - Type of Specimen (e.g. W, H, I, O)

W- In the Wheel Path; for dual tires further specification of Left (L) or Right (R) side, Caravan (C) or Traffic (T) side required

H- In the Hump, caused by shear flow. If the specimen comes from between two dual tires, the specimen is a 100 mm core

I- Outside the hump within the heated area; also out of the wheel path

O- Outside the heated area. Not necessarily adjacent to the measuring point

Bonding - Either Bonded (B), Not Bonded (NB), or Broken Bond (BB). Broken Bond (BB) was bonded but broken during core removal

Specimen heights are measured at four locations for the different asphalt layers

After cores are cut down to 50 mm specimens for testing, the lifts are identified as follows

O (or OL) - The Overlay, either DGAC or ARHM

T (or TL) - The Top Lift of Goal 1 Construction

B (or BL) - The Bottom Lift of Goal 1 Construction

Table B-1 Thickness Data from Before Trafficking.

Section	Point Loc.	Transverse Loc.	Layer	Thickness (mm)	Section	Layer	Average	Std. Dev.
504	504-TL-L2	Outside	Top Lift	75	504	TL	76	1
504	504-TL-L1	Outside	TL	76				
504	504-BL-L1	Outside	BL	81	504	BL	82	2
504	504-BL-L2	Outside	BL	83				
505	12	I	ATPB	70	505	ATPB	73	4
505	6	I	ATPB	76				
505	6	I	BL	75	505	BL	75	0
505	12	I	Bottom Lift	75				
505	12	I	OL	59	505	OL	61	3
505	6	I	OL	63				
505	6	I	TL	75	505	TL	75	0
505	12	I	TL	75				
506	6	I	BL	73	506	BL	78	4
506	10	I	BL	76				
506	3	I	BL	76				
506	10	O	BL	78				
506	6	O	BL	83				
506	3	O	BL	84				
506	10	I	OL	76	506	OL	78	3
506	6	I	OL	77				
506	10	O	OL	77				
506	6	O	OL	78				
506	3	O	OL	81				
506	3	I	OL	82				
506	10	I	TL	75	506	TL	79	3
506	3	I	TL	78				
506	6	I	TL	78				
506	10	O	TL	81				
506	6	O	TL	82				
506	3	O	TL	84				
507		Outside in box	BL	76	507	BL	76	1
507		Outside in box	BL	75				
507		Outside in box	OL	78	507	OL	78	1
507		Outside in box	OL	77				
507		Outside in box	TL	77	507	TL	76	2
507		Outside in box	TL	74				
508	8	I	BL	76	508	BL	82	5
508	5	I	BL	78				
508	11	I	BL	80				
508	8	O	BL	84				
508	5	O	BL	87				
508	11	O	BL	88				
508	5	O	OL	64	508	OL	66	2
508	8	O	OL	64				
508	11	O	OL	65				
508	5	I	OL	66				

Section	Point Loc.	Transverse Loc.	Layer	Thickness (mm)	Section	Layer	Average	Std. Dev.
508	8	I	OL	67				
508	11	I	OL	69				
508	5	I	TL	72	508	TL	75	2
508	11	I	TL	73				
508	8	I	TL	74				
508	11	O	TL	75				
508	5	O	TL	76				
508	8	O	TL	77				
509	8	I	BL	67	509	BL	70	3
509	11	I	BL	68				
509	5	O	BL	68				
509	11	O	BL	72				
509	8	O	BL	72				
509	5	I	BL	74				
509	8	O	OL	68	509	OL	70	1
509	5	O	OL	70				
509	11	O	OL	71				
509	8	I	TL	65	509	TL	70	4
509	5	O	TL	67				
509	5	I	TL	72				
509	11	O	TL	72				
509	8	O	TL	75				
510	5.2	I	ATPB	69	510	ATPB	75	4
510	8	I	ATPB	75				
510	5	I	ATPB	76				
510	5.2	I	ATPB	80				
510	5	I	BL	70	510	BL	74	5
510	5.2	I	BL	71				
510	8	I	BL	78				
510	5.2	I	BL	79				
510	5.2	I	OL	26	510	OL	34	6
510	5	I	OL	37				
510	5.2	I	OL	37				
510	8	I	OL	38				
510	5.2	I	TL	58	510	TL	61	3
510	5	I	TL	61				
510	5.2	I	TL	61				
510	8	I	TL	65				
511	11	I	ATPB	76	511	ATPB	81	5
511	8	I	ATPB	81				
511	5	I	ATPB	85				
511	8	I	BL	81	511	BL	83	3
511	5	I	BL	82				
511	11	I	BL	86				
511	5	I	OL	36	511	OL	38	2
511	8	I	OL	38				
511	11	I	OL	40				

Section	Point Loc.	Transverse Loc.	Layer	Thickness (mm)	Section	Layer	Average	Std. Dev.
511	5	I	TL	65	511	TL	69	3
511	11	I	TL	70				
511	8	I	TL	71				
512	12	I	ATPB	70	512	ATPB	70	1
512	9	I	ATPB	71				
512	12	I	BL	72	512	BL	72	0
512	9	I	BL	73				
512	9	I	OL	51	512	OL	52	1
512	12	I	OL	52				
512	9	I	TL	67	512	TL	69	3
512	12	I	TL	71				
513	12	O	BL	75	513	BL	78	3
513	5	O	BL	80				
513	5	I	BL	80				
513	5	O	OL	76	513	OL	77	1
513	5	I	OL	77				
513	12	O	OL	79				
513	5	I	TL	63	513	TL	67	3
513	5	O	TL	69				
513	12	O	TL	69				

Table B-2 Thickness in the Wheelpaths after Trafficking.

Section	Point Loc.	Transverse Loc.	Layer	Thickness (mm)	Section	layer	location	average	Std. Dev.
504	504-TL-W2	Wheel	TL	62	504	TL	W	66	5.8
504	504-TL-W1	Wheel	TL	70					
504	504-BL-W2	Wheel	BL	85	504	BL		80	6.2
504	504-BL-W1	Wheel	BL	76					
505	9	WC	TL	66	505	TL	W1	68	3.0
505	12	WC	TL	67					
505	6	WC	TL	72					
505	9	WT	TL	67	505	TL	W2	68	0.9
505	12	WT	TL	68					
505	6	WT	TL	69					
505	12	WC	OL	50	505	OL	W1	51	0.5
505	6	WC	OL	51					
505	9	WC	OL	51					
505	12	WT	OL	54	505	OL	W2	55	0.8
505	9	WT	OL	55					
505	6	WT	OL	56					
505	9	WC	BL	68	505	BL	W1	74	5.2
505	6	WC	BL	74					
505	12	WC	BL	79					
505	9	WT	BL	61	505	BL	W2	64	2.4
505	12	WT	BL	63					
505	6	WT	BL	66					
505	12	WC	ATPB	62	505	ATPB	W1	66	5.2
505	6	WC	ATPB	66					
505	9	WC	ATPB	72					
505	6	WT	ATPB	73	505	ATPB	W2	77	4.2
505	9	WT	ATPB	79					
505	12	WT	ATPB	81					
506	10	LW	TL	69	506	TL	W1	72	2.9
506	3	LW	TL	72					
506	6	LW	TL	75					
506	10	RW	TL	68	506	TL	W2	72	3.2
506	3	RW	TL	73					
506	6	RW	TL	74					
506	10	LW	OL	66	506	OL	W1	70	4.9
506	6	LW	OL	71					
506	3	LW	OL	75					
506	10	RW	OL	60	506	OL	W2	66	6.5
506	6	RW	OL	66					
506	3	RW	OL	73					
506	3	LW	BL	71	506	BL	W1	72	1.2
506	6	LW	BL	72					
506	10	LW	BL	74					
506	6	RW	BL	71	506	BL	W2	72	1.3
506	3	RW	BL	73					
506	10	RW	BL	74					

Section	Point Loc.	Transverse Loc.	Layer	Thickness (mm)	Section	layer	location	average	Std. Dev.
507		Wheel	TL	73	507	TL	W	73	
507		Wheel	OL	68	507	OL	W	68	
507	6	W	BL	72	507	BL	W	72	
508	11	W	TL	64	508	TL	W	66	2.0
508	8	W	TL	67					
508	5	W	TL	68					
508	5	W	OL	59	508	OL	W	64	4.2
508	11	W	OL	65					
508	8	W	OL	68					
508	8	W	BL	68	508	BL	W	73	4.5
508	5	W	BL	74					
508	11	W	BL	76					
509	11	WC	TL	67	509	TL	W1	67	
509	11	WT	TL	70	509	TL	W2	71	2.0
509	8	WT	TL	72					
509	8	WC	OL	67	509	OL	W1	68	1.9
509	11	WC	OL	68					
509	5	WC	OL	71					
509	5	WT	OL	71	509	OL	W2	72	0.6
509	11	WT	OL	72					
509	8	WT	OL	72					
509	5	WC	BL	72	509	BL	W1	72	
509	11	WT	BL	66	509	BL	W2	70	4.3
509	5	WT	BL	71					
509	8	WT	BL	74					
510	5.2	W	TL	58	510	TL	W	55	3.7
510	5.2	W	TL	53					
510	5.2	W	OL	31	510	OL	W	30	1.2
510	5.2	W	OL	29					
510	5.2	W	BL	80	510	BL	W	78	1.9
510	5.2	W	BL	77					
510	5.2	W	ATPB	69	510	ATPB	W	68	1.3
510	5.2	W	ATPB	67					
511	5	W	TL	60	511	TL	W	62	1.5
511	11	W	TL	62					
511	8	W	TL	63					
511	8	W	OL	32	511	OL	W	34	2.5
511	5	W	OL	34					
511	11	W	OL	37					
511	8	W	BL	76	511	BL	W	78	3.2
511	5	W	BL	76					
511	11	W	BL	81					
512	9	W	TL	62	512	TL	W	64	1.9
512	12	W	TL	65					
512	6	W	TL	65					
512	12	W	OL	44	512	OL	W	45	0.8
512	9	W	OL	45					

Section	Point Loc.	Transverse Loc.	Layer	Thickness (mm)	Section	layer	location	average	Std. Dev.
512	6	W	OL	46					
512	12	W	BL	69	512	BL	W	73	4.1
512	6	W	BL	74					
512	9	W	BL	77					
512	9	W	ATPB	66	512	ATPB	W	69	3.3
512	12	W	ATPB	69					
512	6	W	ATPB	73					

Table B-3 Thickness of the Humps After Trafficking.

Section	Point Loc.	Transverse Loc.	Layer	Thickness (mm)	Section	layer	location	average	Std. Dev.
504	504-TL-H1	Hump	TL	77	504	TL	H	76	0.9
504	504-TL-H2	Hump	TL	76					
504	504-BL-H2	Hump	BL	83	504	BL	H	82	1.2
504	504-BL-H1	Hump	BL	81					
505	9	Hump	TL	72	505	TL	H	74	1.7
505	6	Hump	TL	74					
505	12	Hump	TL	75					
505	9	MH	TL	71	505	TL	Hm	74	4.2
505	6	MH	TL	77					
505	12	Hump	OL	58	505	OL	H	60	1.6
505	9	Hump	OL	60					
505	6	Hump	OL	61					
505	9	MH	OL	59	505	OL	Hm	60	1.6
505	6	MH	OL	61					
505	9	Hump	BL	71	505	BL	H	73	2.7
505	6	Hump	BL	72					
505	12	Hump	BL	76					
505	9	MH	BL	69	505	BL	Hm	72	4.7
505	6	MH	BL	76					
505	12	Hump	ATPB	68	505	ATPB	H	71	3.0
505	9	Hump	ATPB	72					
505	6	Hump	ATPB	74					
505	9	MH	ATPB	64	505	ATPB	Hm	70	8.7
505	6	MH	ATPB	76					
506	10	Hump	TL	74	506	TL	H	75	1.4
506	3	Hump	TL	76					
506	3	MH	TL	73	506	TL	Hm	74	0.4
506	10	MH	TL	74					
506	10	Hump	OL	76	506	OL	H	79	4.9
506	3	Hump	OL	83					
506	10	MH	OL	79	506	OL	Hm	82	4.6
506	3	MH	OL	85					
506	3	Hump	BL	74	506	BL	H	75	1.1
506	10	Hump	BL	76					
506	3	MH	BL	72	506	BL	Hm	74	3.0
506	10	MH	BL	77					
507	507-TL-HW	Hump	TL	77	507	TL	H	78	0.9
507	507-TL-HE	Hump	TL	79					
507	507-OL-HW	Hump	OL	78	507	OL	H	78	0.1
507	507-OL-HE	Hump	OL	79					
507	507-BL-HE	Hump	BL	74	507	BL	H	74	0.6
507	507-BL-HW	Hump	BL	74					
508	11	Hump	TL	73	508	TL	H	75	2.6
508	5	Hump	TL	74					
508	8	Hump	TL	78					
508	5	Hump	OL	69	508	OL	H	70	0.7

Section	Point Loc.	Transverse Loc.	Layer	Thickness (mm)	Section	layer	location	average	Std. Dev.
508	8	Hump	OL	70					
508	11	Hump	OL	70					
508	8	Hump	BL	76	508	BL	H	77	0.9
508	5	Hump	BL	77					
508	11	Hump	BL	78					
509	11	Hump	TL	70	509	TL	H	71	1.4
509	8	Hump	TL	70					
509	5	Hump	TL	72					
509	5	Hump	OL	64	509	OL	H	70	5.0
509	8	Hump	OL	72					
509	11	Hump	OL	73					
509	11	Hump	BL	62	509	BL	H	68	5.9
509	5	Hump	BL	70					
509	8	Hump	BL	73					
510	5	Hump	TL	63	510	TL	H	64	1.4
510	11	Hump	TL	63					
510	8	Hump	TL	65					
510	5.2	Hump-middle	TL	64	510	TL	Hm	64	
510	8	Hump	OL	36	510	OL	H	38	2.7
510	5	Hump	OL	36					
510	11	Hump	OL	41					
510	5.2	Hump-middle	OL	37	510	OL	Hm	37	
510	5	Hump	BL	66	510	BL	H	76	8.7
510	11	Hump	BL	79					
510	8	Hump	BL	83					
510	5.2	Hump-middle	BL	79	510	BL	Hm	79	
510	8	Hump	ATPB	67	510	ATPB	H	72	6.1
510	11	Hump	ATPB	71					
510	5	Hump	ATPB	79					
510	5.2	Hump-middle	ATPB	62	510	ATPB	Hm	62	
511	5	Hump	TL	66	511	TL	H	69	2.5
511	11	Hump	TL	69					
511	8	Hump	TL	71					
511	5	Hump	OL	37	511	OL	H	39	1.4
511	8	Hump	OL	39					
511	11	Hump	OL	40					
511	8	Hump	BL	80	511	BL	H	82	1.6
511	5	Hump	BL	82					
511	11	Hump	BL	84					
511	11	Hump	ATPB	78	511	ATPB	H	79	0.8
511	5	Hump	ATPB	79					
511	8	Hump	ATPB	80					
512	9	Hump	TL	66	512	TL	H	69	2.7
512	6	Hump	TL	70					
512	12	Hump	TL	70					
512	9	Hump	OL	51	512	OL	H	52	2.1
512	12	Hump	OL	51					

Section	Point Loc.	Transverse Loc.	Layer	Thickness (mm)	Section	layer	location	average	Std. Dev.
512	6	Hump	OL	55					
512	12	Hump	BL	63	512	BL	H	70	8.8
512	9	Hump	BL	68					
512	6	Hump	BL	80					
512	6	Hump	ATPB	70	512	ATPB	H	74	3.2
512	9	Hump	ATPB	74					
512	12	Hump	ATPB	77					

APPENDIX C: AIR-VOID CONTENT DATA

The following key applies to all tables in this Appendix.

Specimen Labeling:
[Test Section]-[Point Location]-[Transverse Location]-[Bonding]
Test Section - Test number (e.g. 503, 514)
Point Location - Test Section Measuring Points (0 - 16, for most sections)
Transverse Location - Type of Specimen (e.g. W, H, I, O)

W- In the Wheel Path; for dual tires further specification of Left (L) or Right (R) side, Caravan (C) or Traffic (T) side required

H- In the Hump, caused by shear flow. If the specimen comes from between two dual tires, the specimen is a 100 mm core

I- Outside the hump within the heated area; also out of the wheel path

O- Outside the heated area. Not necessarily adjacent to the measuring point

Bonding - Either Bonded (B), Not Bonded (NB), or Broken Bond (BB). Broken Bond (BB) was bonded but broken during core removal

Specimen heights are measured at four locations for the different asphalt layers

After cores are cut down to 50 mm specimens for testing, the lifts are identified as follows

O (or OL) - The Overlay, either DGAC or ARHM

T (or TL) - The Top Lift of Goal 1 Construction

B (or BL) - The Bottom Lift of Goal 1 Construction

Table C-1 Air-Void Contents Before Trafficking.

Section	Point Loc.	Transverse Loc.	Layer	Air Void (%)	Section	Layer	Average	Std. Dev.
504	504-TL-L2	Outside	TL	5.4	504	TL	5.2	0.3
504	504-TL-L1	Outside	TL	5.0				
504	504-BL-L1	Outside	BL	3.3	504	BL	4.6	1.8
504	504-BL-L2	Outside	BL	5.9				
505	9	I	TL	4.5	505	TL	5.5	1.7
505	6	I	TL	4.7				
505	12	I	TL	4.8				
505	6	O	TL	8.1				
505	6	I	OL	3.7	505	OL	4.0	0.4
505	9	I	OL	3.8				
505	12	I	OL	4.5				
505	12	I	BL	2.2	505	BL	2.9	1.2
505	6	I	BL	2.4				
505	9	I	BL	2.4				
505	6	O	BL	4.7				
506	3	I	TL	3.8	506	TL	4.6	0.7
506	10	I	TL	3.8				
506	6	I	TL	4.3				
506	6	O	TL	5.1				
506	10	O	TL	5.3				
506	3	O	TL	5.5				
506	6	I	OL	1.8	506	OL	2.9	0.9
506	3	I	OL	2.0				
506	10	I	OL	3.1				
506	3	O	OL	3.6				
506	10	O	OL	3.8				
506	3	I	BL	4.0	506	BL	4.7	0.6
506	6	I	BL	4.1				
506	10	I	BL	4.9				
506	3	O	BL	5.3				
506	6	O	BL	5.3				
507	10	I	TL	3.8	507	TL	4.7	1.4
507		Outside in box	TL	4.0				
507		Outside in box	TL	7.2				
507	6	I	TL	4.3				
507	3	I	TL	4.3				
507	3	I	OL	4.8	507	OL	6.1	1.5
507	6	I	OL	5.3				
507		Outside in box	OL	8.2				
507		Outside in box	OL					
507	10	I	OL	5.9				
507	10	I	BL	3.0	507	BL	4.6	1.4
507		Outside in box	BL	4.2				
507		Outside in box	BL	6.4				
507	6	I	BL	3.8				
507	3	I	BL	5.5				

Section	Point Loc.	Transverse Loc.	Layer	Air Void (%)	Section	Layer	Average	Std. Dev.
508	8	I	TL	5.2	508	TL	6.4	0.7
508	8	O	TL	6.1				
508	11	O	TL	6.2				
508	5	I	TL	6.7				
508	5	O	TL	7.1				
508	11	I	TL	7.2				
508	11	I	OL	7.3	508	OL	10.2	2.3
508	8	I	OL	8.0				
508	5	I	OL	9.6				
508	5	O	OL	11.4				
508	11	O	OL	11.9				
508	8	O	OL	12.9				
508	8	I	BL	2.3	508	BL	3.5	0.9
508	11	I	BL	3.0				
508	8	O	BL	3.1				
508	5	O	BL	4.2				
508	5	I	BL	4.2				
508	11	O	BL	4.4				
509	5	I	TL	6.3	509	TL	8.7	2.4
509	8	I	TL	8.8				
509	11	I	TL	11.1				
509	5	I	OL	7.1	509	OL	7.6	0.7
509	11	I	OL	7.4				
509	8	I	OL	8.4				
509	8	I	BL	3.6	509	BL	4.9	1.7
509	11	I	BL	4.2				
509	5	I	BL	6.7				
510	5.2	I	TL	4.4	510	TL	4.7	0.4
510	5	I	TL	4.4				
510	4.8	I	TL	5.1				
510	5.2	I	TL	5.1				
510	5.2	I	OL	9.4	510	OL	13.0	3.7
510	5.2	I	OL	16.9				
510	4.8	I	OL	12.9				
510	5.2	I	BL	4.4	510	BL	6.5	1.7
510	5	I	BL	5.8				
510	4.8	I	BL	7.4				
510	5.2	I	BL	8.3				
511	8	I	TL	5.6	511	TL	6.4	0.8
511	11	I	TL	6.5				
511	5	I	TL	7.1				
511	11	I	OL	15.4	511	OL	15.8	0.5
511	5	I	OL	16.1				
511	11	I	BL	1.8	511	BL	3.3	1.5
511	8	I	BL	3.2				
511	5	I	BL	4.9				
512	9	I	TL	5.9	512	TL	6.7	1.1

Section	Point Loc.	Transverse Loc.	Layer	Air Void (%)	Section	Layer	Average	Std. Dev.
512	6	I	TL	7.4				
512	6	I	OL	7.0	512	OL	8.5	2.1
512	9	I	OL	10.0				
512	6	I	BL	2.9	512	BL	3.0	0.1
512	9	I	BL	3.0				
513	12	O	TL	5.0	513	TL	6.2	1.1
513	5	O	TL	5.4				
513	5	I	TL	6.9				
513	12	I	TL	7.3				
513	12	O	OL	4.1	513	OL	5.3	1.0
513	12	I	OL	5.0				
513	5	I	OL	6.1				
513	5	O	OL	6.1				
513	5	O	BL	4.4	513	BL	4.7	0.5
513	12	I	BL	4.4				
513	5	I	BL	4.5				
513	12	O	BL	5.5				

Table C-2 Air-Void Contents in Wheelpaths After Trafficking.

Section	Point Loc.	Transverse Loc.	Layer	Air Void (%)	Section	Layer	Location	Average	Std. Dev.
504	504-TL-W1	Wheel	TL	5.0	504	TL	W	4.5	0.7
504	504-TL-W2	Wheel	TL	4.1					
504	504-BL-W1	Wheel	BL	3.3	504	BL		2.7	0.7
504	504-BL-W2	Wheel	BL	2.2					
505	9	WC	TL	5.3	505	TL	W1	4.7	0.7
505	6	WC	TL	4.8					
505	12	WC	TL	4.0					
505	9	WT	TL	4.3	505	TL	W2	4.0	0.3
505	12	WT	TL	3.9					
505	6	WT	TL	3.7					
505	9	WC	OL	3.5	505	OL	W1	3.2	0.5
505	6	WC	OL	3.5					
505	12	WC	OL	2.7					
505	9	WT	OL	2.8	505	OL	W2	2.5	0.3
505	12	WT	OL	2.6					
505	6	WT	OL	2.2					
505	9	WC	BL	3.9	505	BL	W1	3.2	0.7
505	12	WC	BL	3.3					
505	6	WC	BL	2.5					
505	12	WT	BL	2.5	505	BL	W2	2.3	0.2
505	6	WT	BL	2.3					
505	9	WT	BL	2.1					
506	3	LW	TL	4.1	506	TL	W1	3.7	0.3
506	6	LW	TL	3.6					
506	10	LW	TL	3.4					
506	10	RW	TL	3.3	506	TL	W2	3.3	0.1
506	6	RW	TL	3.3					
506	3	RW	TL	3.2					
506	3	LW	OL	2.3	506	OL	W1	2.1	0.3
506	10	LW	OL	2.2					
506	6	LW	OL	1.7					
506	3	RW	OL	3.1	506	OL	W2	2.6	0.7
506	6	RW	OL	2.9					
506	10	RW	OL	1.8					
506	10	LW	BL	4.0	506	BL	W1	3.5	0.5
506	6	LW	BL	3.4					
506	3	LW	BL	3.0					
506	10	RW	BL	4.7	506	BL	W2	4.4	0.2
506	6	RW	BL	4.4					
506	3	RW	BL	4.2					
507	3	W	TL	3.5	507	TL	W	3.0	0.6
507	6	W	TL	2.3					
507	10	W	TL	2.3					
507		Wheel	TL	3.3					
507	507-TL-W	Wheel	TL	3.335341					
507	10	W	OL	2.6	507	OL	W	2.4	0.2
507	3	W	OL	2.3					
507	6	W	OL	2.2					
507		Wheel	OL	2.4					
507	507-OV-W	Wheel	OL	2.4					
507	10	W	BL	4.7	507	BL	W	4.7	0.5

Section	Point Loc.	Transverse Loc.	Layer	Air Void (%)	Section	Layer	Location	Average	Std. Dev.
507	3	W	BL	4.5					
507	6	W	BL	4.1					
507		Wheel	BL	5.2					
507	507-BL-W	Wheel	BL	5.15224					
508	11	W	TL	7.6	508	TL	W	6.7	1.4
508	8	W	TL	7.5					
508	5	W	TL	5.1					
508	5	W	OL	6.7	508	OL	W	5.9	0.6
508	11	W	OL	5.7					
508	8	W	OL	5.5					
508	5	W	BL	3.0	508	BL	W1	2.5	0.5
508	8	W	BL	2.7					
508	11	W	BL	1.9					
509	11	WC	TL	5.3	509	TL	W1	5.0	0.3
509	5	WC	TL	4.8					
509	8	WC	TL	4.8					
509	11	WT	TL	7.7	509	TL	W2	6.0	1.5
509	8	WT	TL	5.1					
509	5	WT	TL	5.1					
509	11	WC	OL	7.4	509	OL	W1	5.0	0.3
509	5	WC	OL	7.4					
509	8	WC	OL	6.9					
509	11	WT	OL	6.9	509	OL	W2	6.7	0.2
509	8	WT	OL	6.6					
509	5	WT	OL	6.5					
509	8	WC	BL	4.8	509	BL	W1	3.8	1.3
509	11	WC	BL	4.4					
509	5	WC	BL	2.3					
509	8	WT	BL	4.3	509	BL	W2	3.5	1.0
509	5	WT	BL	3.8					
509	11	WT	BL	2.4					
510	4.8	W	TL	4.2	510	TL	W	3.6	0.4
510	5.2	W	TL	3.8					
510	5.2	W	TL	3.3					
510	4.8	W	TL	3.2					
510	5.2	W	OL	7.8	510	OL	W	7.4	0.6
510	5.2	W	OL	6.9					
510	4.8	W	BL	3.9	510	BL	W	2.7	0.8
510	4.8	W	BL	2.6					
510	5.2	W	BL	2.2					
510	5.2	W	BL	2.0					
510	5.2	W	ATPB	26.4	510	ATPB	W	25.2	1.7
510	5.2	W	ATPB	24.1					
511	11	W	TL	3.2	511	TL	W	3.0	0.2
511	5	W	TL	3.1					
511	8	W	TL	2.8					
511	8	W	OL	10.7	511	OL	W	10.5	0.4
511	11	W	OL	10.2					
511	8	W	BL	3.9	511	BL	W	3.3	0.9
511	5	W	BL	3.8					
511	11	W	BL	2.3					
512	6	W	TL	5.3	512	TL	W	5.6	0.3

Section	Point Loc.	Transverse Loc.	Layer	Air Void (%)	Section	Layer	Location	Average	Std. Dev.
512	12	W	TL	5.5					
512	9	W	TL	6.0					
512	9	W	OL	4.0	512	OL	W	4.3	0.4
512	12	W	OL	4.3					
512	6	W	OL	4.7					
512	6	W	BL	4.0	512	BL	W	5.3	1.2
512	12	W	BL	5.6					
512	9	W	BL	6.2					
513	12	W	TL	4.0	513	TL	W	5.0	1.4
513	5	W	TL	5.9					
513	12	W	OL	0.9	513	OL	W	2.2	1.8
513	5	W	OL	3.4					
513	12	W	BL	4.0	513	BL	W	4.3	0.4
513	5	W	BL	4.5					

Table C-3 Air-Void Contents in Humps after Trafficking.

Section	Point Loc.	Transverse Loc.	Layer	Air Void (%)	Section	Layer	Location	Average	Std. Dev.
504	504-TL-H2	Hump	TL	6.595215	504	TL	H	6.0	0.8
504	504-TL-H1	Hump	TL	5.411217					
504	504-BL-H1	Hump	BL	3.374314	504	BL	H	2.6	1.1
504	504-BL-H2	Hump	BL	1.761895					
505	6	Hump	TL	4.7956	505	TL	H	4.5	0.3
505	12	Hump	TL	4.697859					
505	9	Hump	TL	4.151217					
505	12	Hump	OL	5.412369	505	OL	H	5.0	0.4
505	6	Hump	OL	4.929212					
505	9	Hump	OL	4.536608					
505	9	Hump	BL	2.035635	505	BL	H	2.0	0.0
505	12	Hump	BL	2.005376					
505	6	Hump	BL	1.964992					
506	10	Hump	TL	4.005226	506	TL	H	3.5	0.3
506	3	Hump	TL	3.504346					
506	10	MH	TL	3.3	506	TL	Hm	3.2	0.0
506	6	MH	TL	3.2					
506	6	Hump	TL	3.316946					
506	10	Hump	OL	3.545935	506	OL	H	3.2	0.4
506	6	Hump	OL	3.335505					
506	3	Hump	OL	2.778296					
506	10	MH	OL	5.2	506	OL	Hm	4.4	0.7
506	3	MH	OL	4.2					
506	6	MH	OL	3.8					
506	10	Hump	BL	4.380079	506	BL	H	4.0	0.6
506	6	Hump	BL	4.227752					
506	3	Hump	BL	3.323451					
506	6	MH	BL	4.1	506	BL	Hm	4.0	0.0
506	10	MH	BL	4.0					
507		Hump	TL	4.985	507	TL	H	4.4	2.5
507		Hump	TL	4.889					
507	3	Hump	TL	4.388					
507	10	Hump	TL	4.081					
507	6	Hump	TL	3.810					
507	10	Hump	OL	6.515761	507	OL	H	5.8	0.5
507	3	Hump	OL	6.195682					
507		Hump	OL	5.508499					
507		Hump	OL	5.399265					
507	6	Hump	OL	5.318382					
507	3	Hump	BL	6.145356	507	BL	H	5.7	0.3
507	10	Hump	BL	5.884026					
507		Hump	BL	5.643258					
507	6	Hump	BL	5.55096					
507		Hump	BL	5.407404					
508	11	Hump	TL	7.781578	508	TL	H	6.5	1.2
508	5	Hump	TL	6.302929					

Section	Point Loc.	Transverse Loc.	Layer	Air Void (%)	Section	Layer	Location	Average	Std. Dev.
508	8	Hump	TL	5.373724					
508	11	Hump	OL	8.53632	508	OL	H	8.0	0.5
508	8	Hump	OL	7.796665					
508	5	Hump	OL	7.648231					
508	5	Hump	BL	3.741143	508	BL	H	3.2	0.5
508	8	Hump	BL	2.971602					
508	11	Hump	BL	2.764736					
509	11	Hump	TL	10.45499	509	TL	H	8.1	2.0
509	8	Hump	TL	7.016738					
509	5	Hump	TL	6.850026					
509	8	Hump	OL	8.092719	509	OL	H	7.8	0.5
509	5	Hump	OL	7.441045					
509	5	Hump	BL	6.474399	509	BL	H	4.7	1.5
509	11	Hump	BL	3.84963					
509	8	Hump	BL	3.756175					
510	5.2	H	TL	6.61476	510	TL	H	5.6	1.6
510	5.2	H	TL	3.295898					
510	5	Hump	TL	6.640371					
510	8	Hump	TL	6.033182					
510	5.2	Hump-middle	TL	4.152405	510	TL	Hm	4.2	
510	5.2	H	OL	11.71392	510	OL	H	9.6	1.6
510	5.2	H	OL	8.466188					
510	5	Hump	OL	9.746918					
510	8	Hump	OL	8.389841					
510	5.2	Hump-middle	OL	9.300275	510	OL	Hm	9.3	
510	5.2	H	BL	6.141637	510	BL	H	4.3	1.7
510	5.2	H	BL	2.790537					
510	5	Hump	BL	3.888655					
510	5.2	Hump-middle	BL	2.441123	510	BL	Hm	2.4	
510	5.2	H	ATPB	27.43923	510	ATPB	H	27.2	0.3
510	5.2	H	ATPB	26.99787					
510	5.2	Hump-middle	ATPB	14.54426	510	ATPB	Hm	14.5	
511	11	Hump	TL	6.451608	511	TL	H	5.4	1.5
511	8	Hump	TL	6.062247					
511	5	Hump	TL	3.738789					
511	11	Hump	OL	14.0263	511	OL	H	13.7	0.3
511	8	Hump	OL	13.70538					
511	5	Hump	OL	13.47509					
511	5	Hump	BL	4.420391	511	BL	H	3.1	1.3
511	8	Hump	BL	2.917772					
511	11	Hump	BL	1.857105					
512	9	Hump	TL	7.119397	512	TL	H	8.7	1.6
512	12	Hump	TL	8.710821					
512	6	Hump	TL	10.3202					
512	9	Hump	OL	7.445052	512	OL	H	8.2	1.1
512	6	Hump	OL	9.027715					
512	6	Hump	BL	2.92595	512	BL	H	4.4	2.5

Section	Point Loc.	Transverse Loc.	Layer	Air Void (%)	Section	Layer	Location	Average	Std. Dev.
512	9	Hump	BL	3.057596					
512	12	Hump	BL	7.331451					

APPENDIX D: DEFLECTIONS AND BACK-CALCULATED MODULI

Table D-1 Deflection data on rutting test sections (3/1/1997).

Section	Line	Chainage (ft.)	D1	D7	Experiment type	
504 RF	A	60	87	21		
504 RF	A	70	76	20		
504 RF	A	80	82	21		
508 RF	A	90	92	21		
508 RF	A	100	89	21	ARHM-GG 62 mm	
508 RF	A	110	83	20		
511 RF	A	130	73.5	18.5		
511 RF	A	140	68.5	19	ARHM-GG 38 mm	
511 RF	A	150	65	17.5		
507 RF	B	75	87	20		
507 RF	B	85	89.5	21	DGAC	
507 RF	B	95	97.5	20		
509 RF	B	85	82	20		
509 RF	B	95	92	18	ARHM-GG 62 mm	
509 RF	B	105	86	17		
513 RF	D	95	97.5	20		
513 RF	D	105	97	19	DGAC	
513 RF	D	115	137	20.5		
510 RF	B	135	76	19		
510 RF	B	145	68	19	ARHM-GG 38 mm	
510 RF	B	155	65	17		
512 RF	D	135	81	18.5		
512 RF	D	145	73.5	19.5	DGAC	
512 RF	D	155	73	17		
506 RF	E	75	85	22		
506 RF	E	85	90.5	23	DGAC	
506 RF	E	95	96.5	23		
505 RF	D	135	86	18		
505 RF	D	145	79	20	DGAC	
505 RF	D	155	81	17		

Table D-2 Deflection data on rutting test section after construction (4/1/1997).

Section	Line	Chainage	D1	D7	Experiment type
504 RF	A	60	75	20	
504 RF	A	70	72	21	
504 RF	A	80	77	20	
508 RF	A	90	84	21	
508 RF	A	100	82	20	ARHM 62mm
508 RF	A	110	72	20	
511 RF	A	130	70	20	
511 RF	A	140	63	17.5	ARHM 38mm
511 RF	A	150	64	17.5	
507 RF	B	75	75	20	
507 RF	B	85	76	20	DGAC
507 RF	B	95	82	20	
509 RF	B	85	76	20	
509 RF	B	95	82	20	ARHM 62mm
509 RF	B	105	78	20	
513 RF	D	95	82	20	
513 RF	D	105	78	20	DGAC
513 RF	D	115	75	19	
512 RF	D	135	72	20	
512 RF	D	145	65	18	DGAC
512 RF	D	155	64	18	
510 RF	B	135	72	20	
510 RF	B	145	65	18	ARHM 38mm
510 RF	B	155	64	18	

APPENDIX E: TEMPERATURE DATA

Table E-1 Average Temperature, Sections 510RF and 511RF.

	Depth	510 RF		511 RF	
		Avg. Temp.	Std. Dev.	Avg. Temp.	Std. Dev.
Traffic Side	0	53	2.13	51	1.7
	37	51	1.9	50	1.45
	50	50	1.85	49	0.99
	112	47	1.8	46	0.97
	187	43	1.85	43	1.12
Caravan Side	0	52	2.34	51	1.48
	37	51	4.19	50	1.01
	50	50	1.35	50	0.91
	112	48	3.73	48	0.78
	187	46	1.8	45	0.89

Table E-2 Average Temperature, Section 512 RF

	Depth	512 RF	
		Avg. Temp.	Std. Dev.
Traffic Side	0	42	1.23
	50	41	0.98
	76	40	0.93
	145	39	0.84
	230	37	0.89
Caravan Side	0	42	1.24
	50	41	1.02
	76	40	0.98
	145	39	0.86
	230	37	0.86

APPENDIX F: AVERAGE TRANSVERSE SURFACE PROFILES VERSUS LOAD REPETITIONS

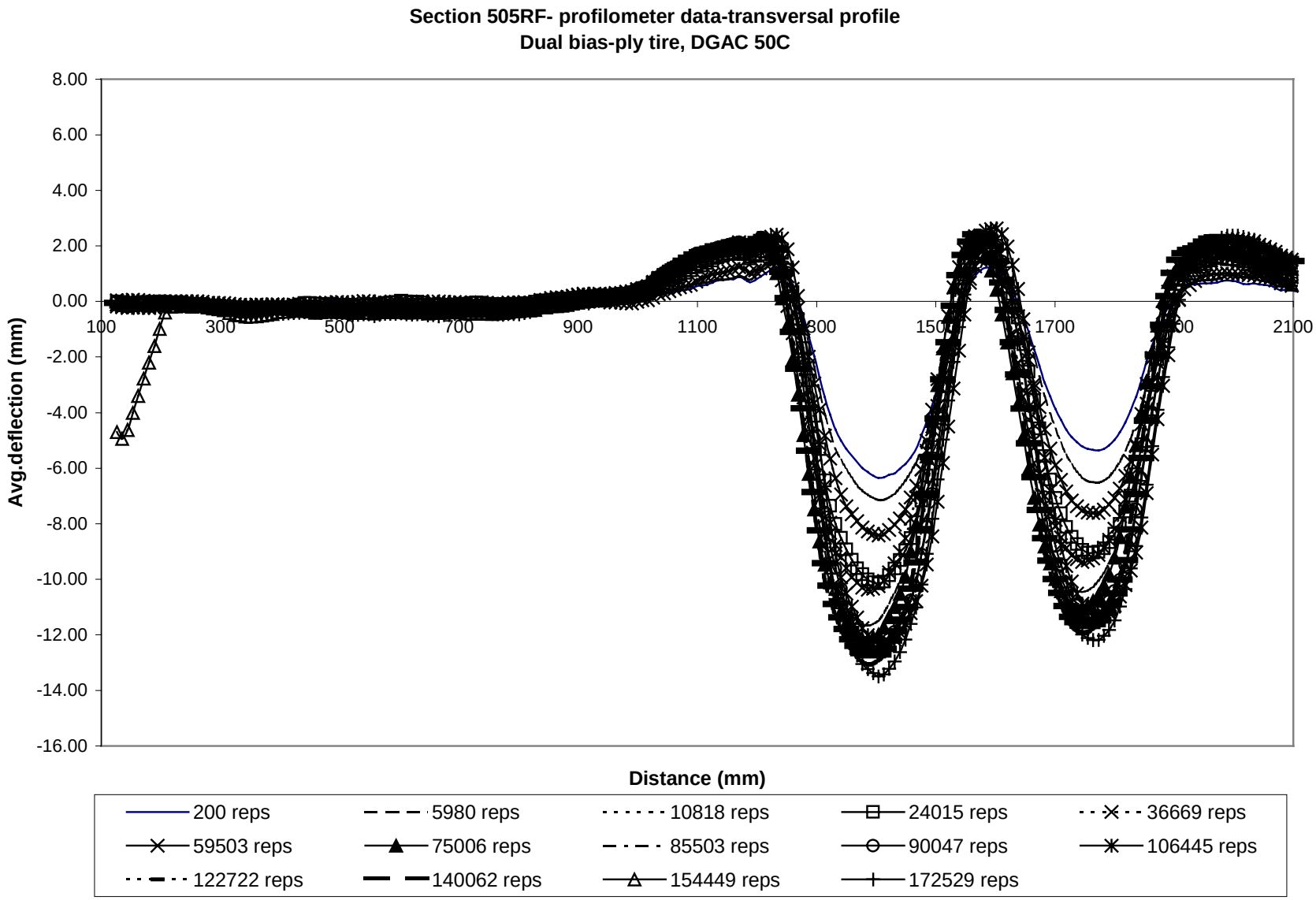

Figure F-1. Profilometer data from Section 505RF.

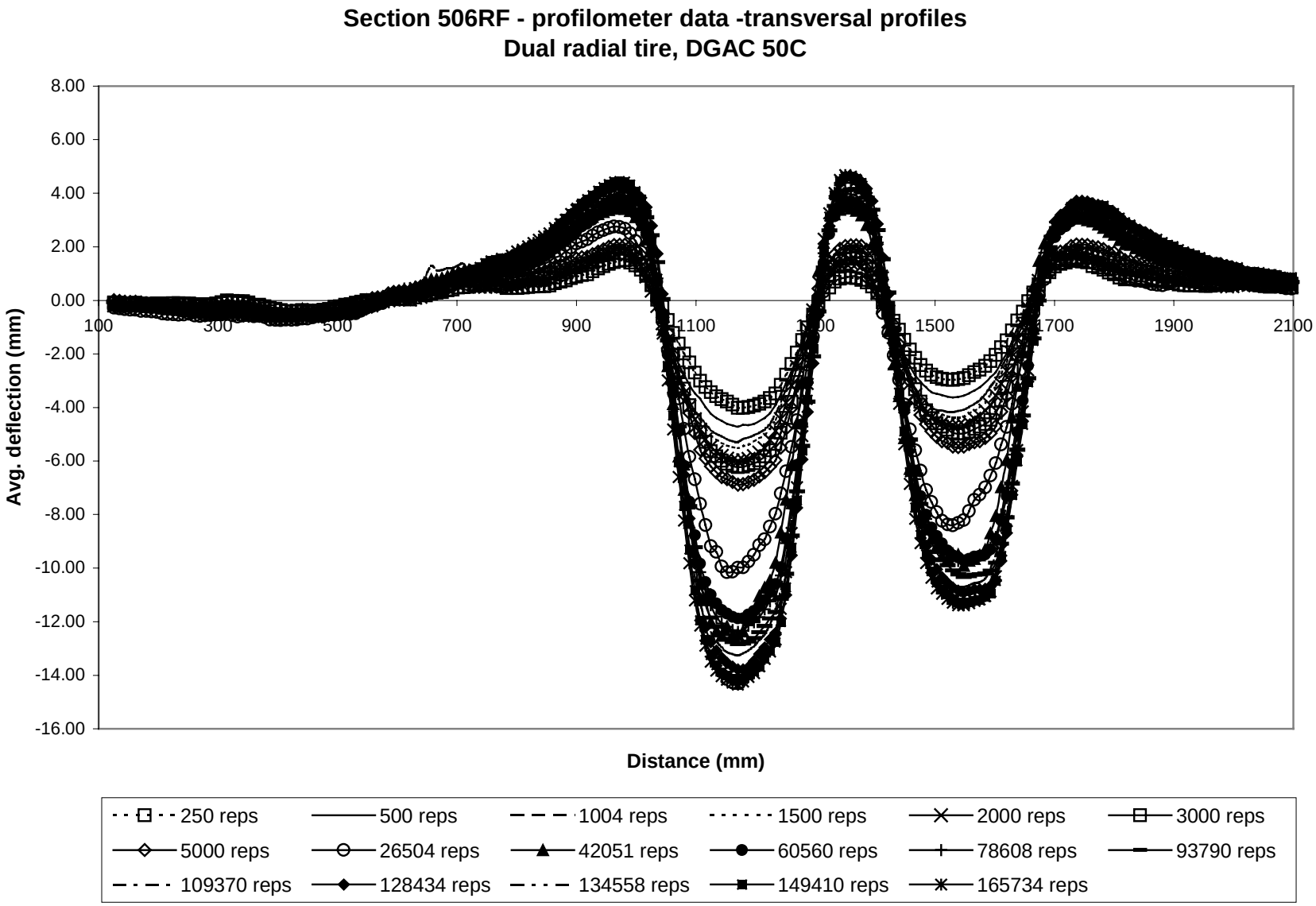

Figure F-2. Profilometer data from Section 506RF.

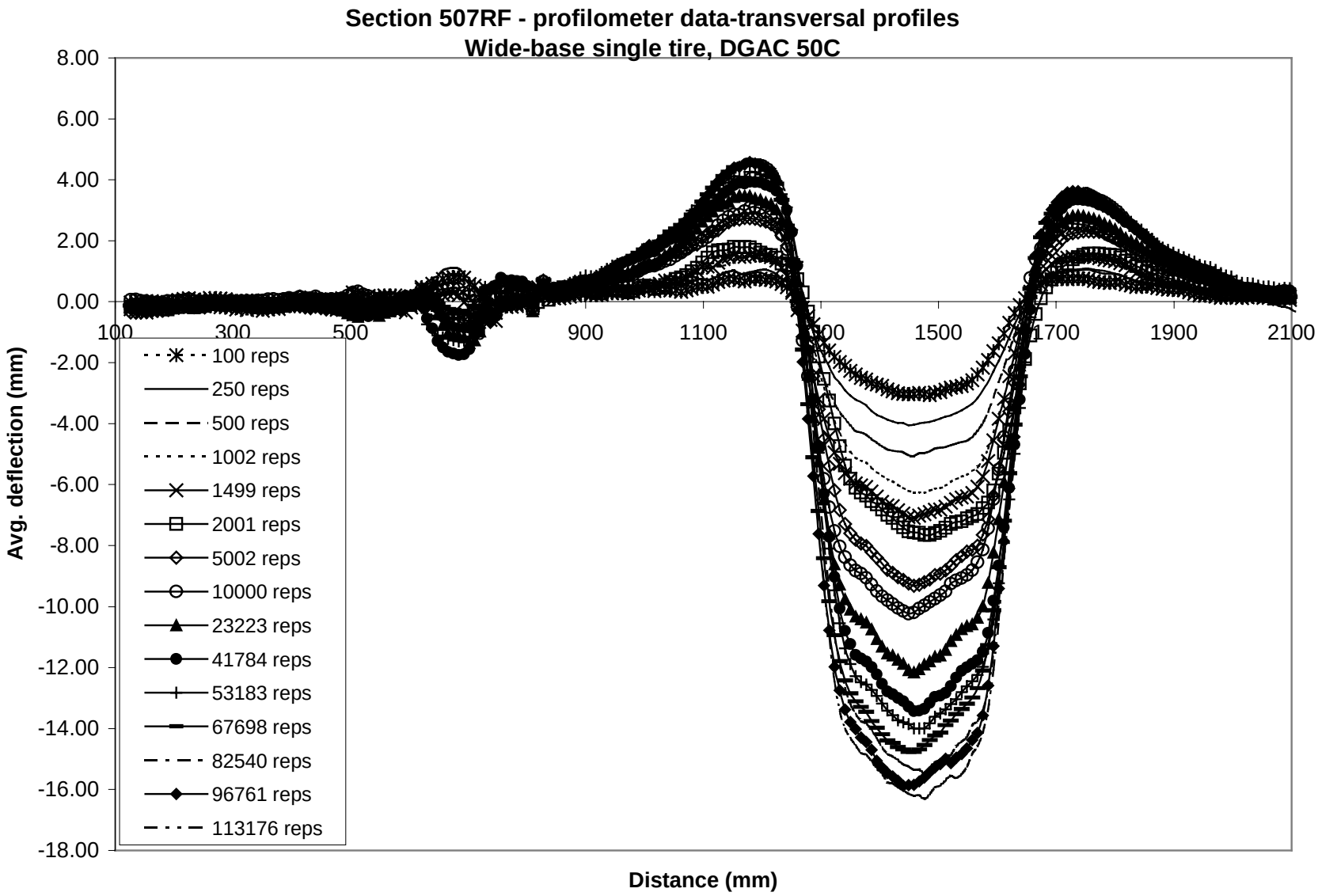

Figure F-3. Profilometer data from Section 507RF.

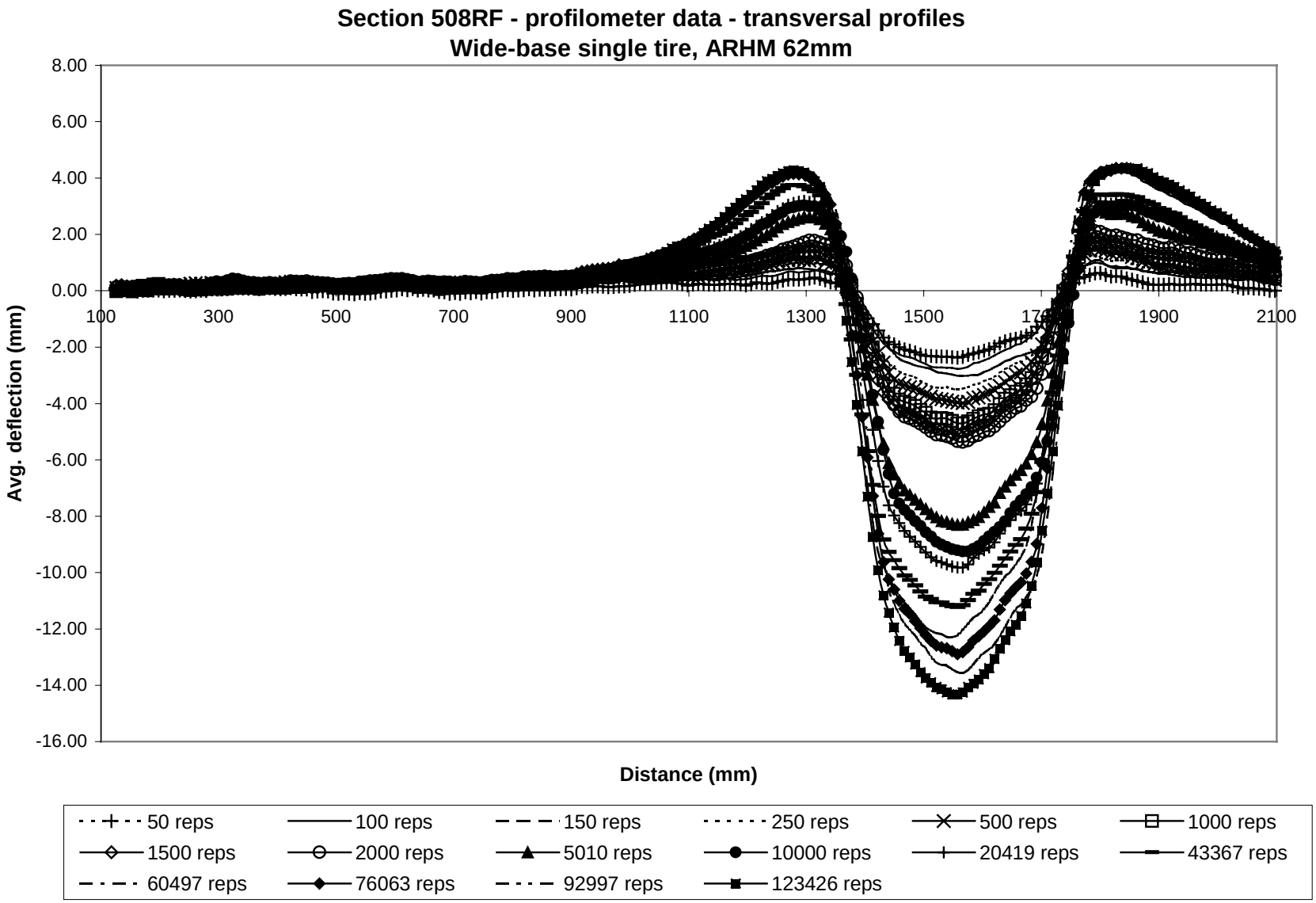

Figure F-4. Profilometer data from Section 508RF.

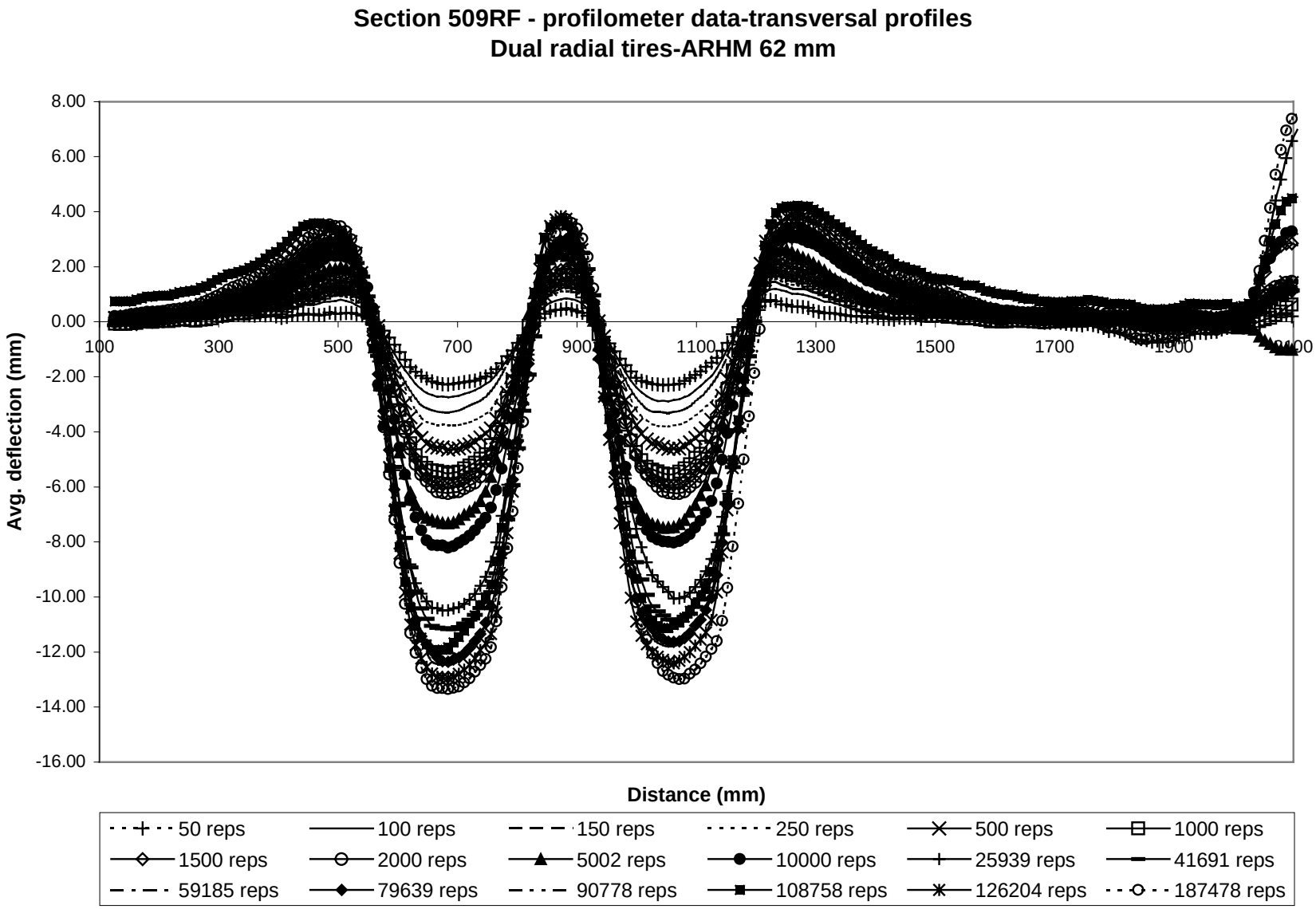

Figure F-5. Profilometer data from Section 509RF.

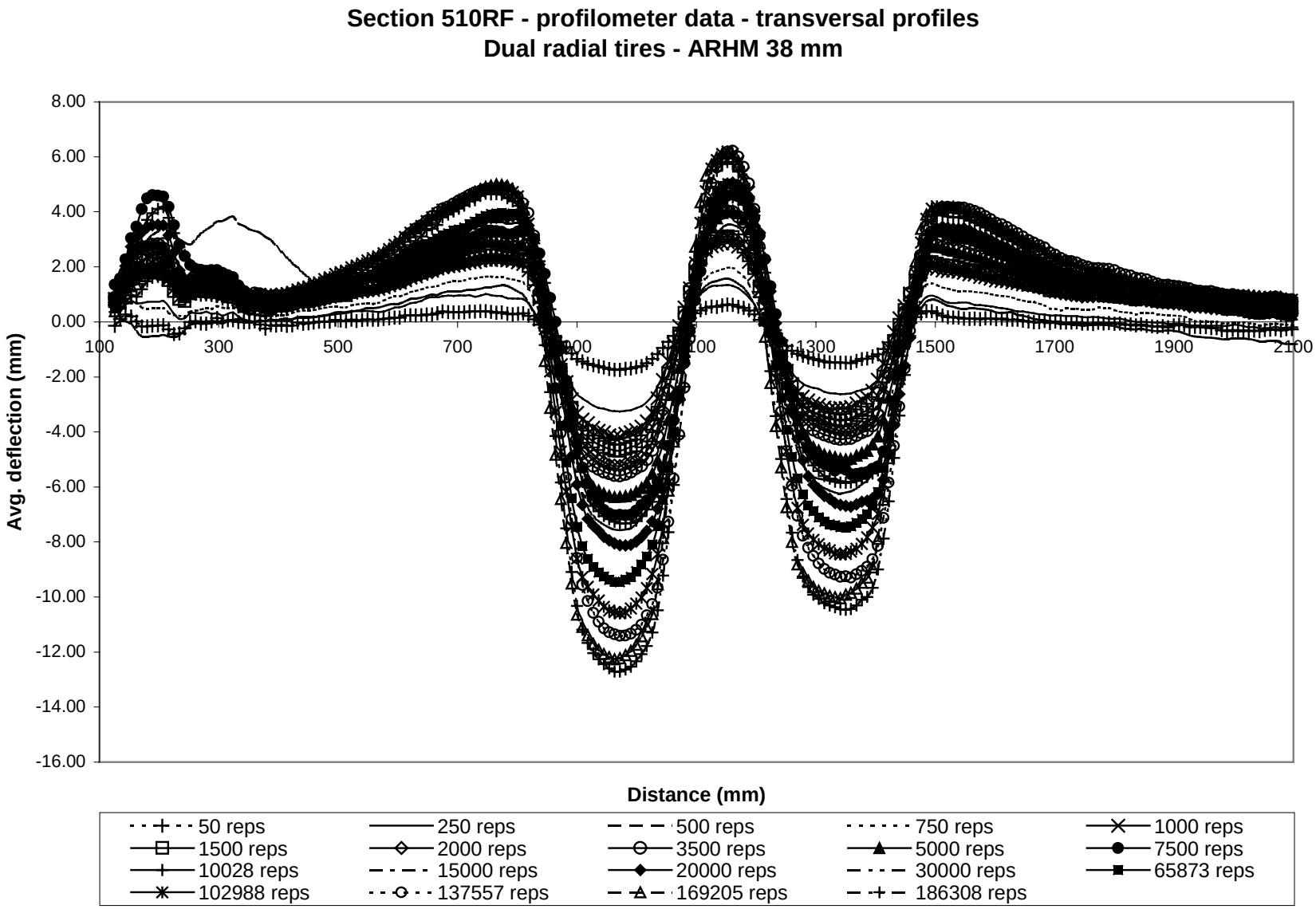

Figure F-6. Profilometer data from Section 510RF.

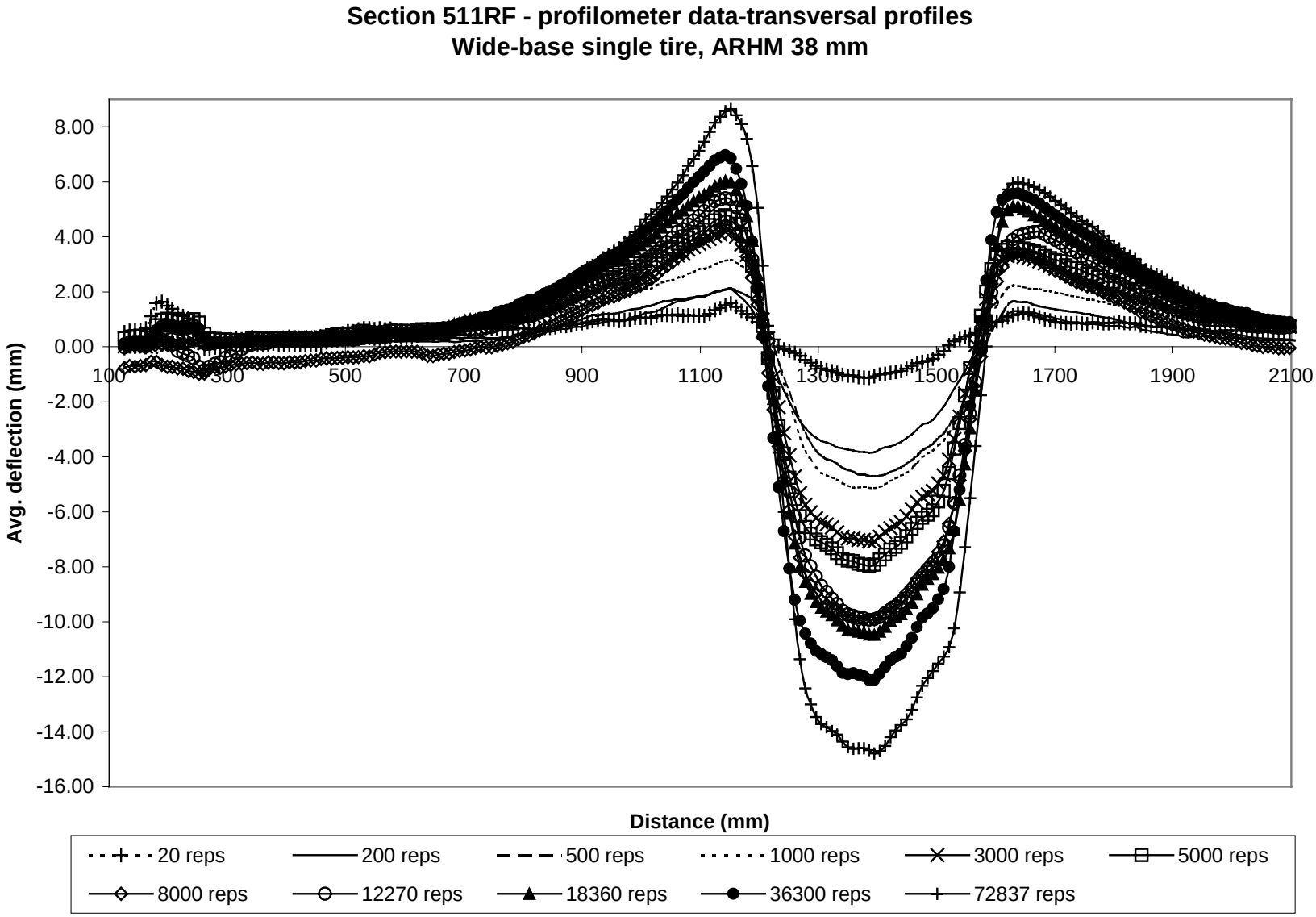

Figure F-7. Profilometer data from Section 511RF.

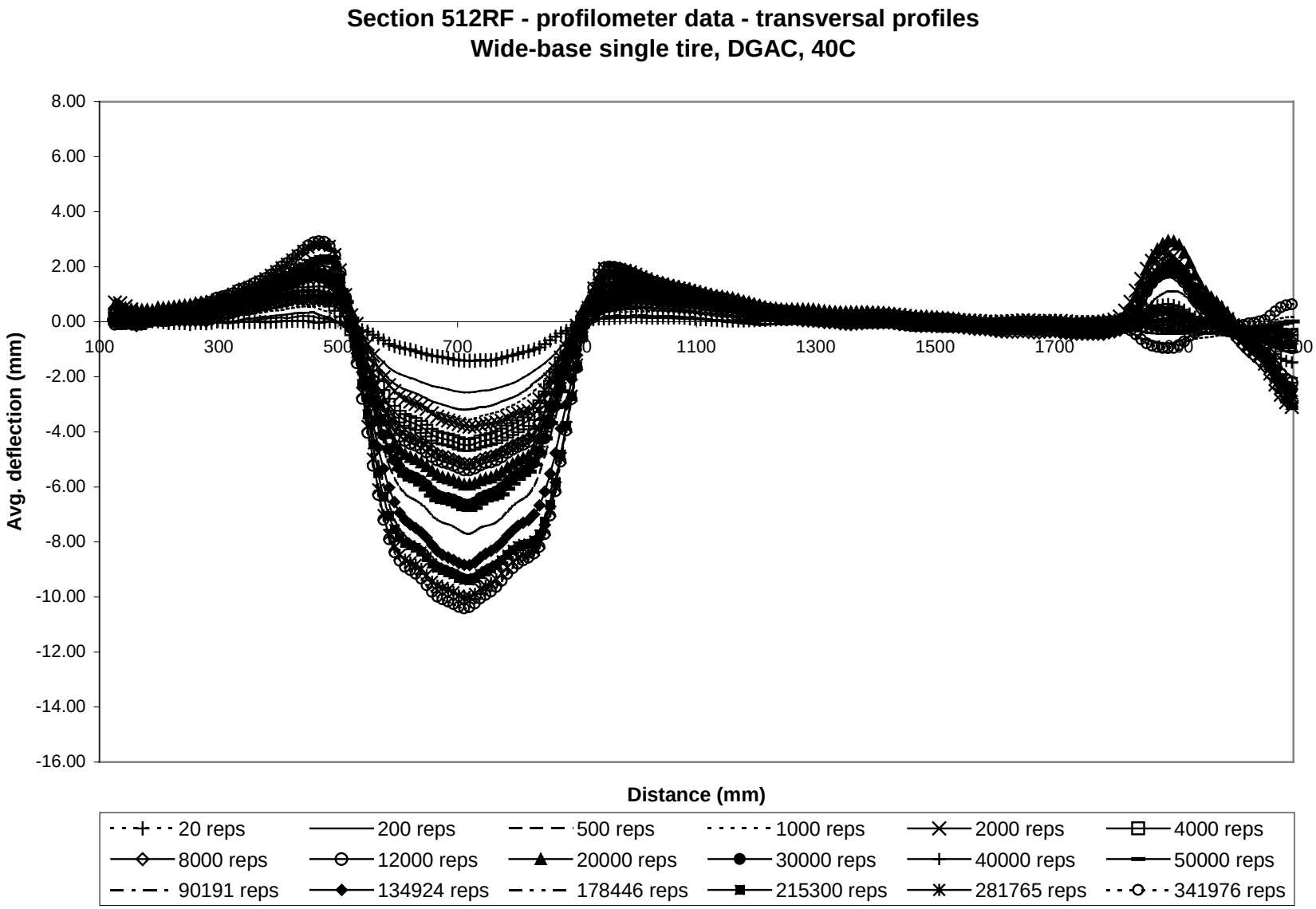

Figure F-8. Profilometer data from Section 512RF.

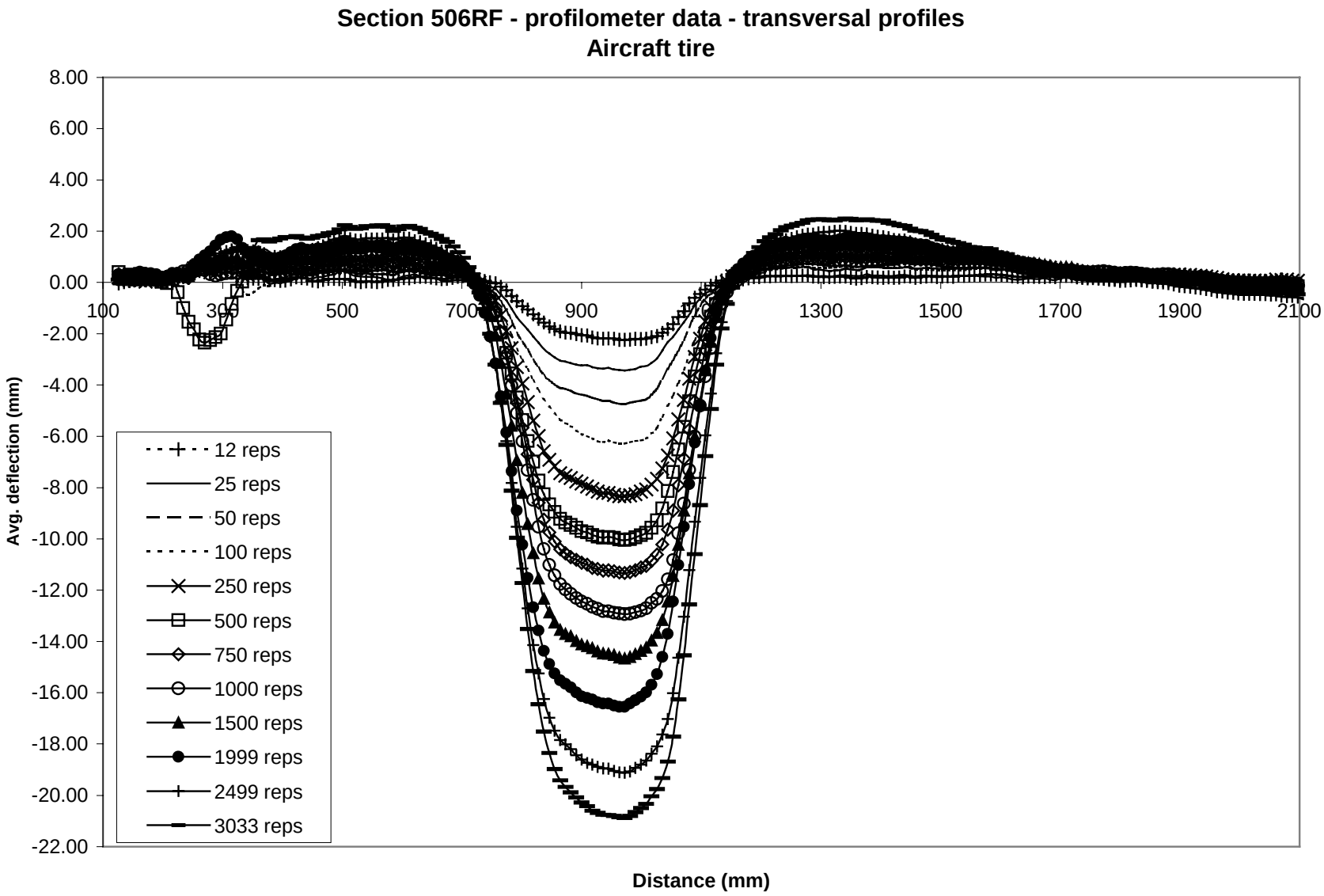

Figure F-9. Profilometer data from Section 513RF.

APPENDIX G TRANSVERSE PROFILES FROM AC SLABS FROM TRENCHES

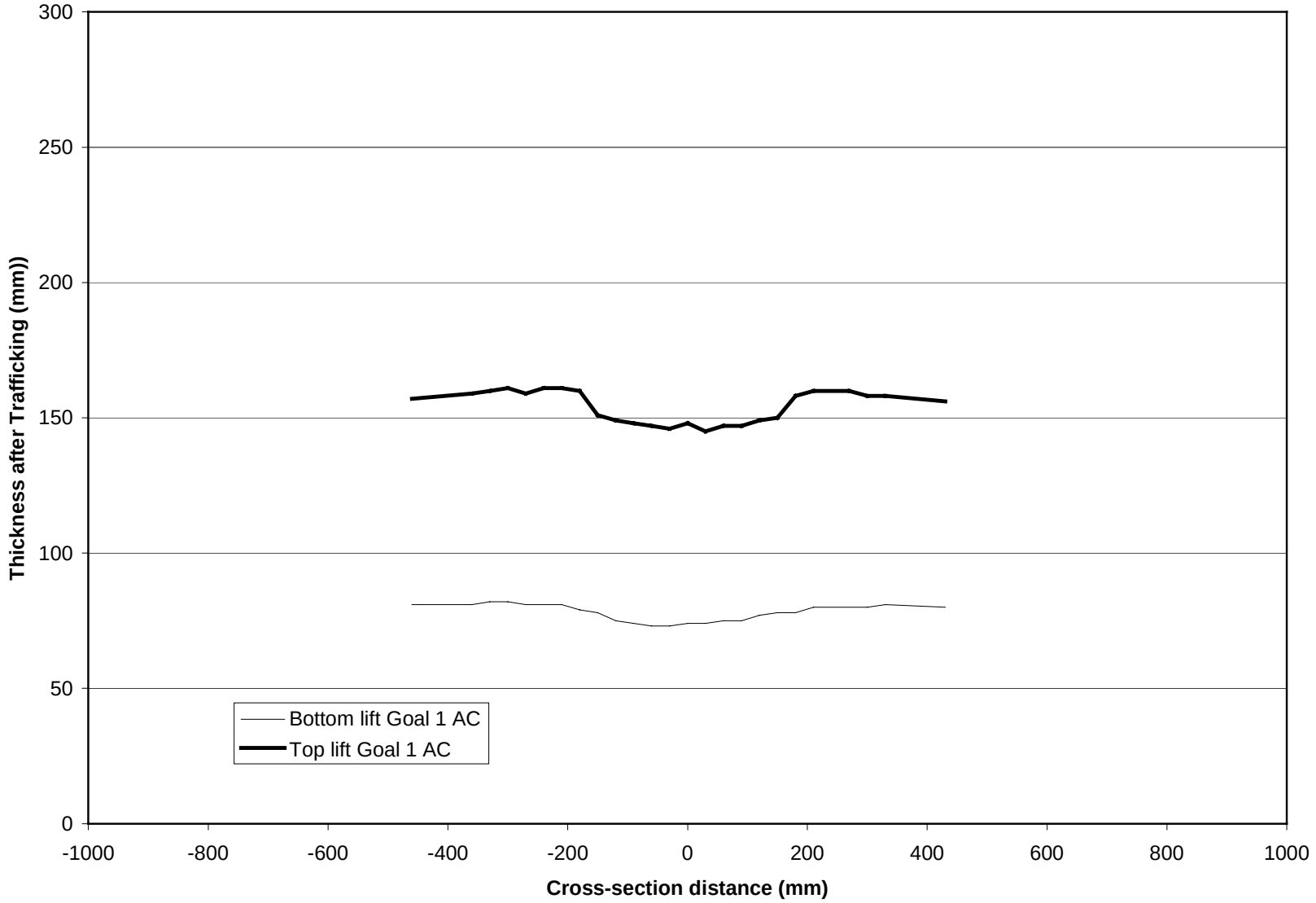

Figure G-1. Transverse profile of trenched AC slab from Section 504RF.

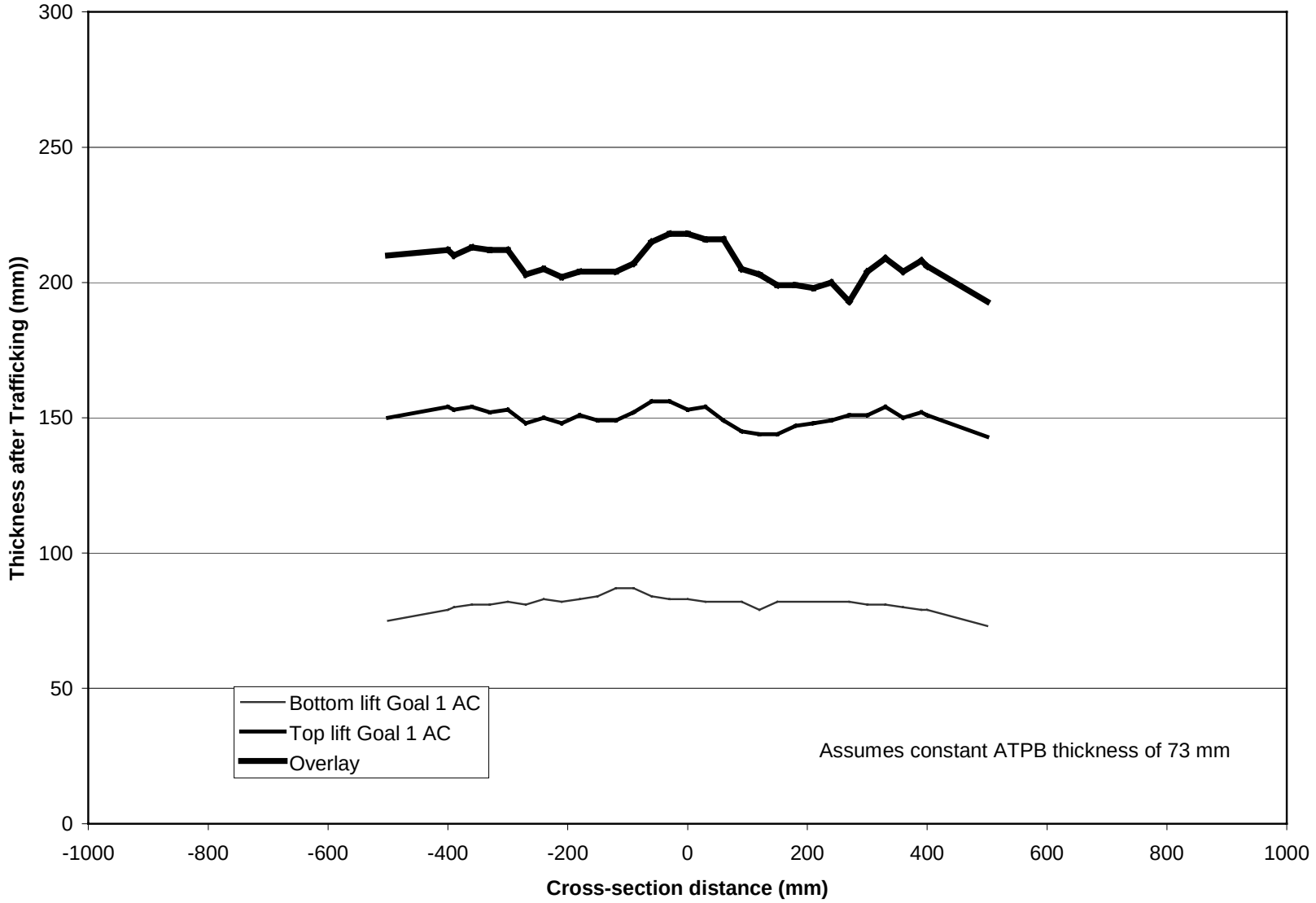

Figure G-2. Transverse profile of trenched AC slab from Section 505RF.

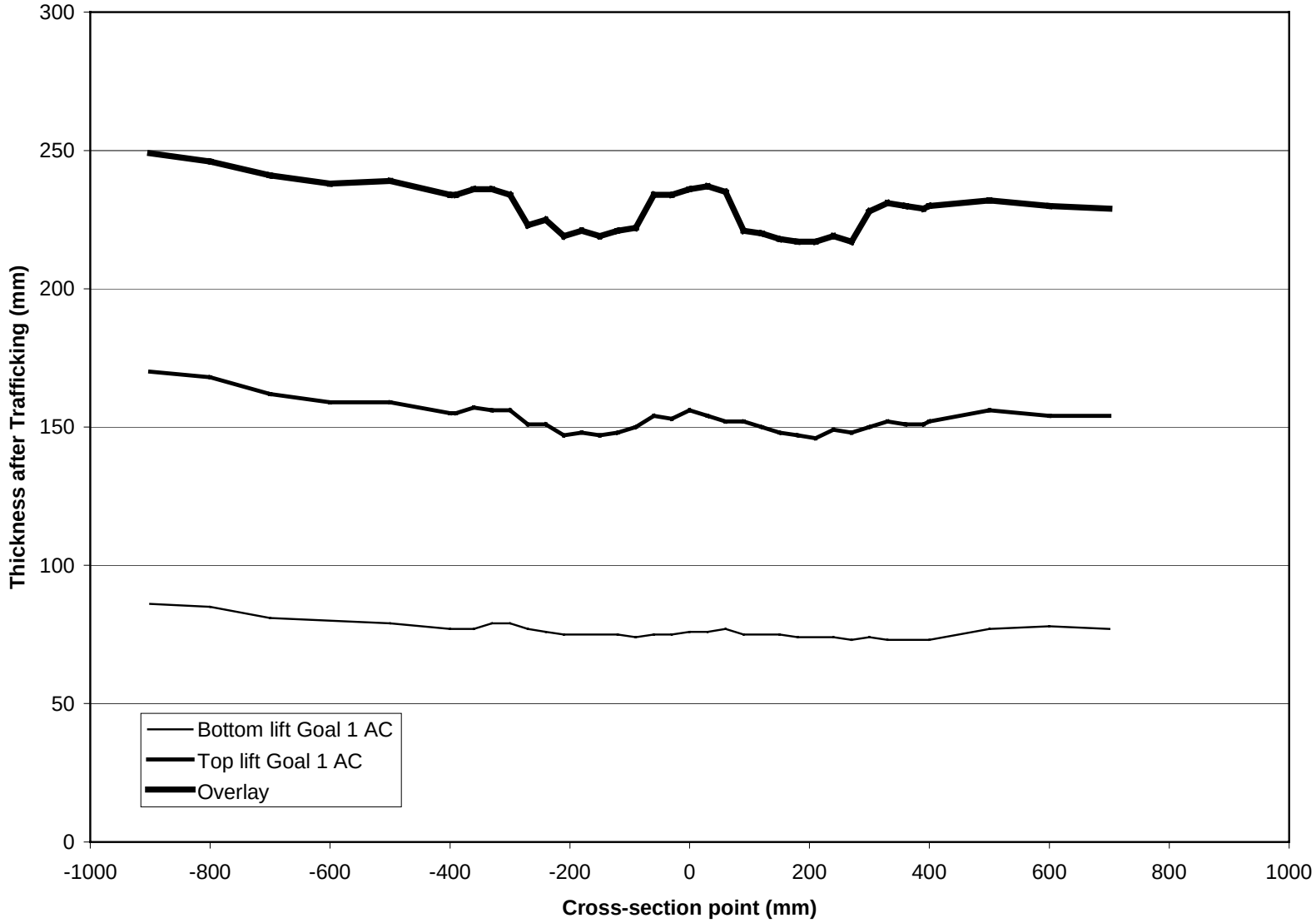

Figure G-3. Transverse profile of trenched AC slab from Section 506RF.

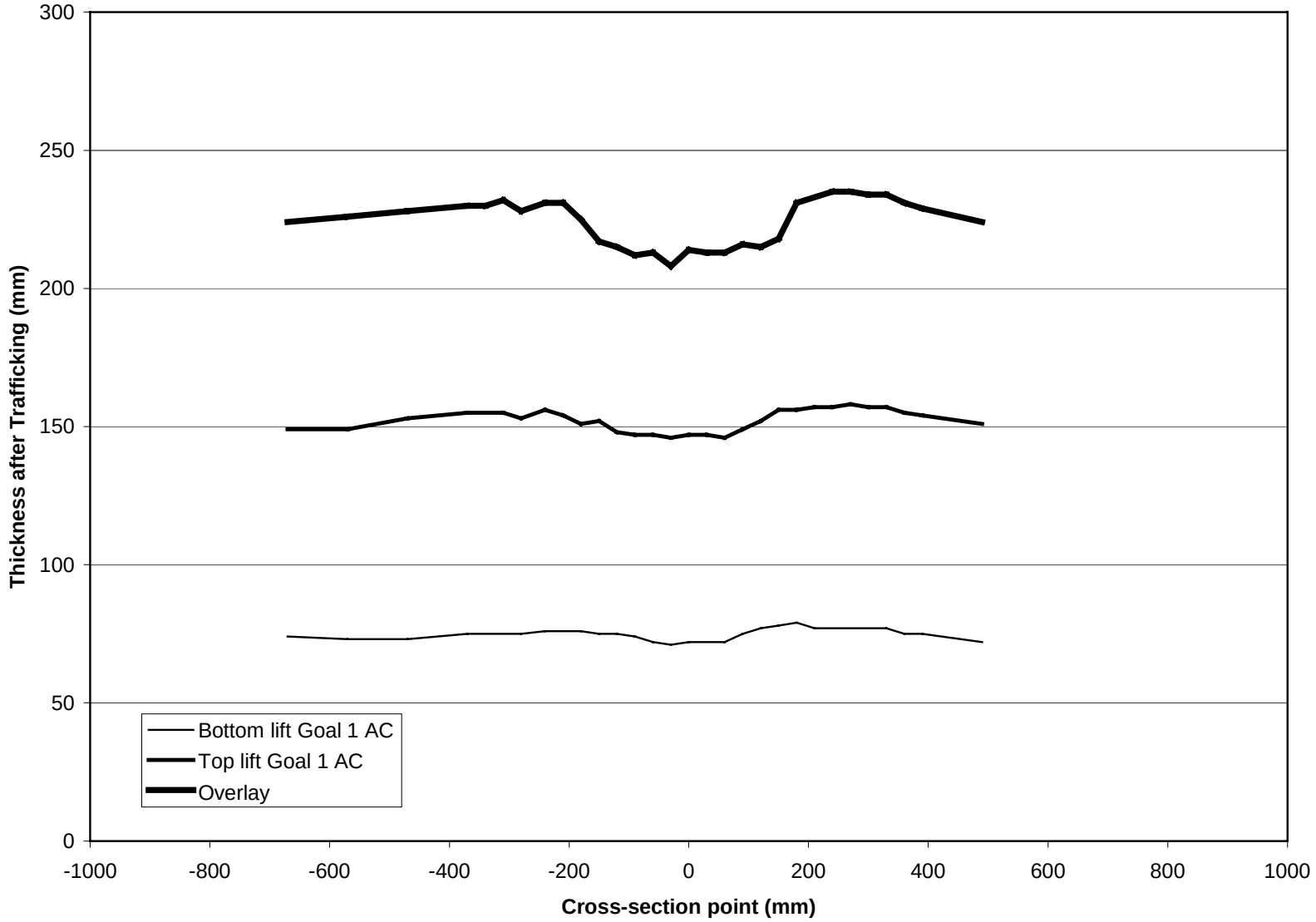

Figure G-4. Transverse profile of trenched AC slab from Section 507RF.

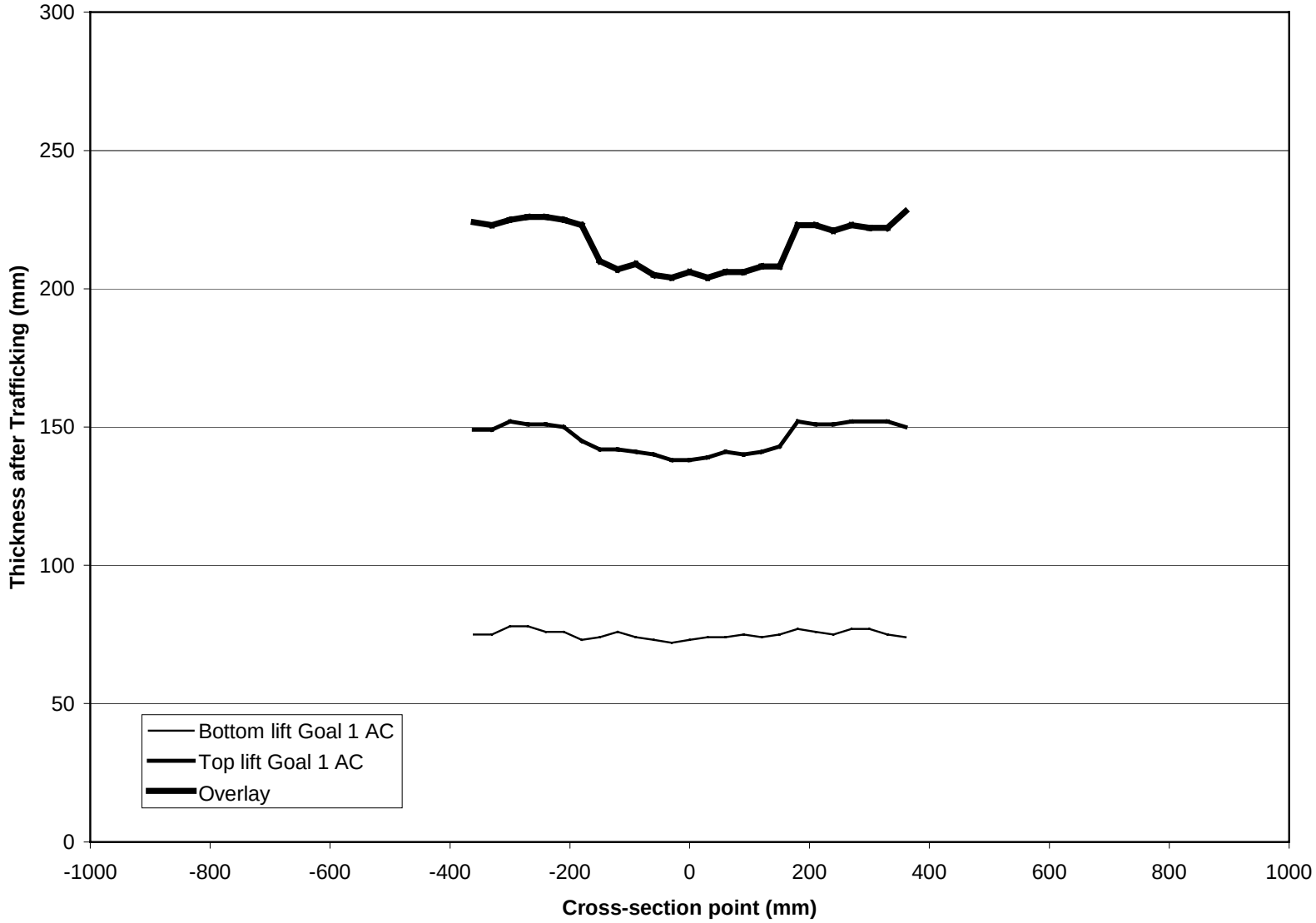

Figure G-5. Transverse profile of trenched AC slab from Section 508RF.

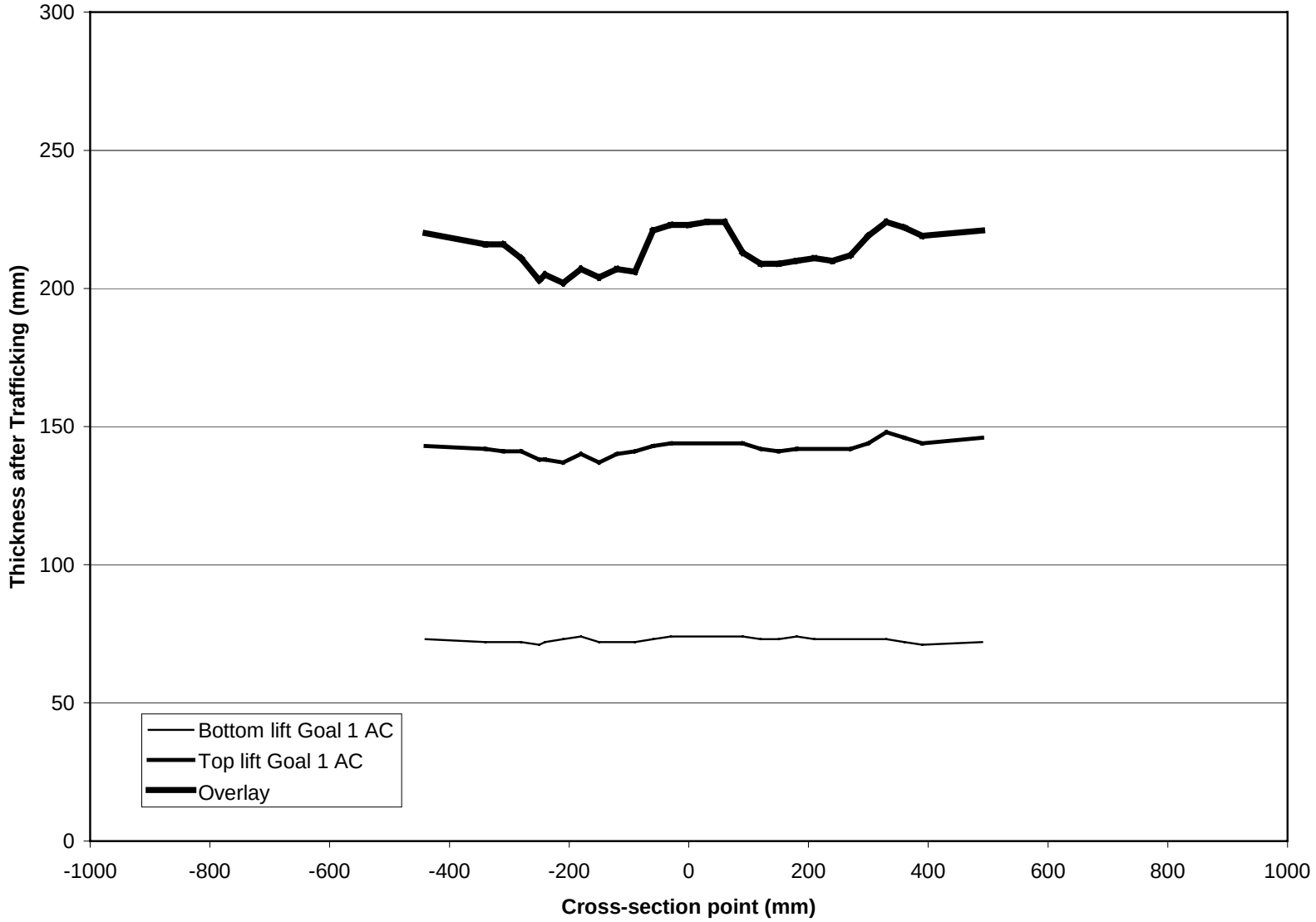

Figure G-6. Transverse profile of trenched AC slab from Section 509RF.

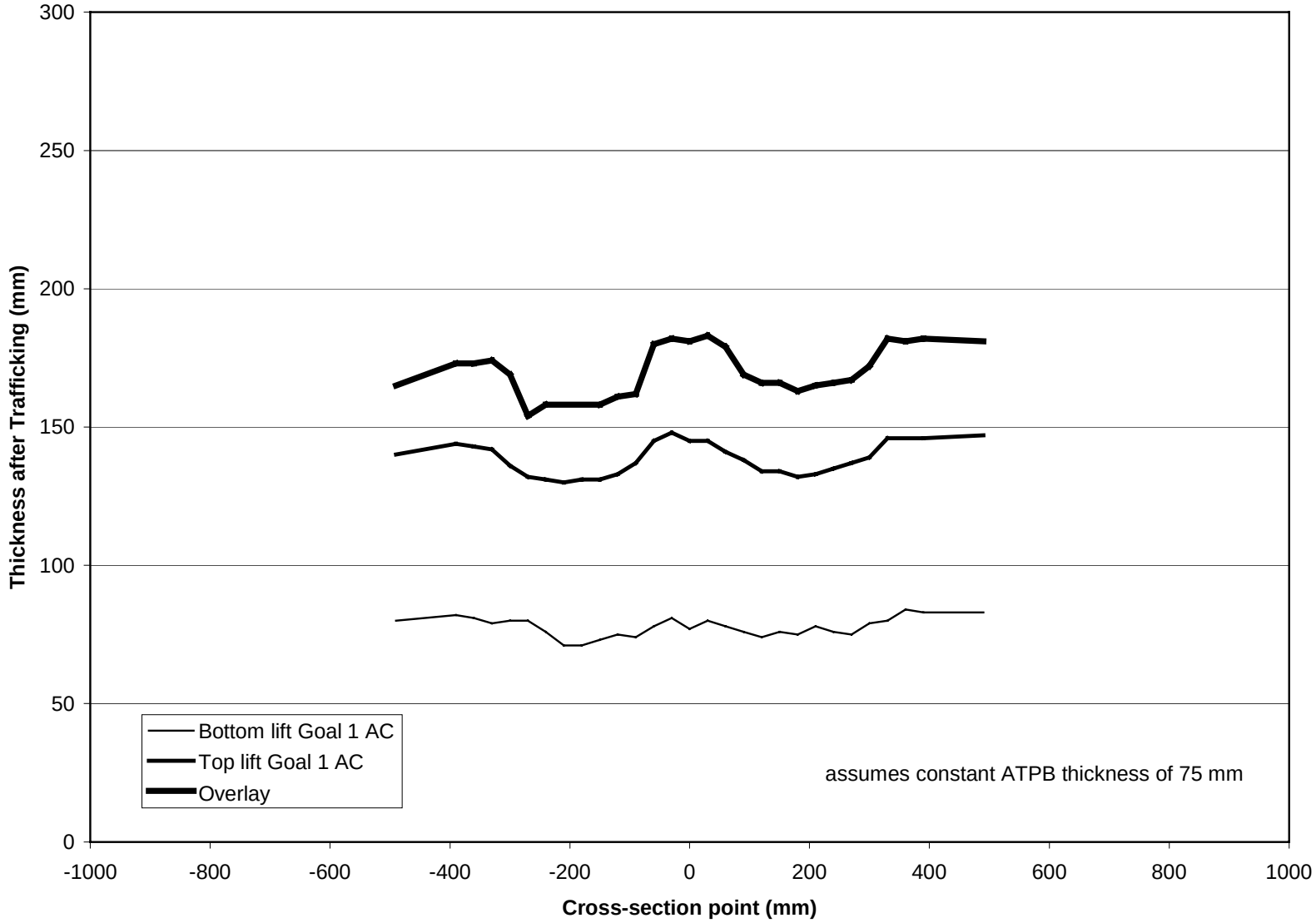

Figure G-7. Transverse profile of trenched AC slab from Section 510RF.

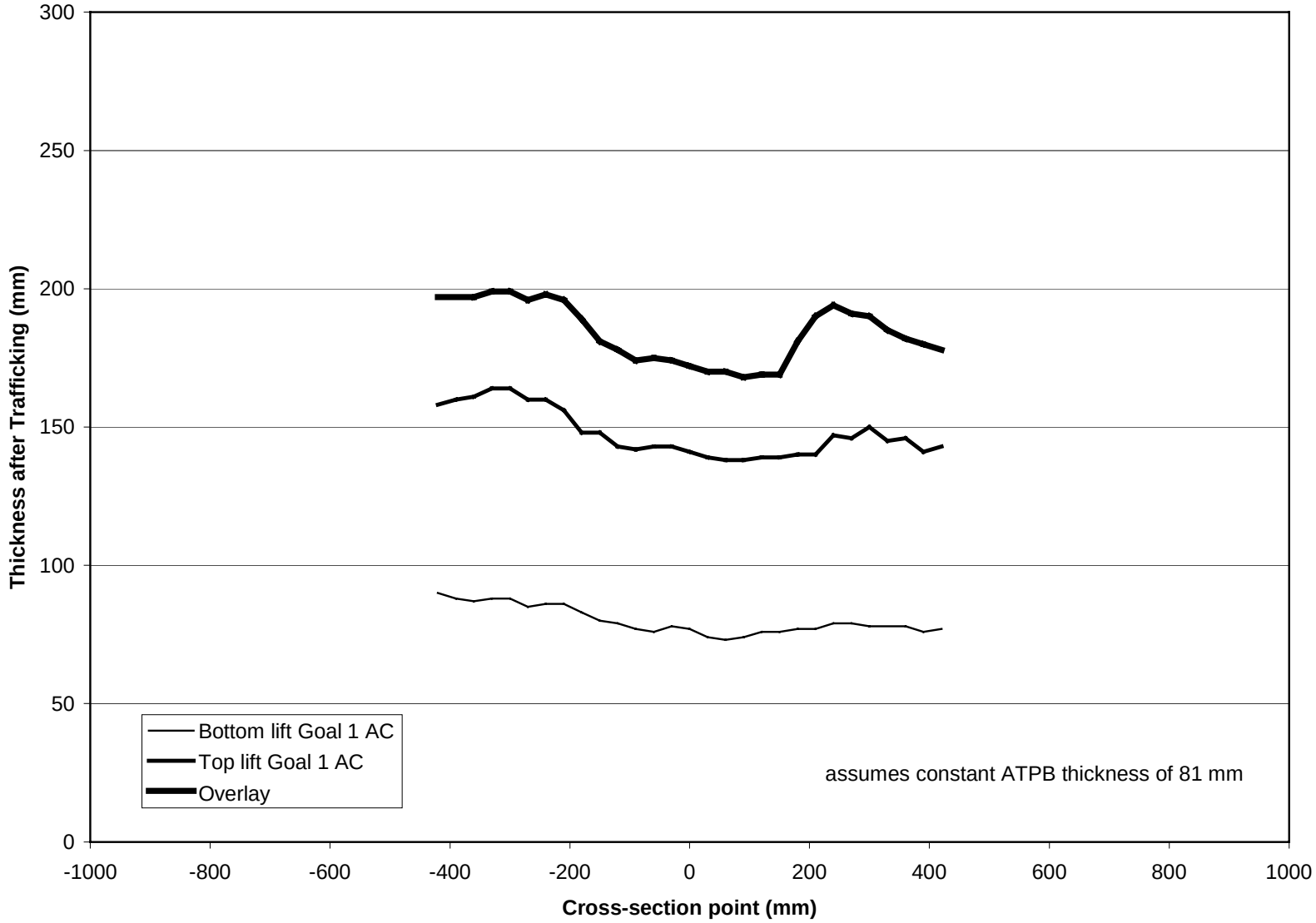

Figure G-8. Transverse profile of trenched AC slab from Section 511RF.

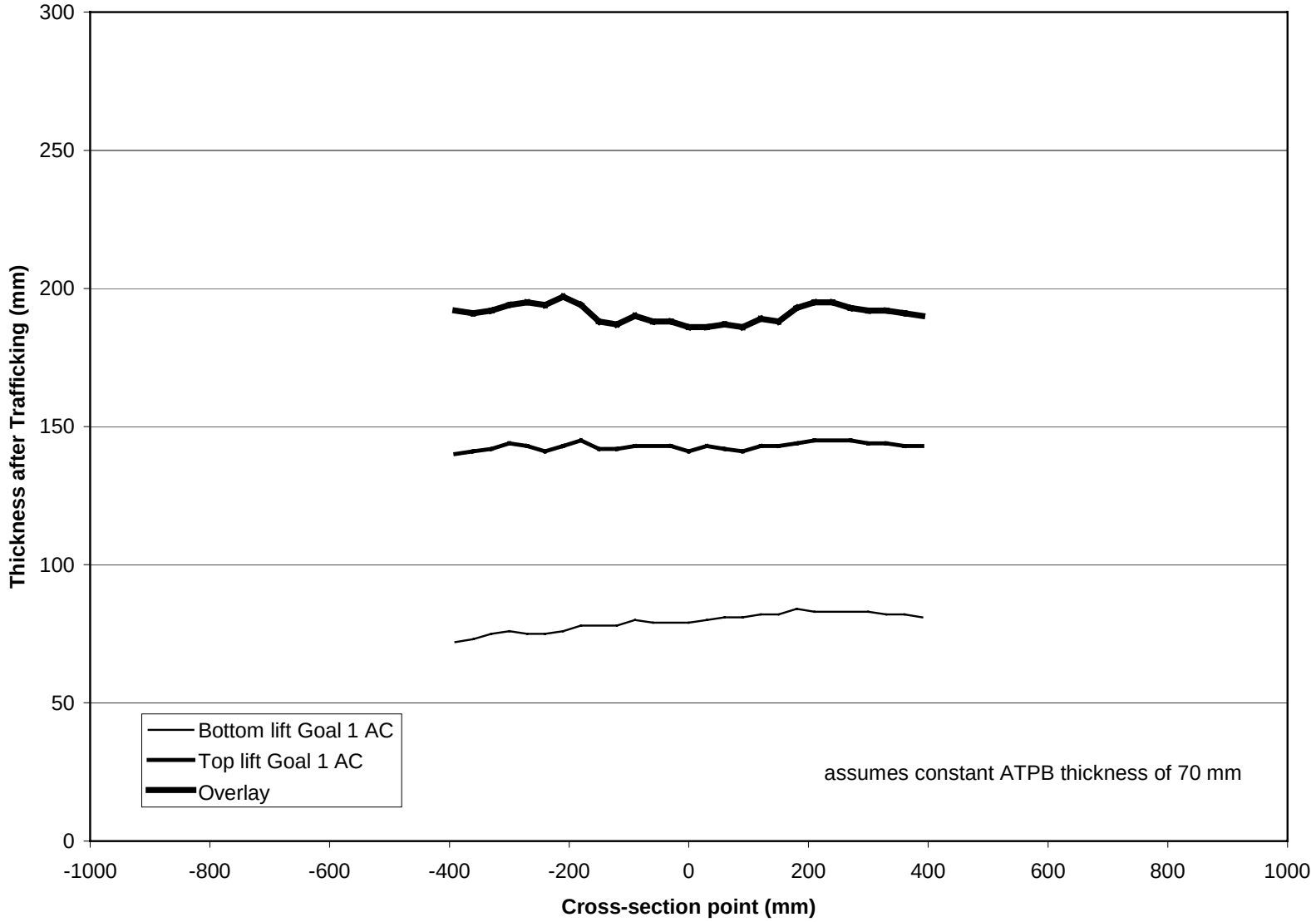

Figure G-9. Transverse profile of trenched AC slab from Section 512RF.

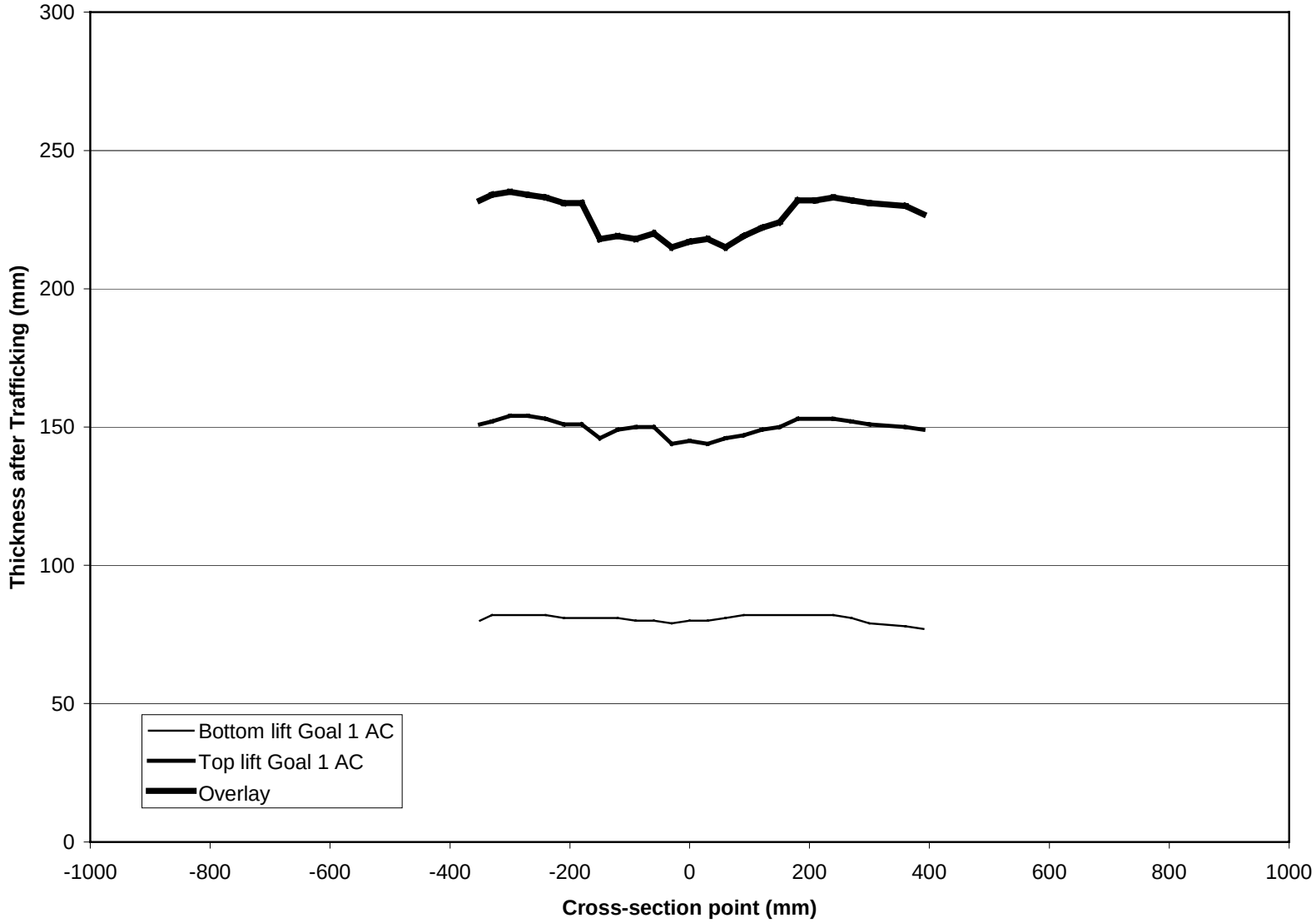

Figure G-10. Transverse profile of trenched AC slab from Section 513RF.

APPENDIX H DEVELOPMENT OF RUT AND HUMP VOLUME UNDER TRAFFICKING FROM TRANSVERSE SURFACE PROFILES

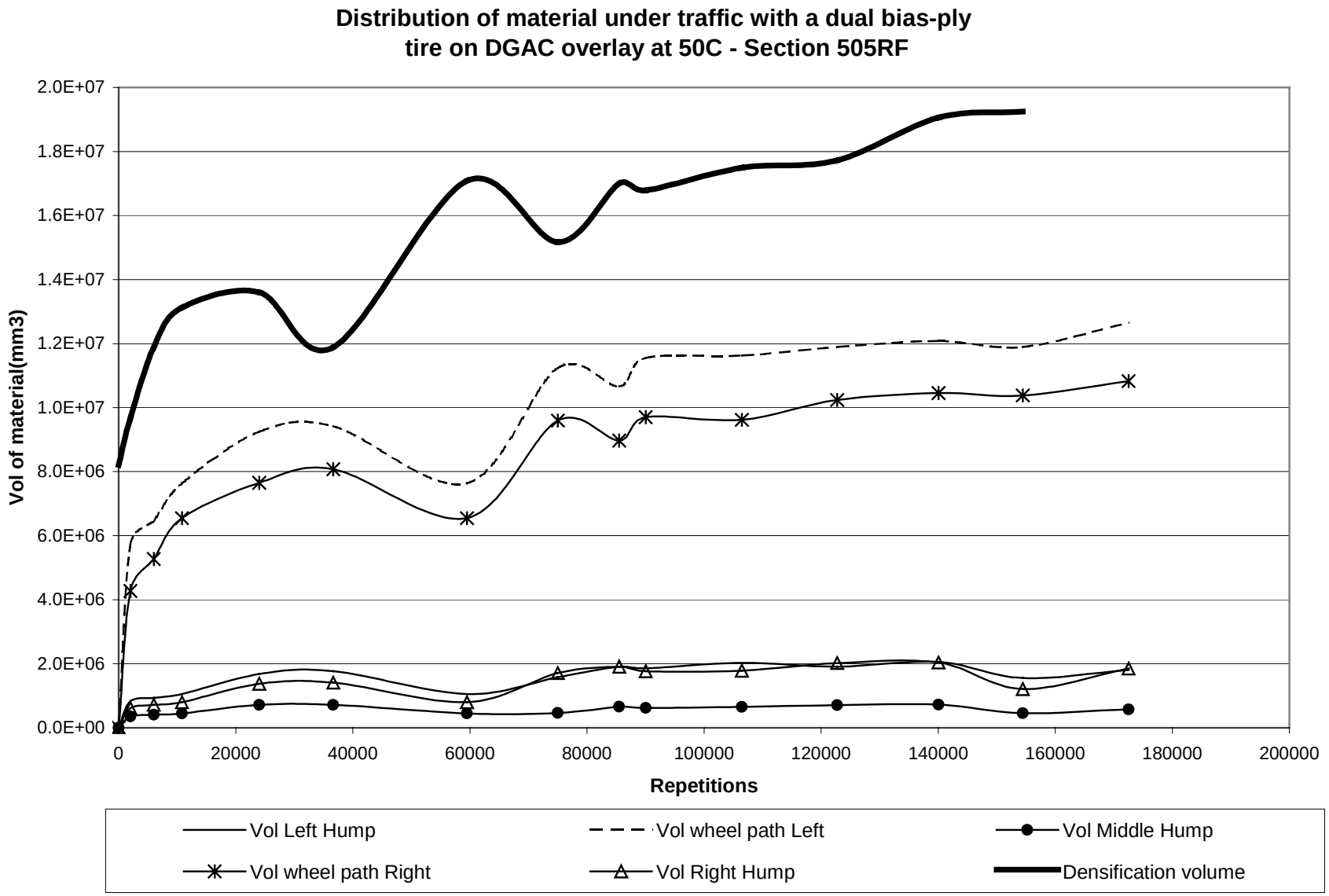

Figure H-1. Development of Rut and Hump Volume Under Trafficking from Transverse Surface Profiles, Section 505RF.

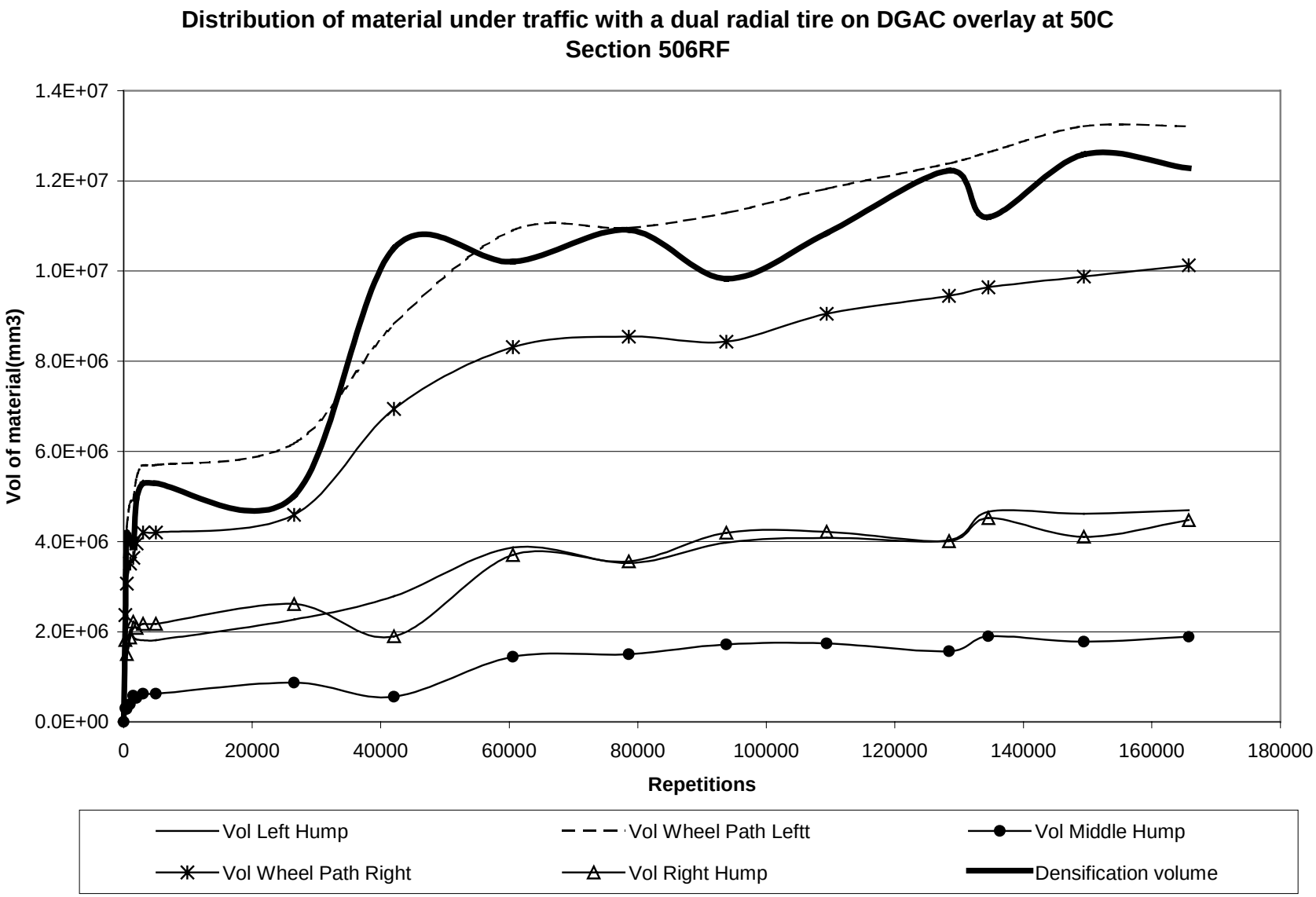

Figure H-2. Development of Rut and Hump Volume Under Trafficking from Transverse Surface Profiles, Section 506RF.

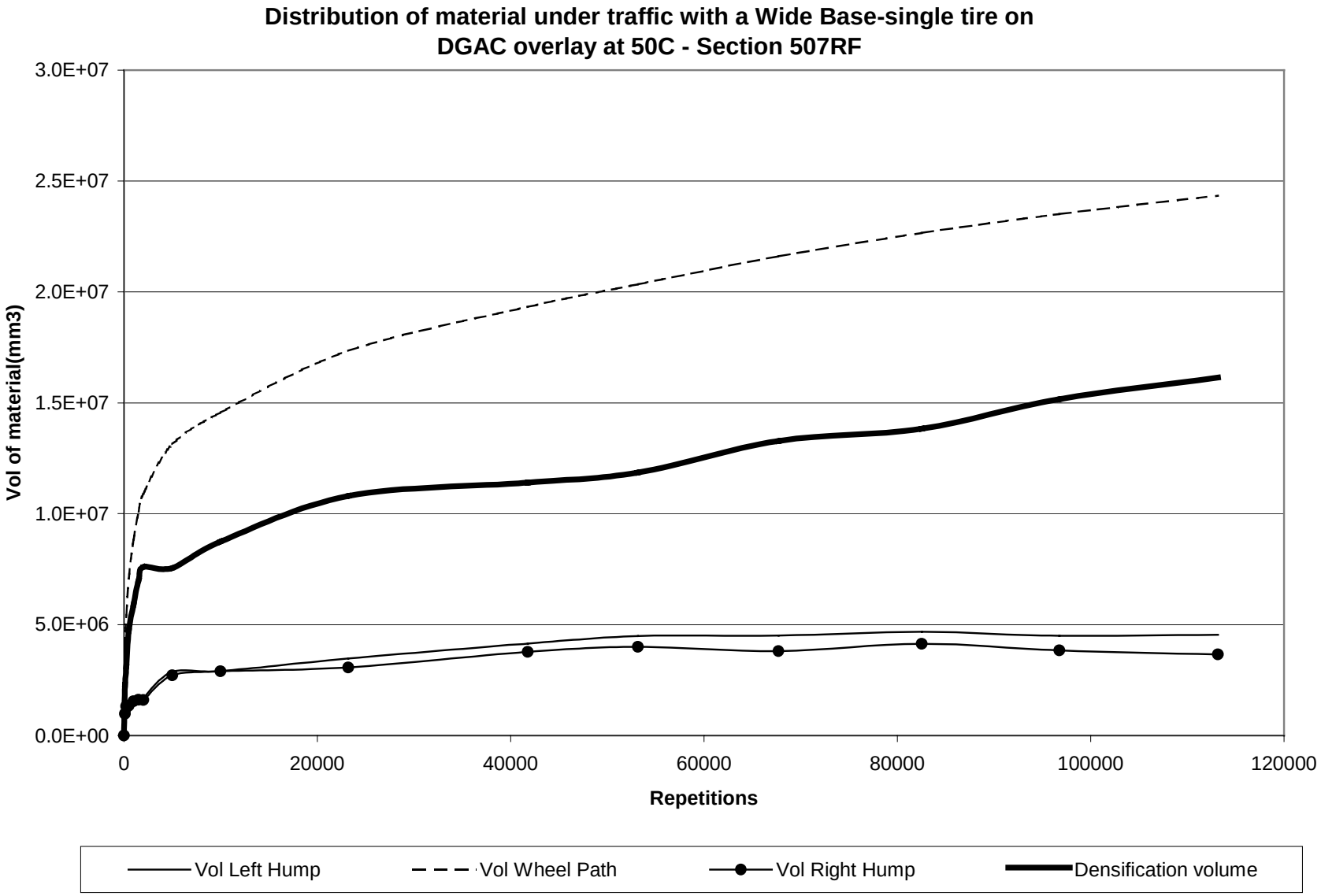

Figure H-3. Development of Rut and Hump Volume Under Trafficking from Transverse Surface Profiles, Section 507RF.

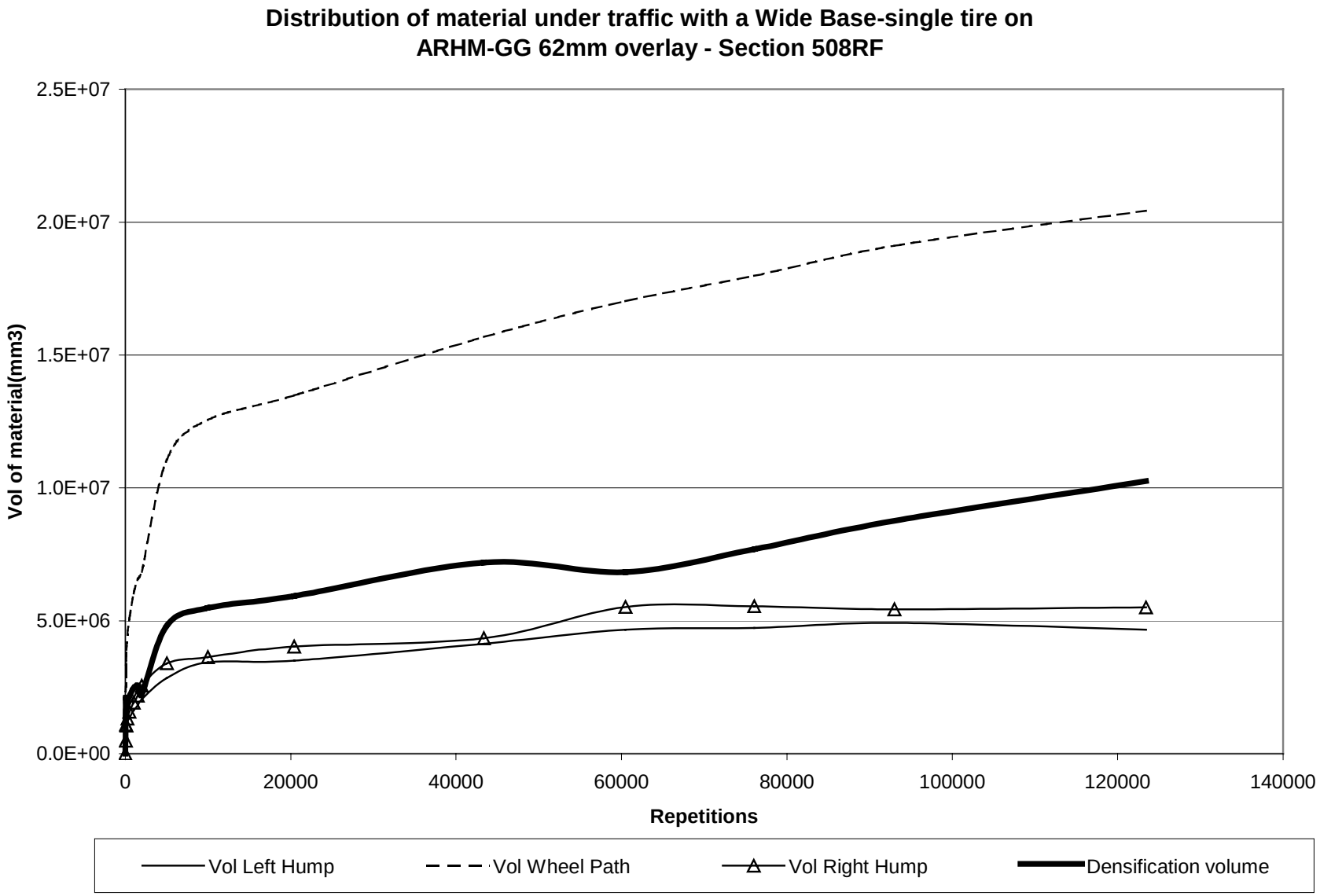

Figure H-4. Development of Rut and Hump Volume Under Trafficking from Transverse Surface Profiles, Section 508RF.

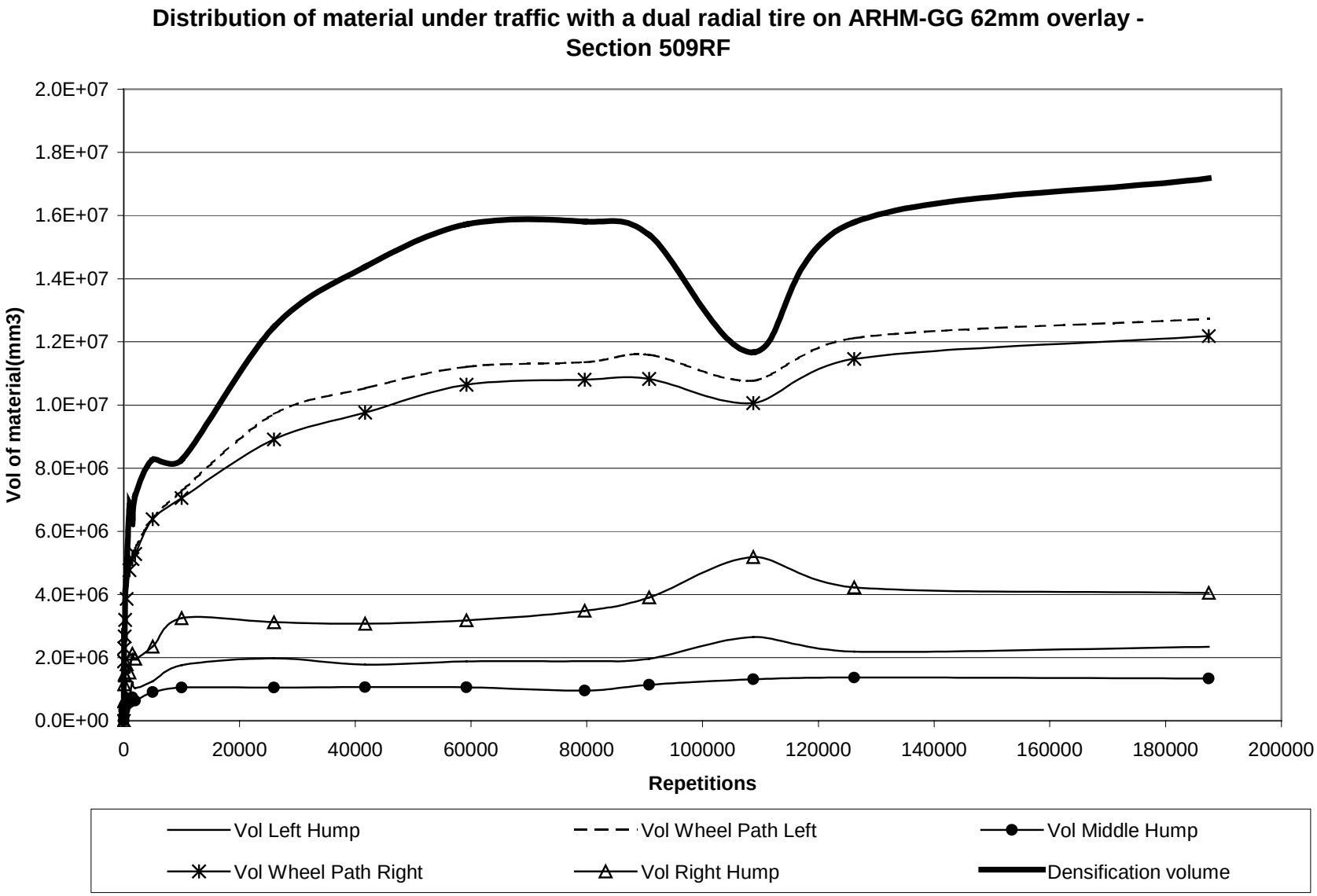

Figure H-5. Development of Rut and Hump Volume Under Trafficking from Transverse Surface Profiles, Section 509RF.

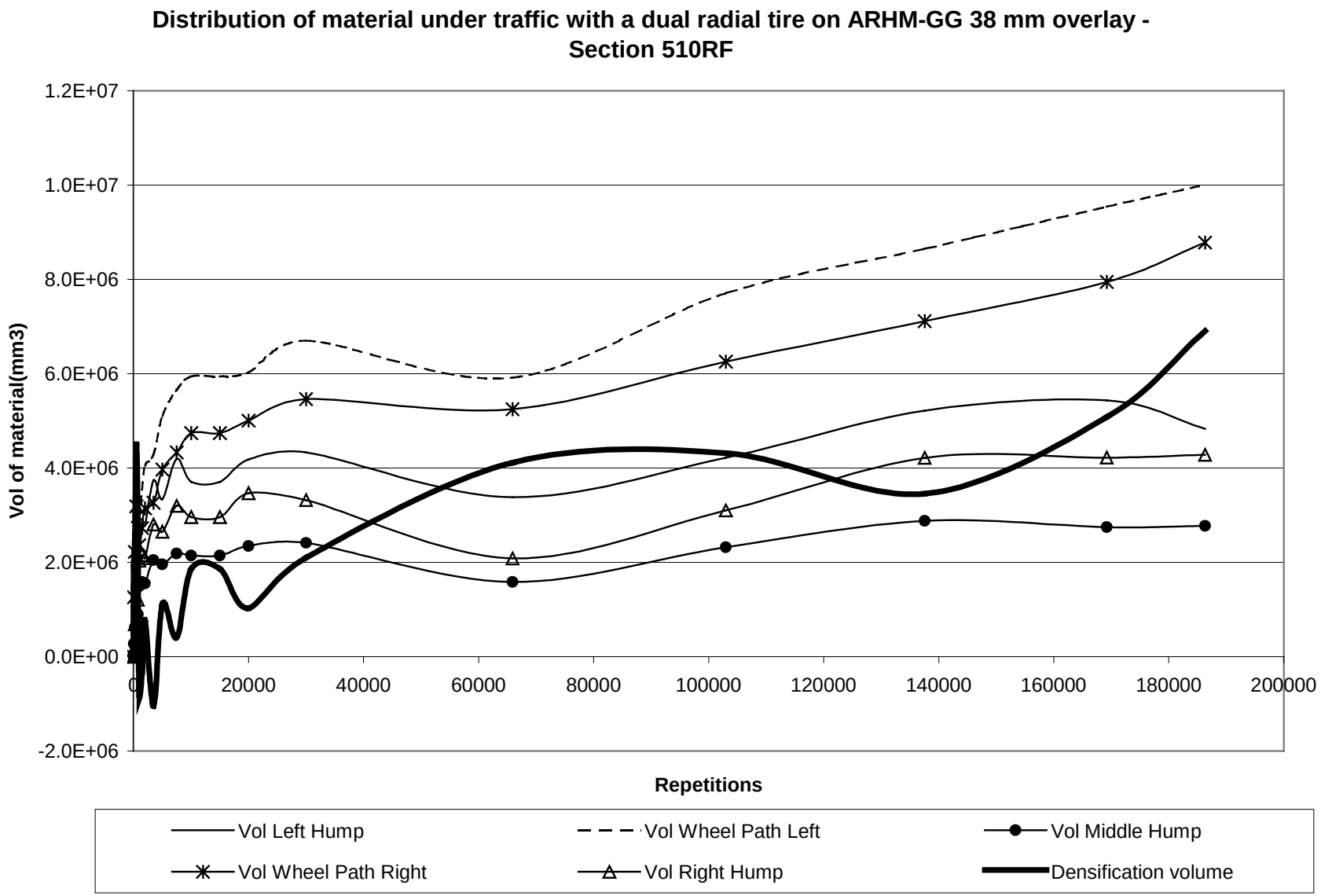

Figure H-6. Development of Rut and Hump Volume Under Trafficking from Transverse Surface Profiles, Section 510RF.

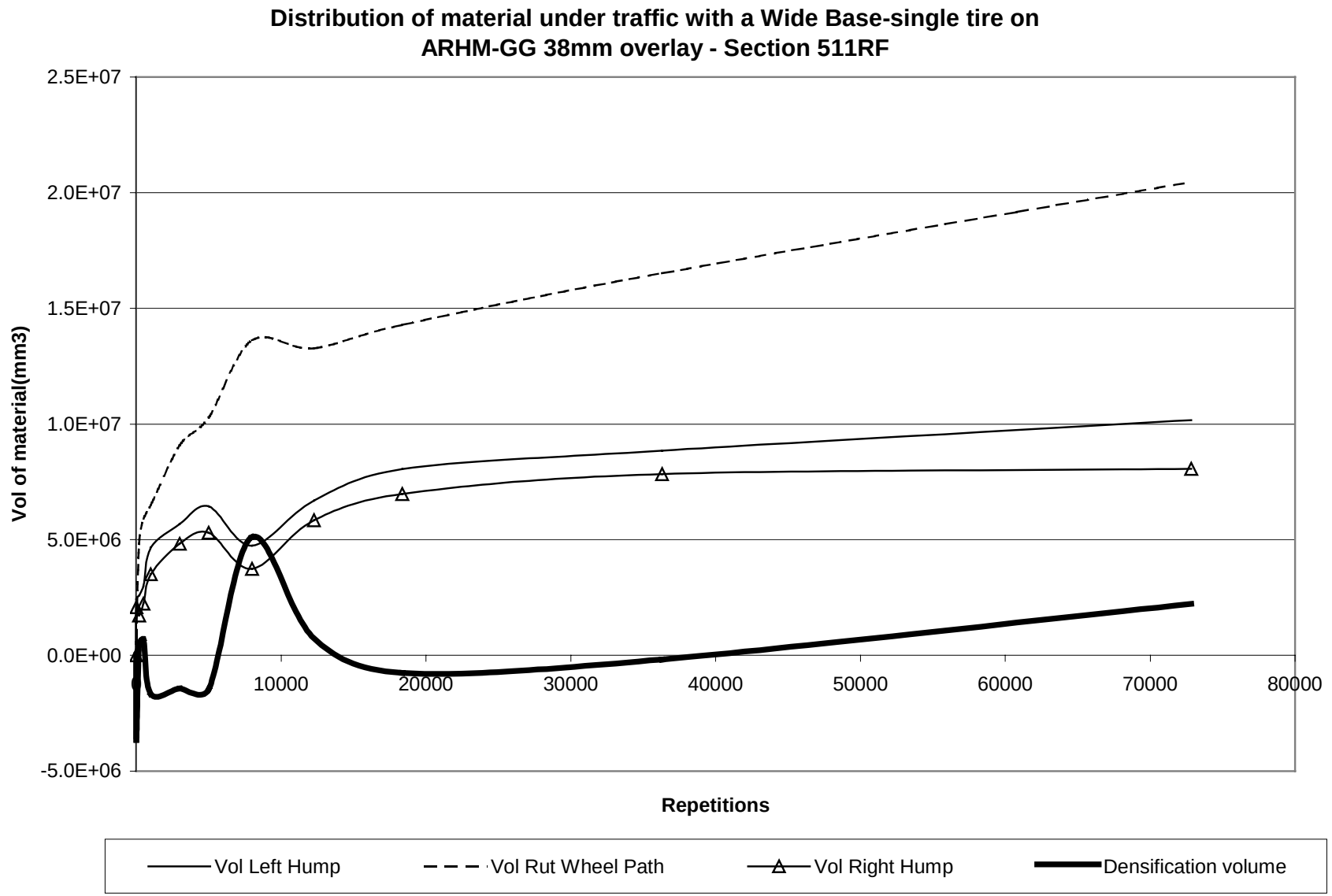

Figure H-7. Development of Rut and Hump Volume Under Trafficking from Transverse Surface Profiles, Section 511RF.

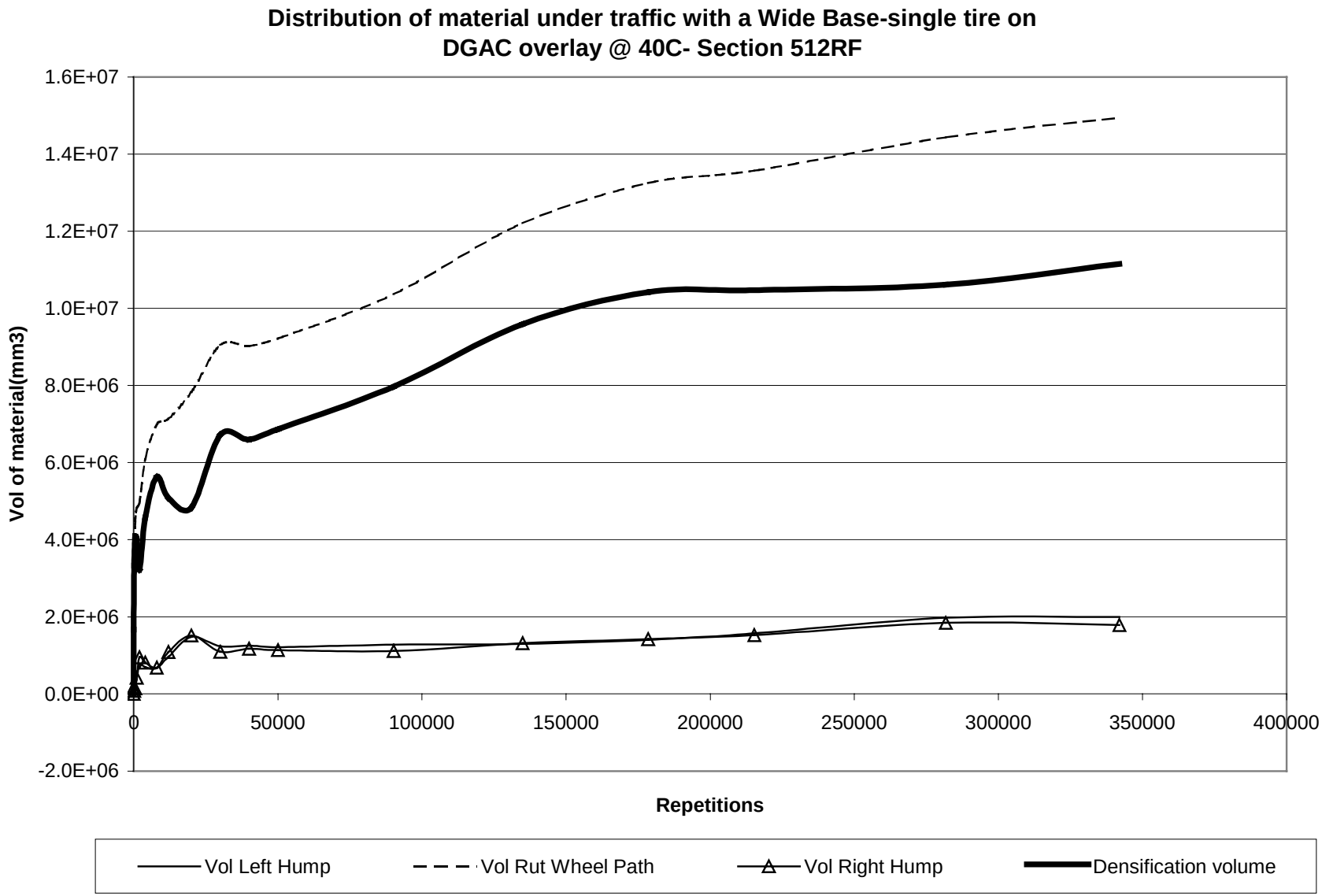

Figure H-8. Development of Rut and Hump Volume Under Trafficking from Transverse Surface Profiles, Section 512RF.

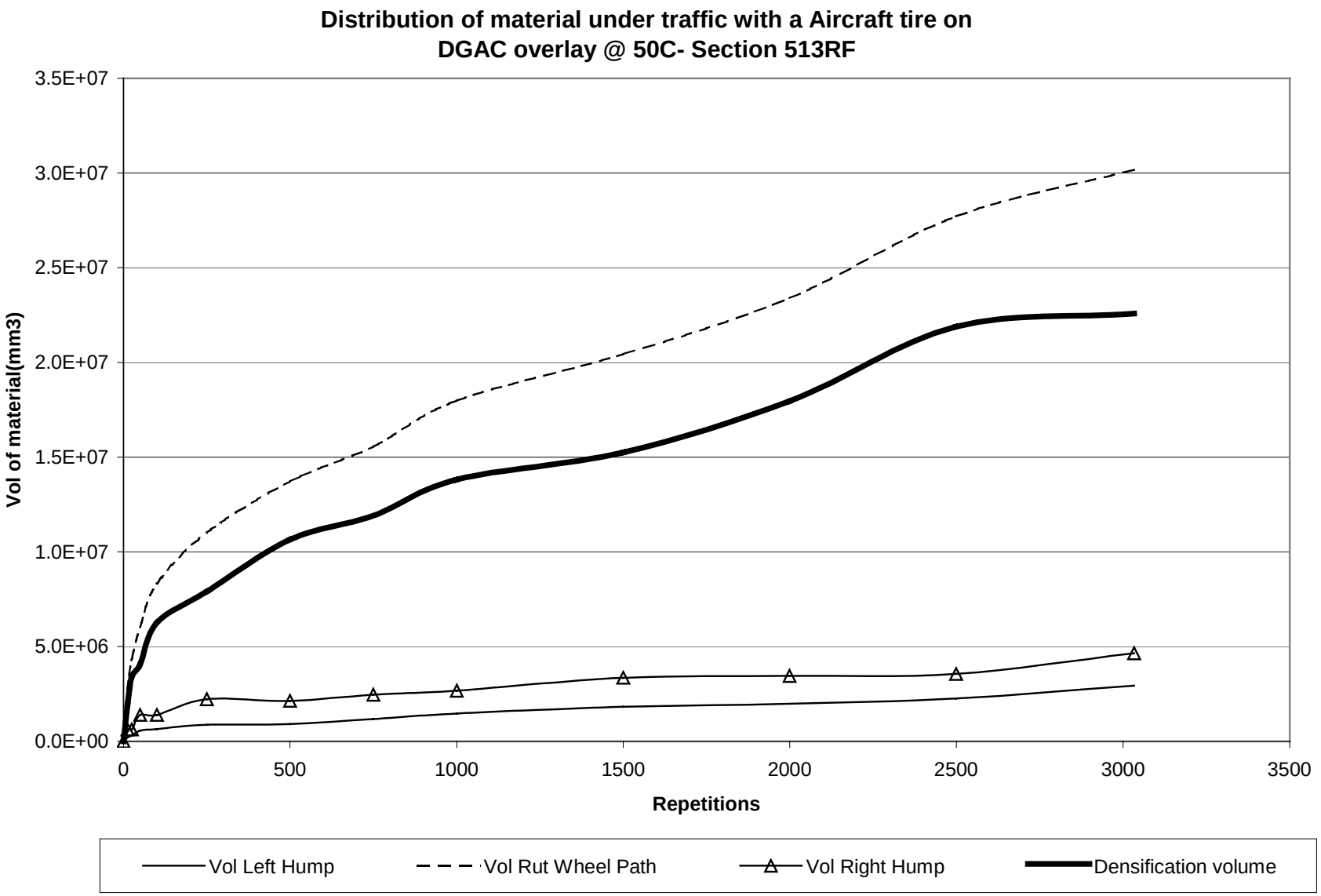

Figure H-9. Development of Rut and Hump Volume Under Trafficking from Transverse Surface Profiles, Section 513RF.

APPENDIX I TRANSVERSE AGGREGATE BASE SURFACE PROFILES AT TERMINATION OF TRAFFICKING

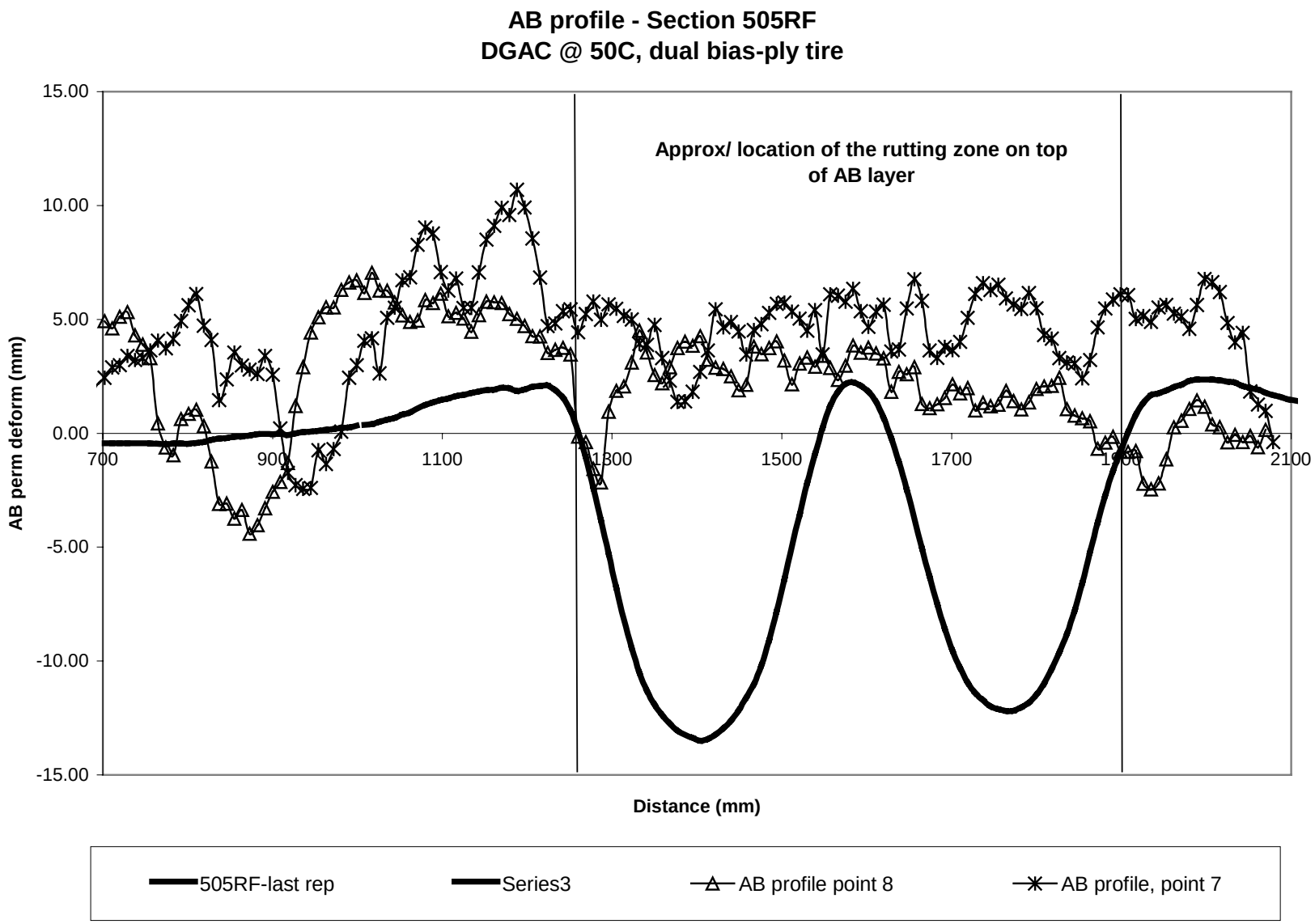

Figure I-1. Transverse Aggregate Base Surface Profile at Termination of Trafficking, Section 505RF.

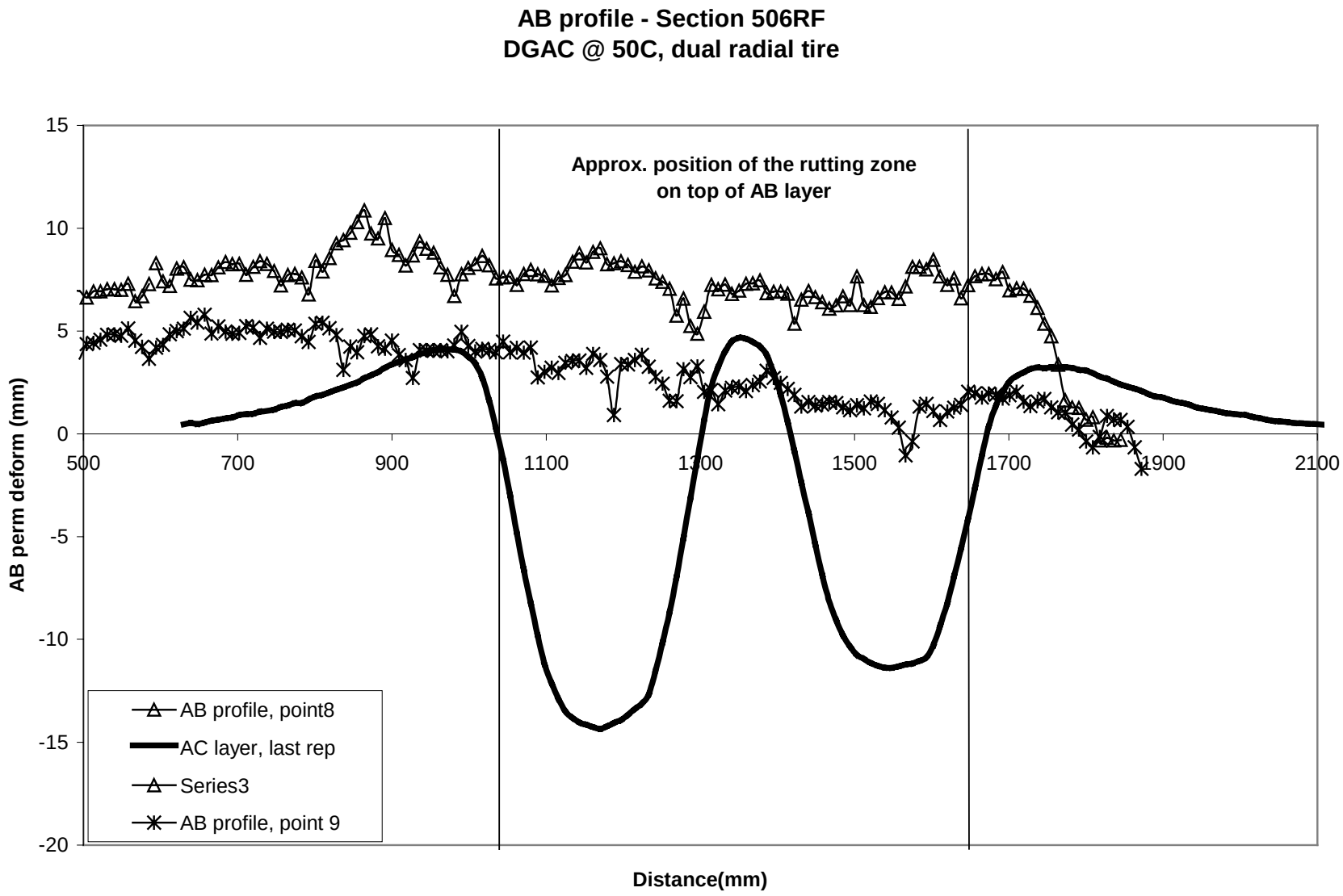

Figure I-2. Transverse Aggregate Base Surface Profile at Termination of Trafficking, Section 506RF.

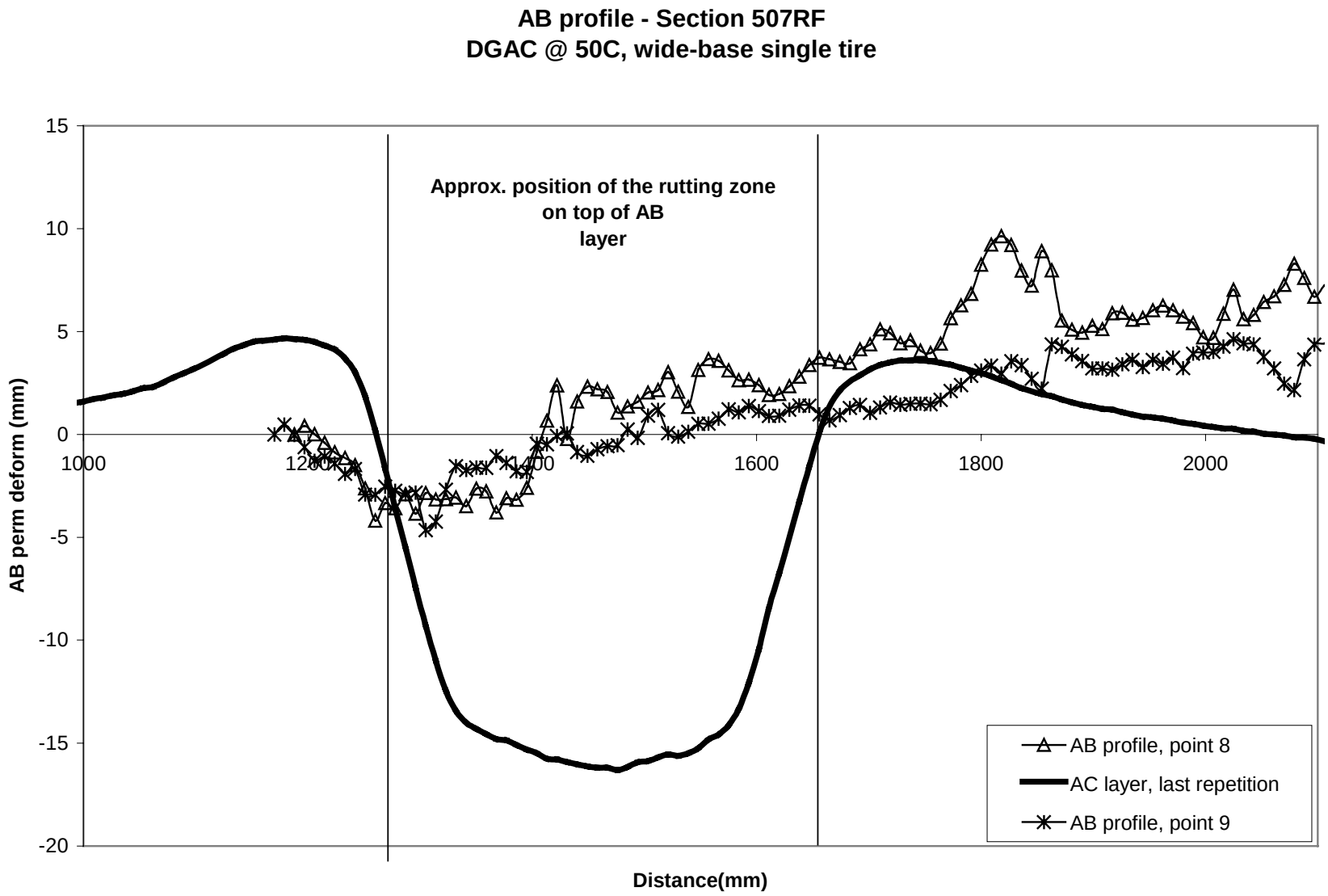

Figure I-3. Transverse Aggregate Base Surface Profile at Termination of Trafficking, Section 507RF.

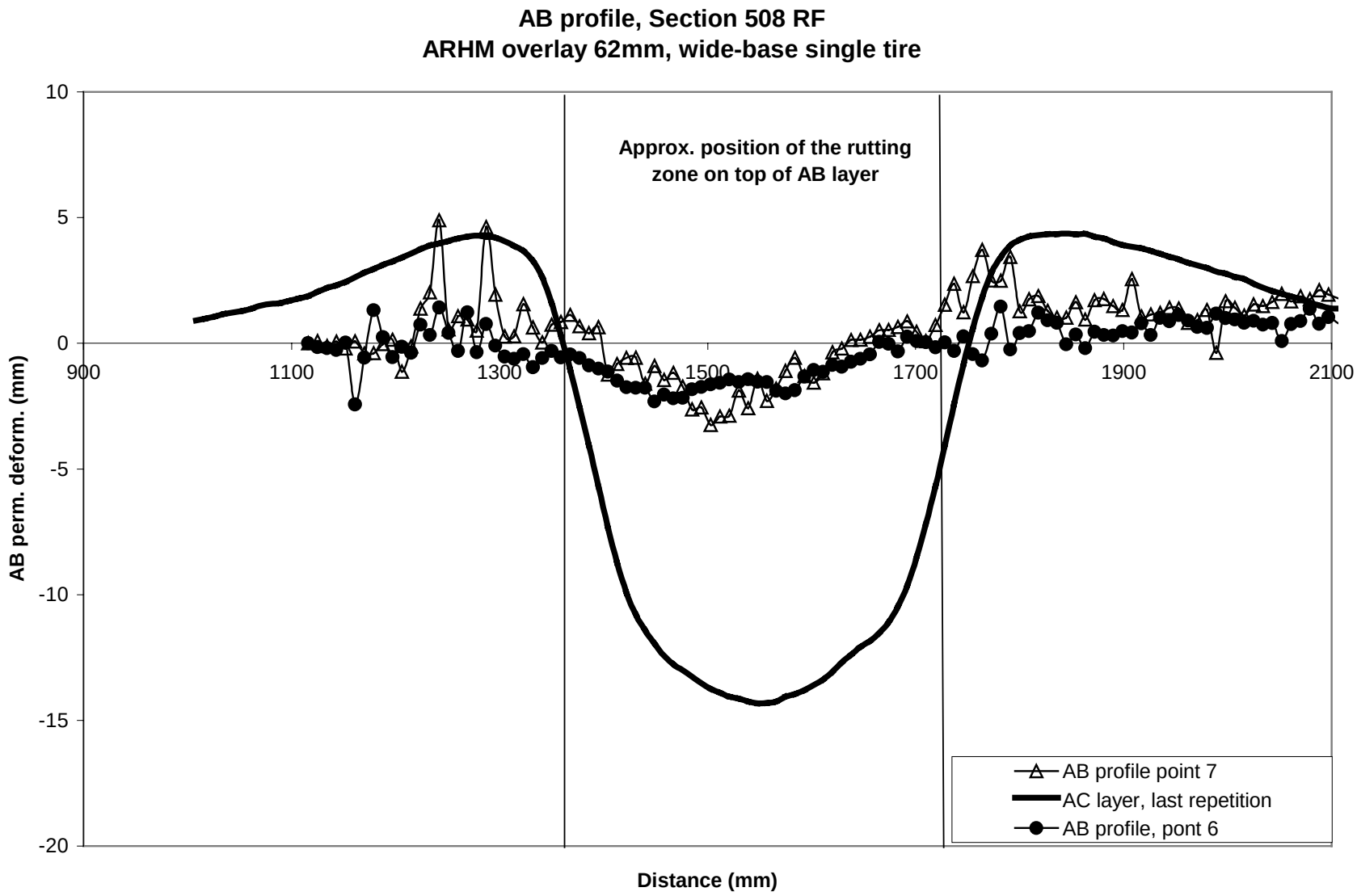

Figure I-4. Transverse Aggregate Base Surface Profile at Termination of Trafficking, Section 508RF.

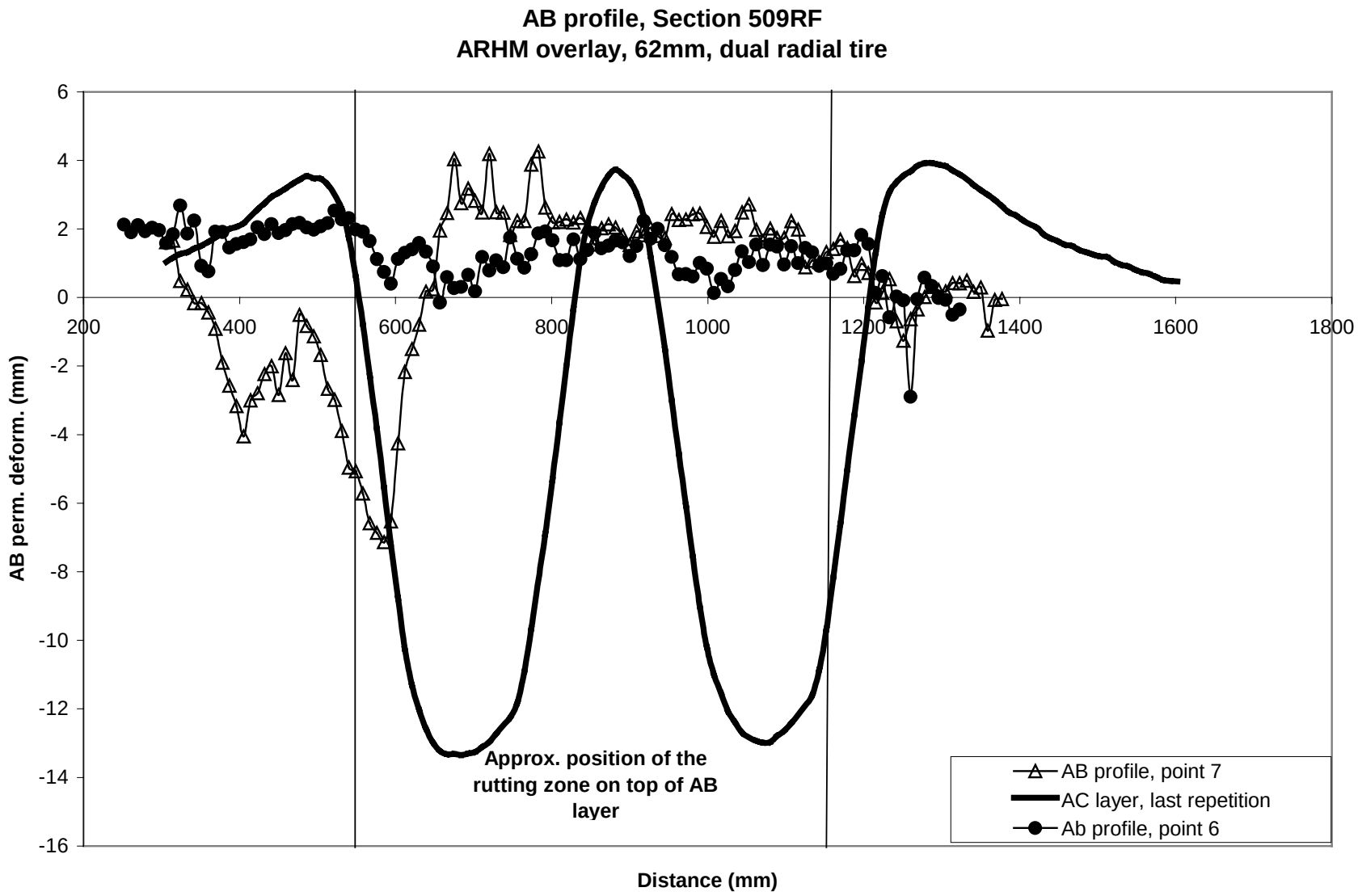

Figure I-5. Transverse Aggregate Base Surface Profile at Termination of Trafficking, Section 509RF.

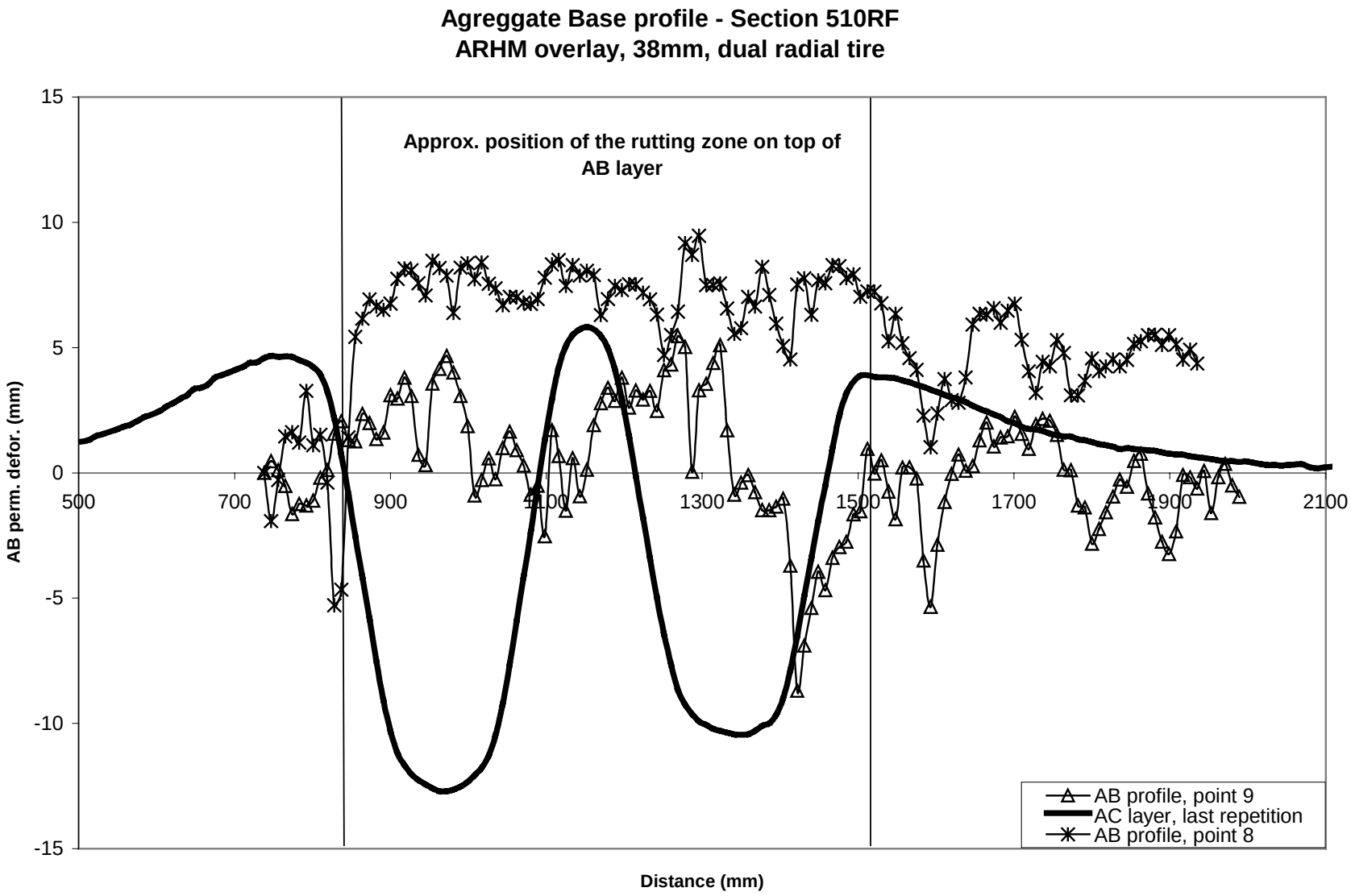

Figure I-6. Transverse Aggregate Base Surface Profile at Termination of Trafficking, Section 510RF.

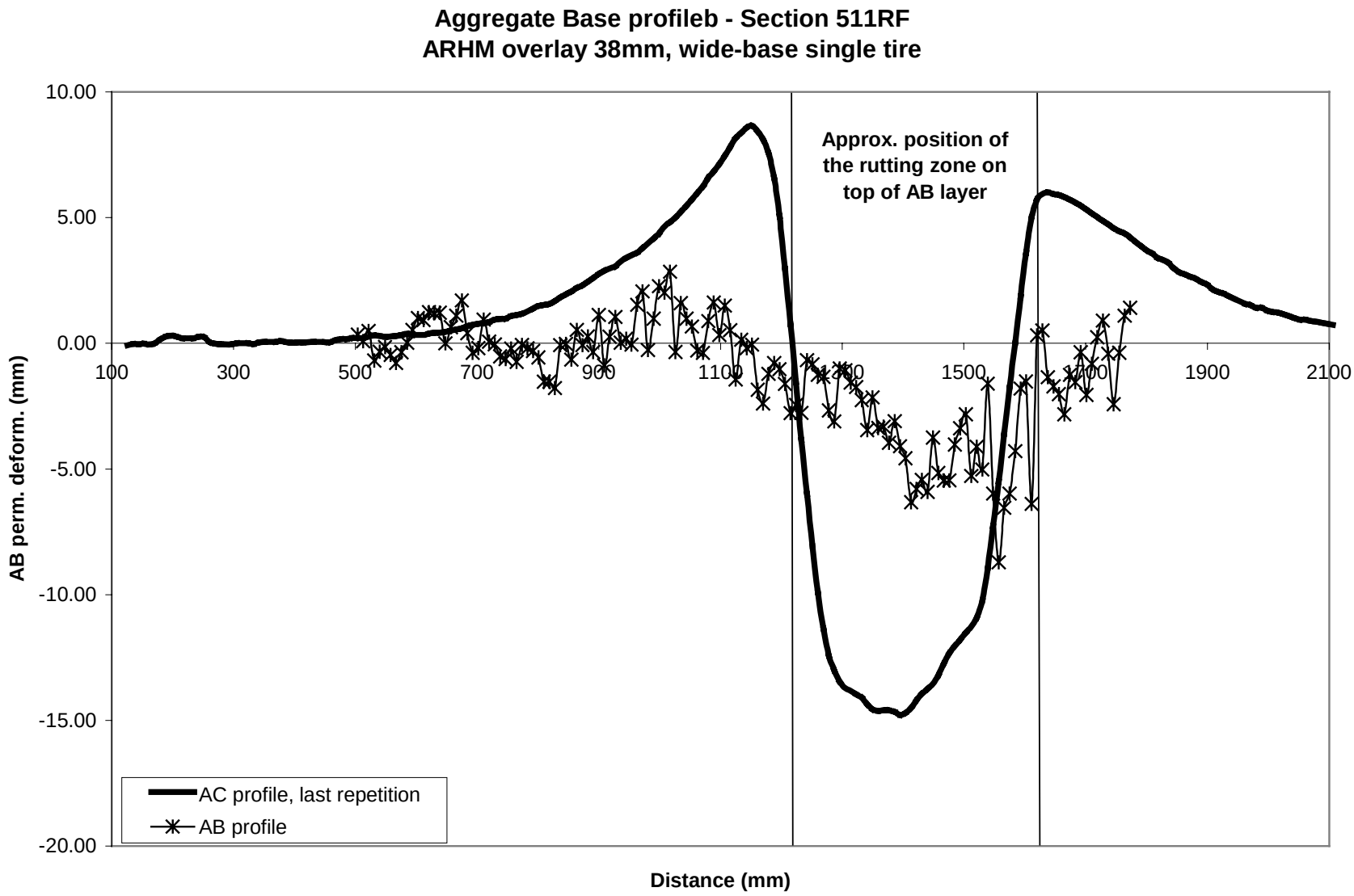

Figure I-7. Transverse Aggregate Base Surface Profile at Termination of Trafficking, Section 511RF.

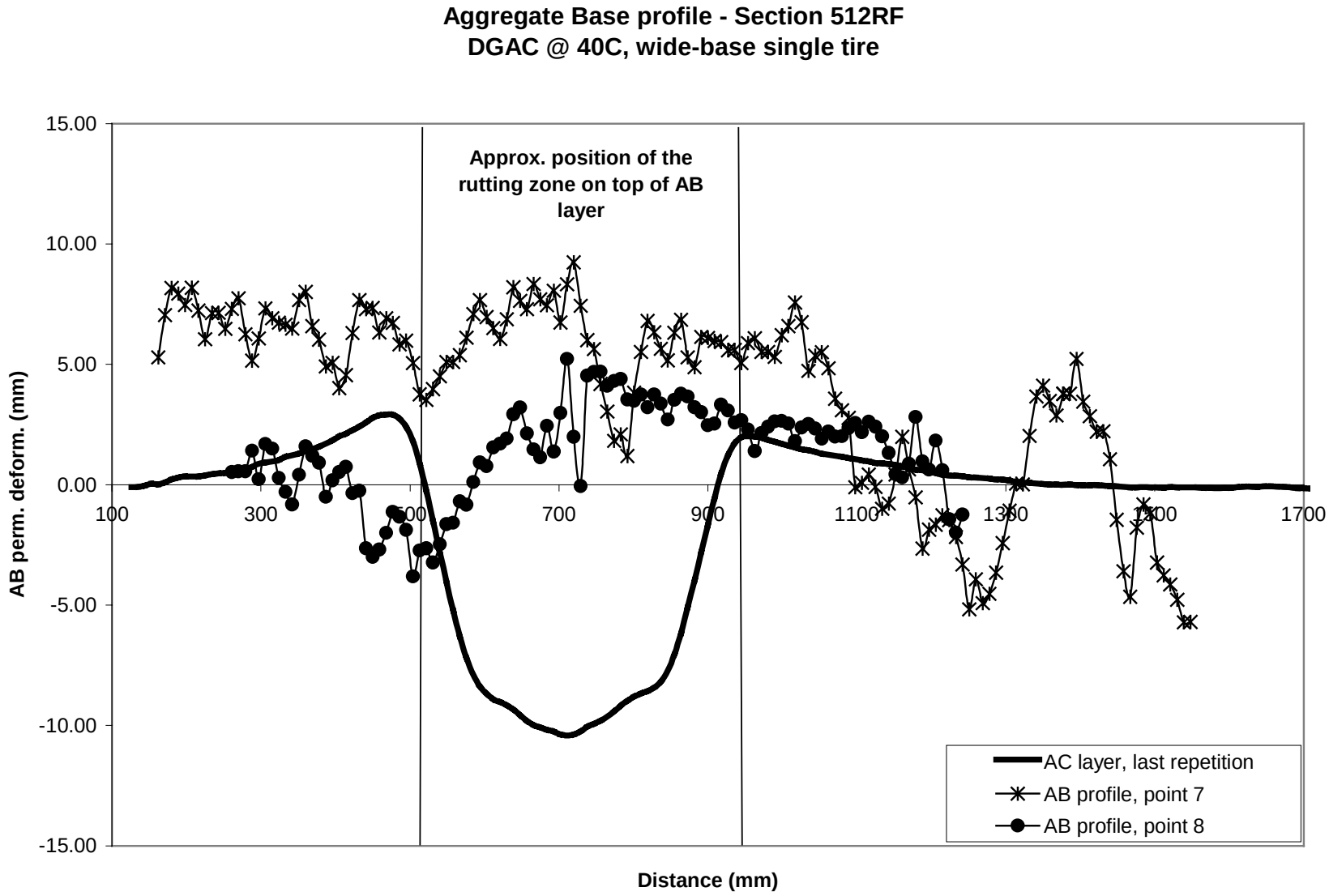

Figure I-8. Transverse Aggregate Base Surface Profile at Termination of Trafficking, Section 512RF.

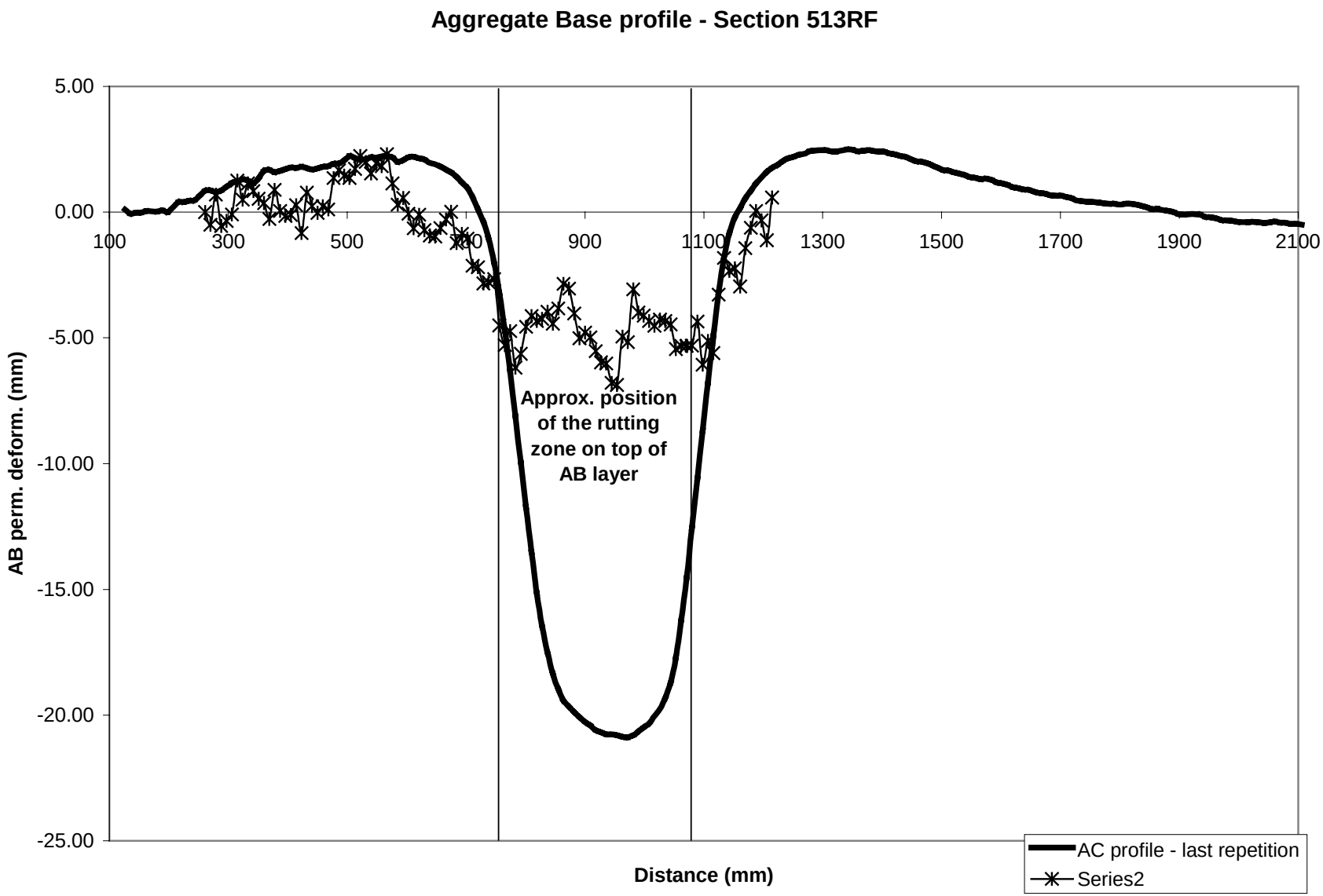

Figure I-9. Transverse Aggregate Base Surface Profile at Termination of Trafficking, Section 513RF.